Wireless Sensor Networks for Smart Communications

Lead Guest Editor: Mu Zhou
Guest Editors: Qilian Liang, Hongyi Wu, Weixiao Meng, and Kunjie Xu

Wireless Sensor Networks for Smart Communications

Wireless Sensor Networks for Smart Communications

Lead Guest Editor: Mu Zhou
Guest Editors: Qilian Liang, Hongyi Wu, Weixiao Meng, and Kunjie Xu

Editorial Board

Contents

Editorial
Wireless Sensor Networks for Smart Communications

Mu Zhou [ID],[1] **Qilian Liang,**[2] **Hongyi Wu,**[3] **Weixiao Meng,**[4] **and Kunjie Xu**[5]

[1]*School of Communication and Information Engineering, Chongqing University of Posts and Telecommunications, Chongqing 400065, China*
[2]*Department of Electrical Engineering, University of Texas at Arlington, Arlington 76019, USA*
[3]*Department of Electrical and Computer Engineering, Old Dominion University, Norfolk 23529, USA*
[4]*Communications Research Center, Harbin Institute of Technology, Harbin 150001, China*
[5]*Intel Corporation, Santa Clara 95054, USA*

Correspondence should be addressed to Mu Zhou; zhoumu@cqupt.edu.cn

Received 14 October 2018; Accepted 14 October 2018; Published 22 October 2018

In the first edition of the special issue titled "Wireless Sensor Networks for Smart Communications", a total of 22 manuscripts were received and 6 of these were accepted. This issue demonstrated that network congestion, user mobility, and adjacent spectrum interference are the main reasons for the degradation of communication quality in Wireless Sensor Networks (WSNs).

In WSNs, the lifetime of network can be extended by exploiting an optimal routing tree algorithm. Besides, by integrating the subgradient-based congestion-optimal Wi-Fi offload and virtualized congestion-optimal Wi-Fi offload algorithms, we can obtain the optimal offload rate of each Access Point (AP). What is more, by using the Device-to-device (D2D) resource allocation and K-nearest Neighbor (KNN) assisted machine learning algorithms, we can obtain effective spectrum resource allocation schemes, and meanwhile by exploiting the mobile state detection algorithms and training of Artificial Neural Network (ANN) model based on ZigBee nodes, we can estimate the heading directions and locations of mobile users.

This special issue has successfully attracted many interesting original articles discussing the optimization of WSNs for smart communications. For example, L. Wang et al. investigated the problem of inefficient spectrum utilization caused by the spectrum sharing and power interference between different communities as well as used the dynamic game theory to optimize the spectrum resource allocation scheme in D2D communication cellular network. The proposed allocation scheme not only quantifies the impact of D2D transmitter power interference on user data transmission rate, but also quantifies the impact of the social relations between different mobile users on data transmission rate. This scheme comprehensively measures the impact of the two factors above on data transmission rate and meanwhile relies on the Nash equilibrium based utility function to design a resource allocation approach based on resource priority searching, which is then used to optimize spectral efficiency. In a subsequent study, Y. Sun et al. proposed a device-free wireless localization system based on the ANN model and used the ZigBee nodes to construct a hardware platform for the communications between different sensor nodes in WSNs. By setting the variance of RSS data and their corresponding indices as the input and the coordinates of known locations as the output for the ANN model training, a satisfactory localization result without the use of special terminals can be obtained. Subsequently, H. A. Shah et al. reported a strategy of using the spectrum-aware KNN algorithm in Cognitive Radio (CR) networks to enhance spectrum utilization. In training phase, this strategy makes global decision based on the perceptual report generated by each CR user, i.e., sending information or keeping silent. At the same time, the majority decisions of different CR users are merged into global one, which is then returned to each CR user. In addition, at each CR user, according to the comparison between global decision and the actual primary user activity determined by confirmation signal, the sensing classes are formed. Then, in classification phase, by comparing each CR user's current sensing report with the existing sensing class formed in training phase, the distance vector and posterior probability of each perceptual class are calculated to indicate

the presence or absence of primary users. In all, this strategy uses a decision-making combination scheme to infer the reliability of each CR user, which is able to determine sending information or keeping silent based on global decision. In response to the Wi-Fi offloading problem, B. Liu et al. studied the problem of network congestion and user mobility management in smart communications. They proposed a Congestion-optimized Wi-Fi Offload (COWO) algorithm to obtain the optimal offload ratio of Wi-Fi networks, which is considered for the enhancement of network throughput as well as mitigation of network congestion. In addition, they improved the COWO algorithm through equivalent transformation and developed a simple Virtual Congestion-optimal Wi-Fi Offload (VCOWO) algorithm, which can well approximate the optimal result obtained by COWO. Finally, extensive simulation results show that the VCOWO is capable of achieving higher network throughput and lower network congestion compared with the existing state-of-the-art. In terms of user mobility, Z. Deng et al. pointed out three special states of human motion, i.e., random hand movement, change of heading direction, and terminal location variation. The performance of heading direction estimation depends on the discrimination of these three states, which can be well achieved according to the user movement states detection, namely, Rotation Matrix and Principal Component Analysis (RMPCA). Besides, the outlier elimination algorithm is also used to improve the accuracy of heading direction estimation of pedestrian. Finally, P. Cao et al. proposed to use multiple Central Processing Unit (CPU) cores to accelerate the process of constructing the optimal routing tree corresponding to the maximal lifetime of WSNs. The goal of this approach is to break down the lifetime maximization problem into several separate subproblems which can be easily solved on each CPU core at the same time. To achieve this goal, they propose three decomposition algorithms, in which two of them are based on the assumption that routing tree does not involve any cycle and the other one is based on the assumption that any node in routing tree has at most one parent node. According to the numerical testing carried out on an 8-core desktop platform, the proposed approach is verified with faster computation speed compared with the conventional ones using only one CPU core.

Therefore, from our perspective, this special issue brings new insights into the WSNs for smart communications. We hope that this information will be helpful to pave the way for the development of intelligent and cognitive communications with wireless sensors in further study.

Conflicts of Interest

I declare that I and the other guest editors have no conflicts of interest or private agreement with companies.

Mu Zhou
Qilian Liang
Hongyi Wu
Weixiao Meng
Kunjie Xu

Research Article

Reliable Machine Learning Based Spectrum Sensing in Cognitive Radio Networks

Hurmat Ali Shah and **Insoo Koo**

School of Electrical Engineering, University of Ulsan, Republic of Korea

Correspondence should be addressed to Insoo Koo; iskoo@ulsan.ac.kr

Spectrum sensing is of crucial importance in cognitive radio (CR) networks. In this paper, a reliable spectrum sensing scheme is proposed, which uses K-nearest neighbor, a machine learning algorithm. In the training phase, each CR user produces a sensing report under varying conditions and, based on a global decision, either transmits or stays silent. In the training phase the local decisions of CR users are combined through a majority voting at the fusion center and a global decision is returned to each CR user. A CR user transmits or stays silent according to the global decision and at each CR user the global decision is compared to the actual primary user activity, which is ascertained through an acknowledgment signal. In the training phase enough information about the surrounding environment, i.e., the activity of PU and the behavior of each CR to that activity, is gathered and sensing classes formed. In the classification phase, each CR user compares its current sensing report to existing sensing classes and distance vectors are calculated. Based on quantitative variables, the posterior probability of each sensing class is calculated and the sensing report is classified into either representing presence or absence of PU. The quantitative variables used for calculating the posterior probability are calculated through K-nearest neighbor algorithm. These local decisions are then combined at the fusion center using a novel decision combination scheme, which takes into account the reliability of each CR user. The CR users then transmit or stay silent according to the global decision. Simulation results show that our proposed scheme outperforms conventional spectrum sensing schemes, both in fading and in nonfading environments, where performance is evaluated using metrics such as the probability of detection, total probability of error, and the ability to exploit data transmission opportunities.

1. Introduction

Cognitive radio (CR) has been proposed to address the issue of spectrum scarcity resulting from inefficient utilization of spectrum resources [1, 2]. A CR user has unlicensed access to the spectrum under the constraint that primary user (PU) communication is not affected. To ensure this, the spectrum is continuously monitored for PU activity. Spectrum sensing can also be used to detect spectral holes and enable CR users to transmit opportunistically. The performance gain of a CR system is further improved by cooperative spectrum sensing (CSS), where multiple CR users cooperate to detect spectral holes.

While matched filtering outperforms other techniques such as cyclostationary detection and energy detection used for spectrum sensing, its complexity makes it impractical for

most systems. Energy detection is the simplest technique, given the limited resources (e.g., energy and computational power) of most CR users. Common spectrum sensing problems such as multipath fading and shadowing can be overcome by exploiting spatial diversity using CSS, thereby ensuring that PU constraints are met [3]. In CSS, individual CR users share their data with a fusion center (FC) that combines local reports to make a global decision. CR users can report the actual amount of received energy, i.e., the not quantized into different levels and then reporting the quantized level which can be represented by fewer bits than the number of bits required for representing the actual amount of energy received. This is called soft-decision combination and results in optimal detection performance but theoretically requires infinite bandwidth [4]. Alternatively, CR users can make a hard decision based on the received energy and

report a single bit representing either the presence or absence of the PU to the FC [5]. Hard reporting saves bandwidth but produces inferior results as compared to soft reporting. Linear soft combination has nearly the same performance as likelihood ratio tests [6].

To balance performance and bandwidth efficiency a combination of both soft and hard decisions can be used where the energy range can be quantized, as in [4, 7]. In [4], the authors used a so-called softened hard combination scheme, in which the observed energy is quantized into four regions using two bits, where each region is represented by a label. This achieves an acceptable trade-off between the improved performance resulting from soft reporting and information loss during quantization process. The FC uses a decision combination rule to combine decisions reported by CR users and make a global decision. The decisions of CR users are in quantized form; i.e., instead of reporting a one-bit decision or the actual amount of energy received to the FC, the CR users quantize the received energy into multiple levels and send multiple bits denoting the quantization zone. This is called quantized-hard decision combination [8].

Along with other factors such as the number of participating CR users, the sensing environment, and sensing capabilities of CR users, the FC's global decision combination rule determines the detection performance of the CR system. For instance, an OR rule results in good protection for the PU but has the lowest spectral hole exploration capability [9], whereas an AND rule improves spectral hole detection but lowers the PU protection capacity. Likewise, poor sensing and/or malicious CR users reduce the performance of the k-out-N decision combination rule. More sophisticated combination rules such as Bayesian analysis and the sequential probability ratio test (SPRT) have better PU protection and spectral hole exploration but require prior information which may not always be available in a given CR environment [10].

The notion of learning from the environment is embedded in the concept of cognitive radios. CR users are meant to monitor the environment and adapt their operating characteristics (operating frequency, transmitting power, etc.) to the changing conditions. To enable CR users to learn from the environment, several authors have considered machine learning algorithms [11–16]. Machine learning in spectrum sensing becomes a task of extracting a feature vector from a pattern and classifying it into a hypothesis class corresponding either to the absence or presence of PU activity. Fading and shadowing can make estimating the channel condition difficult, and hence spectrum sensing cannot reliably determine the PU status based on the current sensing slot only [17]. However, machine learning-based spectrum sensing is capable of implicitly learning the surrounding environment. Another advantage of machine learning-based spectrum sensing is that it can reliably detect PU activity without requiring any prior knowledge of the environment.

Machine learning algorithms are classified into two types: supervised and unsupervised. K-nearest neighbor (KNN) is a supervised machine learning algorithm. In KNN, training instances (spectrum sensing feature vectors) are used to form K neighborhood classes. A test instance is then classified into one of K neighbors based on majority voting. The voting is based on statistical information gained from finding the distance between the test instance and the training instances. The distance should be calculated accurately as to truly reflect the classifying class [18]. KNN is the simplest of machine learning algorithms, suitable for the low-complexity requirements of CR users. KNN is also the most stable machine learning algorithm [19].

Authors in [20–22] have considered KNN for spectrum sensing. In [20] the authors have considered a binary hypothesis testing and have proposed to optimize the distance between the two classes. The drawback of their scheme is that they have considered soft-decision combination and have used a one-time spectrum sensing which cannot be checked against ground reality. In [21], KNN is used in conventional way as a counting mechanism to fill the spaces in building a TV white space database. The use of KNN is limited to reconstruction of the missing spectrum sensing points and thus, the full capacity of KNN as a classifier is not exploited. In [22], authors have found a global energy detection threshold for different conventional rules of decision combination. These rules are used in conjunction with different classification schemes to classify a test instance which takes the signal strength as a feature vector. The authors in [22] also have used KNN as a counting mechanism and, moreover, the global decision combination rule does not take into consideration the weight of individual CR users and their performance history.

Authors in [23] used multiple antennas for centralized spectrum sensing while in [24] a scheme based on multiple energy detectors and adaptive multiple thresholds for cooperative spectrum sensing was presented. For regional area networks, some improved energy detectors were presented in [25, 26]. Authors in [25] proposed a two-stage energy detector where decisions of both the detectors are fused at a decision device while in [26] multiple antennas were used for spectrum sensing in regional area networks. In [27] both a fixed energy detector and adaptive double threshold were used for cooperative spectrum sensing. In [28] multiple antennas based energy detector utilizing adaptive double threshold for spectrum sensing was proposed while in [29] a comparison between cyclostationary detection technique and adaptive double threshold based energy detection scheme was carried out.

In this paper, we propose a machine learning-based reliable spectrum sensing algorithm in which the FC uses a weight-based decision combination rule. In the training phase, CR users perform spectrum sensing, and based on an acknowledgment signal (ACK) and the global decision, the sensing report is assigned to a sensing class. The sensing class corresponds to the behavior of a CR user in a changing environment which is due to the changing activity of the PU. These sensing classes reliably reflect the activity of the PU and the CR user's behavior in response to it. After enough information is gathered about the surrounding environment, the classification phase begins. In the training phase the CR users form a local decision. The local decision is in quantized-hard form. The local decisions of the CR users are sent to the FC and the FC takes a global decision. The CR users stay silent or transmit according to the global decision. If the

CR users transmit and ACK is received in the next time slot then the transmission was successful. Based on the global decision and the status of ACK signal sensing classes are formed. The training phase is over when enough training data for the sensing classes is gathered. In the classification phase, the KNN algorithm is used, where the sensing classes obtained in the training phase are treated as neighbors for the test instance, which is the current sensing report. The Smith-Waterman algorithm (SWA) is used to accurately find the distance between the current sensing report and the neighboring classes. Based on quantitative variables like the conditional probability and posterior probability, which are calculated through KNN, the current sensing report is classified into one of the sensing classes, corresponding to either the absence or presence of the PU. The local decision is then reported to the FC, where the local decisions of all CR users are combined to make a global decision, taking into consideration the reliability of each CR user.

The proposed scheme uses the quantized information as opposed to the soft-decision combination scheme that is proposed in [30]. The spectrum is sensed multiple times in a sensing slot, which makes the proposed scheme more reliable since temporal diversity to the spectrum sensing process is added as wireless channel changes rapidly. The scheme proposed in [30] was based on one-time spectrum sensing while we add a verification mechanism in case that the spectrum sensing decision is absence of PU activity. The classification problem in the proposed scheme is a multilabel one where the current spectrum sensing report is classified into eight different classes. These eight different classes belong to either hypothesis. But the division of the binary hypothesis into subclasses makes the proposed scheme more accurately analyze the PU activity. In addition, the scheme proposed in [30] used the KNN in the traditional way as a counting mechanism. On the other hand, we in the proposed scheme use posterior probability to find the nearest neighbor and utilize KNN to calculate the conditional and prior probabilities.

In the reference of [31], KNN was simply used for data recovery in white space database as a mechanism for majority voting. The classification problem in [31] is also a binary one and the KNN decides a label based on majority labels of the neighboring data points. The proposed spectrum sensing scheme is different from that of [31] in that quantized energy levels are used to train the classifier and then the sensing reports are used to find the class label of the current sensing report by finding the distance between them. Instead of majority voting, we have used an efficient distance measuring algorithm, Smith-Waterman algorithm (SWA) to calculate the similarity of the current sensing report and the training reports.

Mikaeil et al. proposed different classification schemes which work on thresholds calculated through different fusion rules [22]. In the paper, we utilize a different fusion rule at the fusion center which takes into consideration the weight of different CR users before taking a global decision. The focus of [22] is to find the thresholds for different schemes and KNN is used as one of the classifications schemes. On the other hand, in the proposed scheme, the fusion rule utilizes the distance between the test report and the training reports

intrinsically at the CR user level and at the FC the historical accuracy of each CR user is also taken into consideration. In this way, the global fusion rule at the FC makes use of the training reports as well as the history of performance of each CR user. Therefore, the global fusion rule is more robust as well as reliable.

Spectrum sensing has been incorporated into satellite communications, 5G as well as MIMO schemes. The growing need for spectrum has made spectrum sensing crucial for next generation's communication technologies. Authors in [32] employed CR for future broadband satellite-terrestrial communications under the broader framework toward 5G, while the authors in [33] employed joint spectrum sensing and channel selection optimization for satellite communication based on cognitive radios. The concept of the PU as employed by the CR network was employed for satellite cluster communications where the presence of the primary satellite system was detected using the concepts of spectrum sensing by J. Min et al. [34]. The spectral efficiency of MIMO systems which has hybrid architectures were investigated by [35] by investigating the optimal number of users in the system while in [36] the upper limit of downlink spectral efficiency and energy efficiency were investigated in massive MIMI systems with hybrid architecture.

The rest of the paper is organized as follows: Section 2 describes the system model; Section 3 describes the spectrum sensing scheme which consist of KNN algorithm, SWA, the training phase, and the classification phase in detail; Section 4 describes the cooperative spectrum sensing and the global decision combination in detail; Section 5 discusses the results; and Section 6 concludes the paper.

2. System Model

In this section the energy detection method used and the quantization method which is employed are discussed. This section deals with forming of sensing report which is used both in training phase and classification phase of the spectrum sensing scheme. We consider N CR users that continuously sense the spectrum report their local decisions to the FC through a dedicated control channel [4]. The CR user transmits information if a spectral hole exists which is determined by the FC. CR users can either transmit or receive at a given time; i.e., they operate in half-duplex mode. CR users are assumed to be close to the PU and outside the range of other PUs. The system model is presented in Figure 1.

CSS introduces spatial diversity, while temporal diversity is introduced by dividing the sensing slot into minislots. We consider a slotted time-frame structure, where the first slot is used for spectrum sensing and the second slot is used for transmitting CR user data. The authors in [37] investigated the optimal sensing slot duration. In this work a suboptimal sensing slot duration is considered. The sensing result may change when fading and shadowing phenomena are present. Temporal diversity counters these effects by sensing the spectrum n times in the sensing slot. In this work, the sensing slot is further divided into minislots. In each minislot, the spectrum is sensed independently. The sensing performance can be improved if the number of minislots and
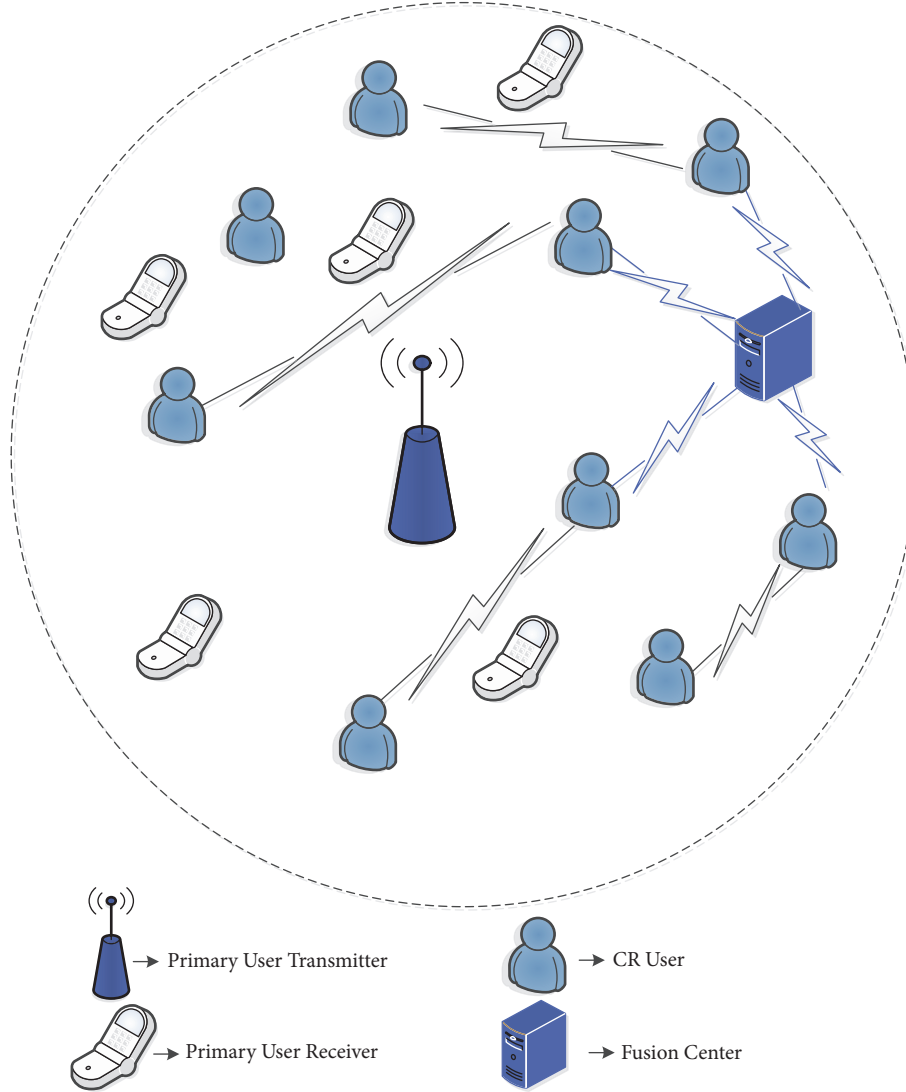
FIGURE 1: Basic system model.

hence the sensing duration are increased but that results in lesser duration for the transmission slot. The authors in [37] investigated the optimal number of minislots for sensing-throughput trade-off in CRNs. According to [37], diversity reception is introduced in the sensing process by sensing the channel independently in minislots within the same sensing phase. In our proposed scheme the results of these minislots are combined to form a sensing report which later is used in the classification phase as given in Section 3.2. The sensing reports were previously used in [8] to calculate trust of each CR user in a CRN which is under-attack by malicious users. In this work the sensing reports are used to train the classifiers and then later used for classifying the current sensing report. A half-duplex CR user system is considered in which in the sensing slot the CR users remain silent. If in the sensing slot it is decided that the PU is absent then the CR users transmit in the transmission slot; otherwise the CR users remain silent.

When the duration of one-time frame, which consists of a sensing slot and a transmission slot, is over the CR users sense the spectrum again. Energy detection is used in each minislot. The energy received in the w-th sensing slot by the i-th CR user at the k-th minislot, $X_{k,w,i}$, can be expressed as

$$X_{k,w,i} = \sum_{j=1}^{N_0} \left| e_{k,w,i}(j) \right|^2 \tag{1}$$

where $k \in \{1, 2, 3, \ldots, n\}$, n is total number of minislots, $e_{k,w,i}(j)$ is the j-th energy sample received at the k-th minislot of the w-th sensing slot by the i-th CR user, and N_0 is the total number of samples, given by $N_0 = 2TB$. T and B are the detection time and signal bandwidth in Hertz, respectively. The number of samples received in a particular minislot is dependent upon the bandwidth of the sensed spectrum and

the sensing time. The received signal $e_{k,w,i}(j)$ in the absence of PU (H_0) and presence of PU (H_1) is given as follows:

$$e_{k,w,i}(j) = \begin{cases} v_{k,w,i}(j); & H_0 \\ s_{k,w,i}(j) + v_{k,w,i}(j); & H_1 \end{cases} \quad (2)$$

where $v_{k,w,i}(j)$ is zero-mean additive white Gaussian noise (AWGN) and $s_{k,w,i}(j)$ is the j-th sample of the PU signal received at the k-th minislot of the of the w-th sensing slot by the i-th CR user.

It was shown in [37] that if the primary signal is absent the probability density function of the energy of the received signal at the i-th CR user ($X_{k,w,i}$) follows a central chi-square distribution with mean μ_0 and variance σ_0^2; otherwise it follows a noncentral chi-square distribution with mean μ_1 and variance σ_1^2, which can be estimated as

$$\begin{aligned} \mu_0 &= N_0 \\ \sigma_0^2 &= 2N_0 \\ \mu_1 &= N_0(\gamma_i + 1) \\ \sigma_1^2 &= 2N_0(2\gamma_i + 1) \end{aligned} \quad (3)$$

where γ_i is the signal to noise ratio (SNR) of the received signal at the i-th CR user.

When the total number of samples, N_0, is large, the energy signal received, $X_{k,w,i}$, under both hypotheses H_0 and H_1 can be approximated by a Gaussian random variable. In our scheme, the energy signal at each minislot is quantized into discrete zones. Multiple bits representing the corresponding zone are transmitted to the FC, rather than transmitting a continuous energy variable (a soft decision) or a single bit (a hard decision). An M-level quantizer of an input variable is represented by a set of quantization levels and a set of quantization thresholds. These quantization thresholds determine the accuracy to which the quantization levels represent the actual received signal.

In the paper, the slotted-frame structure is considered where a frame is one unit of accessing the spectrum. The first slot, called the sensing slot, in each frame is used to sense the spectrum to decide whether the PU is active or not. If it is decided in the sensing slot that the PU is absent, the CR users transmit in the transmission slot. Otherwise, they remain silent for the duration of the transmission slot. When the duration of transmission slot is over, the CR users will start sensing the spectrum again.

Because wireless channel changes rapidly, the spectrum is sensed multiple times instead of only once so as to consider the changing behavior of the channel. To do this, in the paper, the sensing slot is divided into minislots. In each minislot, the spectrum is sensed independently and based on the result, a sensing report is formed. A sensing report is formed according to the quantized decision of each minislot, which is expressed by (4) and will be used in the classification phase later. For spectrum sensing, the energy detection is utilized where samples of received energy are summed and compared with a threshold and based on the comparison result it is decided that whether PU is present or absent.

In this work the number of quantization levels is four, i.e., M = 4. These levels or quantization zones are represented by Z_1, Z_2, Z_3, and Z_4. Zones Z_1 and Z_2 represent low energy or the absence of the PU, while Z_3 and Z_4 represent high energy or the presence of the PU. The quantized energy zones are given as

$$u_{k,w,i} = \begin{cases} H_0 \begin{cases} Z_1; & X_{k,w,i} \le \lambda_{Z_1} \\ Z_2; & \lambda_{Z_1} < X_{k,w,i} \le \lambda_{Z2} \end{cases} \\ H_1 \begin{cases} Z_3; & \lambda_{Z_2} < X_{k,w,i} \le \lambda_{Z3} \\ Z_4; & X_{k,w,i} > \lambda_{Z_3} \end{cases} \end{cases} \quad (4)$$

where $u_{k,w,i}$ represents the quantized energy for the k-th minislot of the w-th sensing slot of the i-th CR user and λ_{Z_1}, λ_{Z_2}, and λ_{Z_3} are the thresholds that differentiate different quantization zones. The set of quantization zones is $q \in \{Z_1, Z_2, Z_3, Z_4\}$ and the set of thresholds is $\lambda \in \{\lambda_{Z_1}, \lambda_{Z_2}, \lambda_{Z_3}\}$. Equation (4) signifies that, in case of H_0, the average received energy at i-th CR user at the k-th sensing slot ($X_{k,w,i}$) can be quantized into either Z_1 or Z_2 and in case of H_1, $X_{k,w,i}$ is quantized into either Z_3 or Z_4. According to our quantization scheme Z_1 and Z_2 represent H_0 and Z_3 and Z_4 represent H_1.

At each sensing slot, a sensing report is formed that consists of symbols belonging to q. The report for the i-th CR user at the w-th sensing slot is called sensing report and is represented by $R_{i,w}$, which contains n elements belonging to q (the sensing report formation is further explained in Section 3.1). This report is used as a feature vector for the machine learning algorithm. During the training phase, this report is assigned to a sensing class based on ACK and the global decision, which will be discussed in detail in Section 3.1. The next section describes the spectrum sensing algorithm at the CR user level.

3. Spectrum Sensing

The proposed spectrum sensing scheme aims to improve PU detection capability under varying environments to improve spectral hole detection. The first goal protects the PU's data from harmful interference and is the foremost constraint specified by IEEE 802.21 which is the standard for accessing TV white spaces [38]. The second goal efficiently exploits spectrum access opportunities, enabling the CR user to transmit data. For the i-th CR user at the w-th sensing slot, channel availability is decided on the basis of the energy vector ($R_{i,w}$). To correctly map $R_{i,w}$ to PU activity, the behavior of the PU has to be learned. Thus the energy vector in our case is analogous to a feature vector in the context of machine learning.

To construct a classifier, i.e., to classify the current sensing report into channel available (H_0) or channel busy (H_1) classes, a training phase is needed. Each CR user stores energy vectors of size W, where W is the length of the training or training phase. In training phase, the slotted-frame structure is used as explained in Section 2. As explained in Section 2, a one-time slot has a sensing phase and a transmission phase. There are W slots in the training phase. These vectors are input of a classifier in the classification phase, where the

current sensing report is compared with previously stored sensing reports to decide between H_0 and H_1.

In our proposed scheme, first the CR users learn the behavior of the PU by mapping the generated quantized energy vectors, which are called sensing reports, to the accurate status of the PU. The true status of the PU is found through ACK and a reliable combination of local decisions of CR users determined by the FC. The function of the CR user in the training phase is different from its function in the classification phase. In the training phase, sensing reports are assigned to sensing classes according to the actual activity of the PU and the corresponding behavior of the CR user. In the classification phase, sensing reports are sorted into one of the sensing classes using KNN. To accurately calculate the distance between the current sensing report and existing members of the sensing classes, SWA is used. Section 3.1 describes the training phase, while Section 3.2 describes the classification phase.

3.1. Training Phase. In this phase, the operating environment is learned by gauging the behavior of the CR user to the changing activity of the PU. The i-th CR user generates a sensing report $R_{i,w}$, makes a local decision on the basis of the average received energy in the current sensing slot, sends the local decision to the FC, and based on the result of FC and the status of ACK assigns the sensing report to a sensing class. This section will explain these steps in detail.

Let the energy received in the w-th sensing slot at the i-th CR user be represented by $Y_{i,w}$ which is given as

$$Y_{i,w} = \frac{\sum_{k=1}^{n} X_{k,w,i}}{n} \tag{5}$$

where $X_{k,w,i}$ is given by (1).

The local decision for the i-th CR user at the w-th sensing slot in the training phase is represented by $q_{i,w}$ and is given by [3]

$$q_{i,w} = \begin{cases} H_0 \begin{cases} Z_1; & Y_{i,w} \leq \lambda_{Z_1} \\ Z_2; & \lambda_{Z_1} < Y_{i,w} \leq \lambda_{Z2} \end{cases} \\ H_1 \begin{cases} Z_3; & \lambda_{Z_2} < Y_{i,w} \leq \lambda_{Z3} \\ Z_4; & Y_{i,w} > \lambda_{Z3} \end{cases} \end{cases} \tag{6}$$

The local decision is sent to the FC, which combines local decisions from all CR users and renders a global decision. In the training phase, the simple majority rule is used as the rule of decision combination. The symbol (quantization zone) reported by the majority of CR users determines the global decision at the FC. As can be seen from (6), the local decision during the training phase is in the quantized-hard form, so the global decision at the FC is also in the quantized-hard form. The sensing report of a CR user is as shown in Figure 2. The local sensing report was explained above in the previous section. In Figure 2, the first six minislots constitute a local sensing report. As can be seen every element of the report belongs to q. For every CR user, at every sensing slot a sensing report (the current sensing report is represented by $R_{i,w}$) is formed, and the local decision is taken according to (6).

Next, the global decision is returned to the CR users. The CR users either transmit or remain silent based on the global decision. If the CR global decision is H_0 then this can be verified by the ACK signal which is sent by the CR receiver to the CR sender after the CR receiver receives the transmission. As overlay cognitive radio network is considered, so, there is no interference to the PU communications. The ACK signal is affected by the PU communication only when the spectrum sensing result is wrong and in-fact the ground reality is H_1. Based on the local decision and the global decision, there are eight possible cases for the CR user and the sensing classes according to our system model. These possible cases called observations are given below.

Observation 1. The local decision ($q_{i,w}$) is Z_1 and the global decision is also Z_1. The CR user transmits its data. If ACK is received, it means the sensing result was correct and the actual status of the PU was H_0. Through the ACK signal, the true status of the PU is known. The sensing report corresponding to this decision ($R_{i,w}$) is stored in a class labelled as R_1 while in case of absence of ACK signal it is stored in R_2.

Observation 2. Both the local decision ($q_{i,w}$) and the global decision are Z_1, or the global decision is Z_2 and the local decision is Z_1. The CR user will transmit, but ACK is not received, meaning that the sensing decision was wrong and the PU was available. The CR user will store $R_{i,w}$ in a class labelled R_2. If ACK signal is received it will be stored in R_1. If the local decision is Z_1 and the global decision is Z_3 or Z_4, then $R_{i,w}$ will also be stored in this class.

Observation 3. The local decision ($q_{i,w}$) is Z_2 and the global decision is also Z_2. The CR users follow the procedure as explained in Observation 1. If ACK is received, the sensing decision is correct and the PU is not present. $R_{i,w}$ is stored in a class labelled R_3, otherwise it is stored in R_4.

Observation 4. The local decision is Z_2 and the global decision is Z_1 or Z_2. The CR user transmits, and if ACK is not received, $R_{i,w}$ is assigned to the class with label R_4, otherwise in R_3. If the local decision is Z_2 and the global decision is either Z_3 or Z_4, then again $R_{i,w}$ will be stored in the class labelled as R_4.

Observation 5. The local decision is Z_3 and the global decision is also Z_3. There will be no transmission in this case. The true status of the PU thus cannot be known. $R_{i,w}$ will be assigned to a class which is labelled as R_5. The sensing report will also be stored in class R_5 if the global decision is Z_4 and the local decision is Z_3.

Observation 6. The local decision is Z_3 but the global decision is either Z_1 or Z_2. The CR user will transmit. If ACK is received, $R_{i,w}$ will be stored in a class labelled R_6, otherwise it will be stored in R_5.

Observation 7. Both the local and global decisions are Z_4. There will be no transmission and $R_{i,w}$ will be stored in the class labelled as R_7. $R_{i,w}$ will also be stored in R_7 if the local decision is Z_4 and global decision is Z_3.

FIGURE 2: Local sensing report and local decision during training phase.

Observation 8. The local decision is Z_4, but the global decision is either Z_1 or Z_2. The CR user will transmit. If ACK is received, $R_{i,w}$ will be stored in class R_8. If no ACK is received, $R_{i,w}$ will be stored in R_7.

In the observations above it can be seen that ACK signal is used when the global decision is H_0. When the global decision is H_1 the CR users do not transmit and thus ACK signal cannot be used to ascertain ground reality. So, in the case when H_1 is the global decision at the FC the CR users store the current sensing report in the classes R_5 and R_7 as the current sensing decision cannot be verified in any other way than at the risk of causing interference to the PU transmission.

The observations are given in decision tree form in Figure 3. As the observations do not stem from one set of decisions, there is no unified root of the decision tree. The decision trees are given in four partitions depending on the local decision. The local decision is abbreviated as LD and the global decision as GD in Figure 3. Figure 3(a) corresponds to the case that the local decision is Z_1 and Observations 1 and 2 are obtained. Figure 3(b) corresponds to the case that the local decision is Z_2 and the Observations 3 and 4 are obtained. Figures 3(c) and 3(d), respectively, correspond to the cases that the local decisions are Z_3 and Z_4 and the Observations 5, 6, 7, and 8 are obtained.

These observations help learn the CR user about the surrounding environment and its behavior in response to the environment and also give CR users historical data that can be used in conjunction with the current sensing behavior to more reliably predict the PU status. This process can be seen as cooperative learning where not only is the individual CR user taken into account, but also the impact of other CR users is incorporated through the global decision. This adds spatial diversity to the learning process, where a receiver with better signal to noise ratio (SNR) conditions can drive the behavior of CR users with poorer SNR conditions.

The training phase is run until the CR user is sufficiently trained in the behavior of the surrounding environment, including changing the SNR conditions and changing the behavior of the PU. Fading can also temporarily affect the signal and thus the energy received due to the continuously changing sensing environment. The training scheme developed takes into consideration the presence of fading and thus store sensing reports that may have been the results of either fading or bad sensing in their corresponding categories. As the learning is based on the ACK and reliable decision combination at the FC, classes based on training more reliably reflect the sensing environment and PU activity. The results of either fading or bad sensing at the CR user level are found in the above observations, where the local decision is different from the global decision or when ACK is not received.

The training data is collected locally at each CR user in the training phase. The performance of machine learning techniques is dependent upon the size of the training phase. As the training size increase, the performance also improves. With an increase in the number of CR users a larger area under the PU is covered. Because our training model incorporates the global decision by acting according to it and also through the ACK signal the ground reality is known, the training phase can accurately know the behavior of CR users to the PU activity. With a large number of CR users, each CR user can reflect the ground reality in its training classes through the global decision. With a large training phase, the behavior of CR users to varying nature of the PU activity also can be accurately known. In conventional machine learning techniques, the training phase can gather adequate amount of training data to know the environment. Knowing the exact nature of PU activity is practically not feasible because of the random nature both of wireless channel and of the PU activity. But as will be shown in simulations, given a sufficiently large size of the training phase, the system detection performance can converge even at a very low SNR.

Figure 4(a) presents the frame structure when the FC decides that the PU is present during training phase. The CR users remain silent during the transmission phase in this case. Different operations in the sensing phase happen as first the local decision is made, then the local sensing decision is sent to the FC through a CCC. The FC combines the local sensing decisions and decides whether the PU is present or absent. If the FC decides that the PU is absent then the CR users transmit and hear for the ACK signal over the same channel on which transmission has been done. The CCC is not used for establishing links between the CR users. Rather it the communications happen between the CR user through the spectrum which is licensed to the PU and which is accessed by the CR users if the PU is absent. Figure 4(b) presents the time frame for the case when PU is absent during training phase. On the basis of the ACK signal the sensing report of the sensing slot is assigned into the classes as defined by the observations above. The frame structure is different for training phase from classification phase. In the training phase the sensing classes are updated on the basis of status of the ACK signal which helps in training the CR user to accurately reflect the ground reality.

3.2. Classification Phase. In the previous phase, information was gathered regarding the operating environment and the CR user behavior in response to the changing environment. Learning the environment is made especially difficult by the nature of CR networks. Because of the noisy sensing environment, CR users only obtain partial observations of the environment variables. In addition, CR users must also transmit data. This results in a trade-off between sensing time and

(a) Decision tree for the case that local decision is Z_1

(b) Decision tree for the case that local decision is Z_2

(c) Decision tree for the case that local decision is Z_3

(d) Decision tree for the case that local decision is Z_4
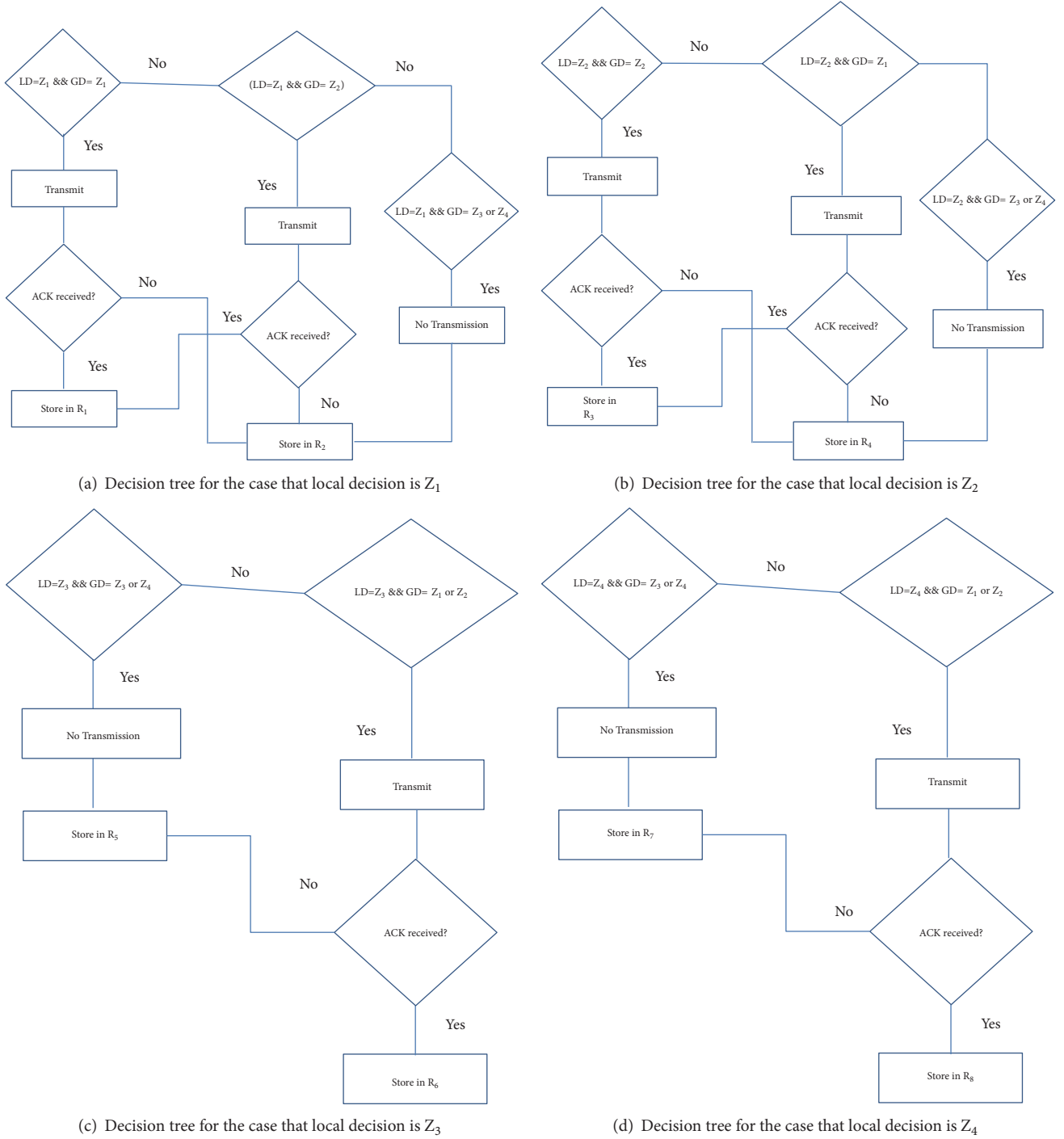
FIGURE 3

throughput: the higher the sensing time, the more accurate the sensing result and thus the more efficient the learning. Therefore, partial observability and capping the sensing time complicate the learning process. A third limitation is that a PU is considered to be autonomous. A CR user may not have any prior information about PU behavior, its operating characteristics, the RF environment, interference levels, or noise power distribution.

Our learning scheme addresses these issues. Partial observability is addressed by incorporating the behavior of other CR users into the learning process through the global decision. The ACK enables CR users to better learn the operating environment and divide the sensing observations into their respective classes more accurately. Our learning scheme requires no prior information and can efficiently map sensing performance to the changing activity of the

Make a local sensing decision according to (6)	Send to FC through CCC	Take a global decision and return to CR users through CCC	Stay silent if global decision is Z_3 or Z_4 and assign sensing reports to sensing classes according to Section 3.1

$\xleftarrow{\hspace{1cm}}$ Sensing slot $\xrightarrow{\hspace{1cm}}$ | $\xleftarrow{\hspace{2cm}}$ Transmission slot $\xrightarrow{\hspace{2cm}}$

$\xleftarrow{\hspace{4cm}}$ One slot $\xrightarrow{\hspace{4cm}}$

(a) Time-frame structure when the FC decision is Z_3 or Z_4 during the training phase

Make a local sensing decision according to (6)	Send to FC through CCC	Take a global decision and return to CR users through CCC	Transmit if FC decides Z_1 or Z_2	Listen to ACK signal on the same channel on which transmission has been done	Assign sensing reports to sensing classes on the status of ACK signal according to Section 3.1

$\xleftarrow{\hspace{1cm}}$ Sensing slot $\xrightarrow{\hspace{1cm}}$ | $\xleftarrow{\hspace{2cm}}$ Transmission slot $\xrightarrow{\hspace{2cm}}$

$\xleftarrow{\hspace{4cm}}$ One slot $\xrightarrow{\hspace{4cm}}$

(b) Time-frame structure when the FC decision is Z_1 or Z_2 during the training phase

Figure 4

PU, thus enabling the CR user to more reliably detect the PU.

A frame structure during the classification phase is presented in Figure 5. In the local decision making phase, the spectrum is sensed and a sensing report is created. The first six minislots in the local decision making part of Figure 5 represent the local sensing report. The second part is the classification phase discussed in Section 3.2.3. The last part of the local decision making slot is the reporting phase, where the local decision is reported to the FC, the global decision is returned and the CR user takes action accordingly. The transmission phase follows the local decision making phase.

In this section, we will present in detail how the current sensing report is classified into one of the training classes. KNN, a machine learning algorithm, is used to accurately classify the current instance into one of the sensing classes and thus reliably detect PU activity. Section 3.2.1 presents the KNN algorithm.

3.2.1. K-Nearest Neighbor Algorithm. KNN is a distribution-free machine learning algorithm that classifies observations into one of several classes based on quantitative variables. KNN, being a distribution-free method, is suitable for the context of cognitive radios. KNN classifies a test instance, in our case the current sensing report as described in Section 3.1, into one of several neighboring classes by majority voting. The voting can be modified to calculate the distance between any two sensing reports. In the context of CR networks, it is highly improbable that any two sensing reports are exactly the same, so we have to measure the similarity between them.

The classification plane is divided into a number of neighbors and the distance of the current sensing report to each of those neighbors is found. For the sake of notational simplicity let us denote the sensing report of the current sensing slot at the i-th CR user by x_i onwards. Let $d(x_i, y)$ be the distance, where y represents the neighbors, or the sensing classes obtained in Section 3.1, given by $y \in \{R_1, R_2R_3, R_4, R_5, R_6R_7, R_8\}$. The distance is calculated to each

of the neighbors representing either H_0 or H_1. Based on the calculated distance, the current sensing report is classified either to H_0 or to H_1. Section 3.2.2 shows how the distance is calculated and Section 3.2.3 shows the procedure for using KNN for classification.

3.2.2. Smith-Waterman Algorithm. The Smith-Waterman algorithm (SWA) [39] is a local alignment algorithm that calculates an accurate distance between two vecto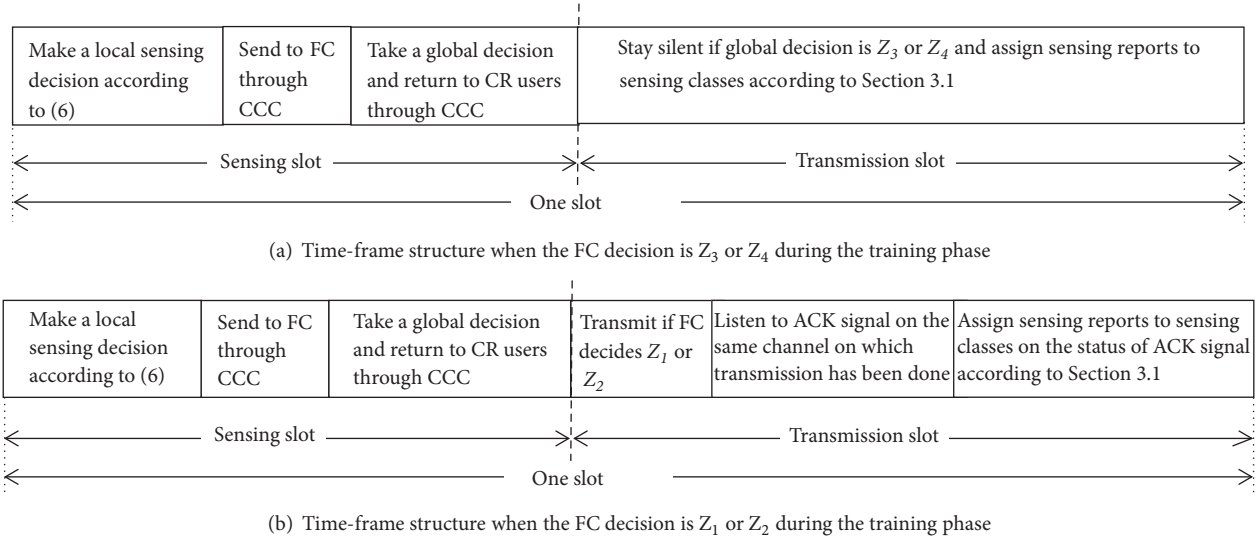rs. The sensing reports in our case can differ from each other due to spatial and temporal diversity, so the voting method conventionally used in KNN, which is based on finding a match or a mismatch, is not applicable here. Instead, we focus on measuring the similarity between sensing reports, using SWA to calculate the distance between the current sensing report and the sensing classes.

SWA consists of three stages: training, matrix fill, and trace back. The three stages are briefly described as follows.

Training: one sensing report is arranged horizontally and the other vertically. The top row and the leftmost column are initialized to 0.

Matrix fill: let the sensing report arranged vertically be $\hat{q}_m$ and the sensing report arranged horizontally be $\hat{q}_j$. Each element of $\hat{q}_m$ ($q_{p,m}$) is compared with every element of $\hat{q}_j$ ($q_{l,j}$) and the score $F(p, l)$ is computed according to the matrix fill equation as follows:

$$F(p,l) = \max \begin{cases} 0 \\ F(p\text{-}1, l\text{-}1) + o\left(q_{p,m}, q_{l,j}\right) \\ F(p\text{-}1, l) \text{-}t\left(q_{p,m}, q_{l,j}\right) \\ F(p, l\text{-}1) \text{-}t\left(q_{p,m}, q_{l,j}\right) \end{cases} \tag{7}$$

where $p, l = 1, 2, \ldots, n$ are indices of the elements of report $\hat{q}_m$ and report $\hat{q}_j$, respectively, $q_{p,m}$ is the p-th element of report $\hat{q}_m$, $q_{l,j}$ is the l-th element of report $\hat{q}_j$, $o(q_{p,m}, q_{l,j})$ is the similarity reward between two characters, and $t(q_{p,m}, q_{l,j})$
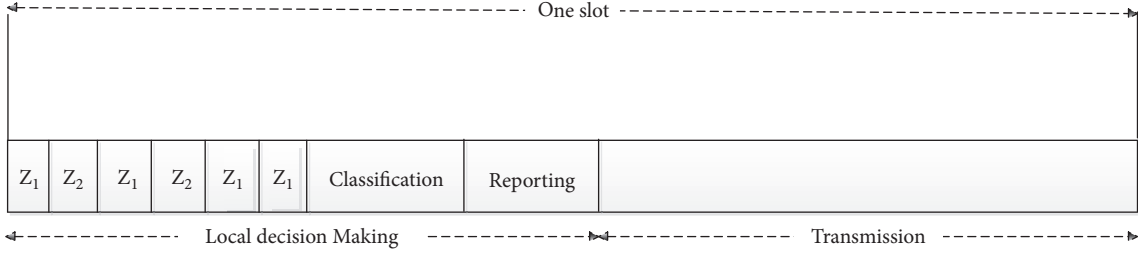
FIGURE 5: Frame structure during classification phase.

is the gap penalty (dissimilarity) that determines the degree of mismatch between $q_{p,m}$ and $q_{l,j}$ to be penalized. Different reward and penalty values are defined for different types of sequences and applications. Here, we use intuitive values based on experimental results. The gap penalty is determined as

$$t\left(q_{p,m}, q_{l,j}\right) = \begin{cases} 4, & \left(q_{p,m} = \text{'}Z_1\text{'}, q_{l,j} = \text{'}Z_4\text{'}\right) \\ 3, & \left(q_{p,m} = \text{'}Z_1\text{'}, q_{l,j} = \text{'}Z_3\text{'}\right) \\ & \text{or } \left(q_{p,m} = \text{'}Z_2\text{'}, q_{l,j} = \text{'}Z_4\text{'}\right) \\ 2, & \left(q_{p,m} = \text{'}Z_2\text{'}, q_{l,j} = \text{'}Z_3\text{'}\right) \\ 1, & \left(q_{p,m} = \text{'}Z_1\text{'}, q_{l,j} = \text{'}Z_2\text{'}\right) \\ & \text{or } \left(q_{p,m} = \text{'}Z_3\text{'}, q_{l,j} = \text{'}Z_4\text{'}\right) \\ 0, & \text{otherwise.} \end{cases} \quad (8)$$

and the similarity reward is calculated as

$$o\left(q_{p,m}, q_{l,j}\right) = \begin{cases} 2, & \left(q_{p,m} = q_{l,j}\right) \\ 1, & \left(q_{p,m} = \text{'}Z_1\text{'}, q_{l,j} = \text{'}Z_2\text{'}\right) \text{ or} \\ & \left(q_{p,m} = \text{'}Z_3\text{'}, q_{l,j} = \text{'}Z_4\text{'}\right) \\ 0, & \text{otherwise.} \end{cases} \quad (9)$$

It is important to note that $o(q_{p,m}, q_{l,j}) = o(q_{l,j}, q_{p,m})$ and $t(q_{p,m}, q_{l,j}) = t(q_{l,j}, q_{p,m})$, which means that the similarity reward and gap penalty have the commutative property. The similarity score between two sensing reports $F_{\widehat{q}_m, \widehat{q}_j}$ is obtained by taking the maximum element of the score matrix (F). The similarity score of the m-th sensing report when compared with the j-th sensing report is given as

$$F_{\widehat{q}_m, \widehat{q}_j} = \max_{p,l=1,2,\dots,n} \left\{F\left(p,l\right)\right\}. \quad (10)$$

Trace back: the third stage of the SWA is called trace back and is performed to align sequences based on the scores computed in the "matrix fill" stage. Since our objective is just to find the similarity score, the trace back stage is not required in our work.

3.2.3. Classification. As is explained a sensing report have n elements belonging to q. The sensing report (x_i) has to be

classified into one of the sensing classes, which are treated as neighbors for x_i. The candidate set of neighbors for x_i is denoted by $N(x_i)$ and contains all classes as found in Section 3.1 such that $N(x_i) \in \{R_1, R_2, R_3, R_4, R_5, R_6, R_7, R_8\}$ and each CR user has its own version of sensing classes.

The current sensing report is compared with every member of each of the sensing classes belonging to $N(x_i)$. The membership counting vector is represented by $\overrightarrow{y_{x_i}}(l)$. Each element of $\overrightarrow{y_{x_i}}(l)$ is the result of comparing x_i with the j-th member of the l-th sensing class which is computed by (10). Let h_1^l be the event that sensing report x_i belongs to class l and h_0^l be the event that sensing report x_i does not belong to class l. Furthermore, let E_ω^l be the event that ω elements in $\overrightarrow{y_{x_i}}(l)$ are greater than a threshold. Then the posterior probability $(P_{x_i}(l))$ that the current sensing report x_i belongs to class l is found as

$$P_{x_i}(l) = P\left(\frac{h_1^l}{E_\omega^l}\right) = \frac{P\left(h_1^l\right) P\left(E_\omega^l / h_1^l\right)}{\sum_{b \in [0,1]} P\left(h_b^l\right) P\left(E_\omega^l / h_b^l\right)}$$
$$= P\left(h_1^l\right) P\left(\frac{E_\omega^l}{h_1^l}\right). \quad (11)$$

Based on the posterior probability, the local decision for the i-th CR user at the r-th sensing slot, represented by $q_{i,r}$, is given as

$$q_{i,r} = \begin{cases} H_0 & P_0 > P_1 \\ H_1 & \text{otherwise} \end{cases} \quad (12)$$

where P_0 is the sum of posterior probabilities of sensing classes representing H_0 and is given as

$$P_0 = P_{x_i}\left(R_1\right) + P_{x_i}\left(R_3\right) + P_{x_i}\left(R_6\right) + P_{x_i}\left(R_8\right) \quad (13)$$

and P_1 is the sum of posterior probabilities of sensing classes representing H_1 and is given as

$$P_1 = P_{x_i}\left(R_2\right) + P_{x_i}\left(R_4\right) + P_{x_i}\left(R_5\right) + P_{x_i}\left(R_7\right). \quad (14)$$

4. Cooperative Spectrum Sensing

The FC receives the local decisions as D_i where $i = 1, 2, 3, \dots, N$. In CSS, the sensing capabilities of CR users are different from each other which results in different local

sensing results [40]. In the proposed scheme, we use a weight-based decision combination at the FC. Each CR user is assigned a weight based on its effectiveness.

A partial global decision at FC, represented by $L_{G,i}$, is made by excluding the result of the i-th CR user as

$$L_{G,i} = \begin{cases} H_0 & N^i_{H_0} > N^i_{H_1} \\ H_1 & \text{otherwise} \end{cases} \tag{15}$$

where $N^i_{H_0}$ is the number of CR users reporting H_0 excluding the local decision of the i-th CR user and is given as

$$N^i_{H_0} = \sum_{i=1,i\neq i}^{N} I_0 (D_i = H_0) \tag{16}$$

where $I_0(D_i = H_0)$ is indicator function for H_0 and is given by

$$I_0 (D_i = H_0) = \begin{cases} 1; & D_i = H_0 \\ 0; & D_i \neq H_0. \end{cases} \tag{17}$$

On the other hand, $N^i_{H_1}$ is the number of CR users reporting H_1 excluding the local decision of the i-th CR user and is given as

$$N^i_{H_1} = \sum_{i=1,i\neq i}^{N} I_0 (D_i = H_1) \tag{18}$$

where $I_0(D_i = H_1)$ is indicator function for H_1 and is given by

$$I_0 (D_i = H_1) = \begin{cases} 1; & D_i = H_1 \\ 0; & D_i \neq H_1. \end{cases} \tag{19}$$

Partial global decisions are found for all CR users. The local decisions are then combined through a majority rule as $L_{G,all}$ and can be expressed as

$$L_{G,all} = \begin{cases} H_0 & N_{H_0} > N_{H_1} \\ H_1 & \text{otherwise} \end{cases} \tag{20}$$

where N_{H_0} is the number of CR users reporting H_0 and N_{H_1} is the number of CR users reporting H_1. Based on (15) and (20), the weight for each CR user, α_i, is calculated as

$$\alpha_i = \begin{cases} \alpha_i + 1 & L_{G,i} \neq L_{G,all} \\ \alpha_i & L_{G,i} = L_{G,all}. \end{cases} \tag{21}$$

The cumulative weight for each hypothesis β_a where $a \in \{H_0, H_1\}$ is then calculated as

$$\beta_a = \sum_{i=1}^{N} \alpha_i I_0 (D_i = a) \quad a \in \{H_0, H_1\} \tag{22}$$

where $I_0(D_i = a)$ is given by

$$I_0 (D_i = a) = \begin{cases} 1; & D_i = a \\ 0; & \text{otherwise.} \end{cases} \tag{23}$$

The final global decision is denoted by L_G and is calculated as

$$L_G = \begin{cases} H_0 & \beta_{H_0} > \beta_{H_1} \\ H_1 & \text{otherwise.} \end{cases} \tag{24}$$

The global decision is returned to CR users and the CR users then transmit or stay silent according to the global decision.

Let $\beta = \sqrt{2\gamma \sum_{k=1}^{n} |h_k|^2 + 1}$ where h_k is the channel gain between the primary user and the i-th CR user during the k-th minislot and γ is the mean SNR as received from the PU. If it is assumed that the system's coefficients are known, then the system probability of false alarm under nonfading channels is given as [37]

$$P_f^S = Q \left(\beta Q^{-1} \left(\overline{P_d} \right) + \sqrt{N_0} \gamma \sum_{k=1}^{n} |h_k|^2 \right) \tag{25}$$

where $Q(.)$ is the complimentary distribution function of the standard Gaussian, i.e., $Q(\chi) = (1/2\pi) \int_{\chi}^{\infty} \exp(-t^2/2) dt$ and $\overline{P_d}$ is the system target probability of detection. The probability of detection and probability of false alarm of the proposed scheme depend both on the probability of the sensing report falling into a particular quantization zone and on the number of minislots in the sensing slot. The target probability of detection and target probability of false alarm are depended upon the number of quantization zones, the portability that under a particular hypothesis the sensing decision will fall in a particular quantization zone and the weight of each quantization zone. The quantization thresholds are adjusted such that the optimal quantization thresholds are found. On the basis of quantization parameters the target probabilities of detection and false alarm are optimized. For cooperative spectrum sensing the target probability of detection, if the weight of the quantization zones is considered the same, i.e., that each quantization zone contributes the same to the final decision combination, can be given as [41]

$$\overline{P_d} = \prod_{m=1}^{M} \left\{ \begin{pmatrix} N - \sum_{s=1}^{l} N_{Z_s} \\ N_{B_m} \end{pmatrix} \left(P_{H_1} (Z_m) \right)^{N_{Z_m}} \right\} \tag{26}$$

where N_{Z_m} is the number of CR users having the local sensing decision in zone Z_m, l is the largest integer less than m, and $P_{H_1}(Z_m)$ is the probability of having the local sensing decision in quantization zone Z_m under H_1.

The system probability of detection can be given as [37]

$$P_d^S = Q \left(\beta Q^{-1} \left(\overline{P_f} \right) + \sqrt{N_0} \gamma \sum_{k=1}^{n} |h_k|^2 \right) \tag{27}$$

where $\overline{P_f}$ is the system target probability of false alarm and is given by [41]

$$\overline{P_f} = \prod_{m=1}^{M} \left\{ \left(\begin{matrix} N - \sum_{s=1}^{l} N_{Z_s} \\ N_{B_m} \end{matrix} \right) \left(P_{H_0}\left(Z_m\right) \right)^{N_{Z_m}} \right\} \qquad (28)$$

and $P_{H_1}(Z_m)$ is the probability of having the local sensing decision in quantization zone Z_m under H_0.

5. Results and Analysis

In this section we observe the behavior of our proposed scheme and compare it to other schemes through system parameters such as probability of detection, probability of error, and probability of spectral holes exploitation. In [8], the effect of introducing multiple bits for reporting and sensing the spectrum multiple times within the same sensing phase was investigated where the scheme utilizing reporting multiple bits and multiple minislots was shown to be robust against all kind of attacks. Authors in [3, 37] have also shown the reliability gain which is brought by using multiple minislots. The number of CR users is 5, the number of iterations is 1000, the sensing slot duration is 1 ms, the sampling frequency is 300 kHz, and the number of energy samples in each sensing slot is 600. The idle probability of PU is 0.5. The SNR range is from -25 to -10 dB. When the number of CR users is large, clusters are formed for spectrum sensing to reduce the overhead. Authors in [42] considered clusters to sense the spectrum where the number of CR users in each cluster was five. That is, when cluster is considered, the CR users send their local decisions to a cluster-head to reduce the number of direct reports sent to the FC. To consider a higher number of CR users, the concept of cluster needs to be adopted. However, it is beyond the scope of the paper. However, according to [42] as the number of clusters and thus the number of CR users increase the sensing performance also improves. The idle probability is used as 0.5 in literature for the sake of fairness ([8, 42]). If the idle probability of PU is increased, it will provide higher opportunities of transmission to the CR user. Therefore, the idle probability of PU in the paper is taken as 0.5 for maintaining fairness among CR and PU systems. As the idle probability of PU is considered equal to that of probability of activity of the PU, the target detection probability for channel without fading is set to be 0.8 at SNR of -20 dB. The detection probability as is set in this paper with a higher active probability of the PU of 0.5 (the authors in [37] considered a low active probability of PU of 0.3) guarantees the protection of the PU data. We measure the performance of our proposed scheme in both the AWGN channels and also in fading channels by observing our scheme's behavior and also of other schemes behavior through varying SNR conditions for different system parameters. The training phase strongly impacts the system performance, as through this phase, the sensing classes are developed. The larger this phase, the greater the number of training instances, which means the current sensing report has more similar reports to match with. We plot the proposed scheme with two variants. In

one, the training phase is 100 iterations and in the other it is 330 iterations. These schemes are compared with a scheme in which the CR users make a one-bit local decision and the local decisions are combined at the FC by using a conventional OR rule.

In this paper, the probability of error (Pe) is given as

$$Pe = Pf \times P\left(H_0\right) + (1 - Pd) \times P\left(H_1\right) \qquad (29)$$

where Pd is the probability of detection, P_f is the probability of false alarm, $P(H_0)$ is the prior probability of H_0, and $P(H_1)$ is the prior probability of H_1. The probability of detection (Pd) is defined as

$$Pd = \frac{n_{(D_G=1 \,\&\&\, H=1)}}{n_{(D_G=1 \,\&\&\, H=1)} + \left(n_{(D_G=0 \,\&\&\, H=1)} \right)} \qquad (30)$$

and the probability of false alarm (P_f) is defined as

$$Pf = \frac{n_{(D_G=1 \,\&\&\, H=0)}}{n_{(D_G=1 \,\&\&\, H=1)} + \left(n_{(D_G=0 \,\&\&\, H=1)} \right)} \qquad (31)$$

where H is the real status of the PU and is equal to a randomly generated stream of ones and zeroes with size equal to the total number of iterations. A one represents the presence of the PU, while a zero represents absence of the PU. The notation $n_{(x \,\&\&\, y)}$ means the number of times the condition in the subscript is satisfied. The probability of spectral hole exploitation is represented by Pnf and can be expressed as

$$Pnf = 1 - Pf. \qquad (32)$$

Soft-decision combination gives the optimal sensing performance [4]. In [4], it is also shown that hard decision combination gives inferior results but only has one-bit overhead while soft combination incurs a lot of overhead. In one-bit hard combination scheme, sensing information was lost during local decision making because of using only one threshold. By using multiple thresholds, the sensing information loss can be reduced, which leads to better performance, and more overhead. In [7], it is also shown that using two bits for reporting the local decision can significantly improve the sensing performance. The effectiveness of using two bits (four quantization levels) was shown for both perfect and imperfect reporting channels. In [43], H. Sakran et al. utilized three bits to report the local decision to the FC. The performance improvement was shown to be better than using two bits for reporting local decision. In summary, it is obvious that trade-off exists between spectrum sensing performance and overhead when we design the quantization levels. Therefore, in the paper we mainly focus on applying machine learning algorithm into Smith-Waterman algorithm-based soft-decision spectrum sensing by considering the case of four quantization levels. To consider more quantization levels than 4 levels, the whole problem formulation such as the observations in Section 3.1 and the classification classes have to be changed and redesigned. Therefore, simulation results are bounded to the case of four quantization levels.

In the training phase the probability of detection of the proposed scheme is equal to that of majority rule which
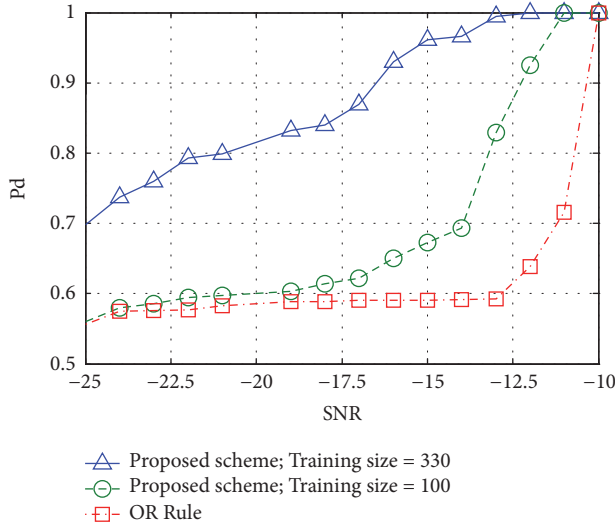
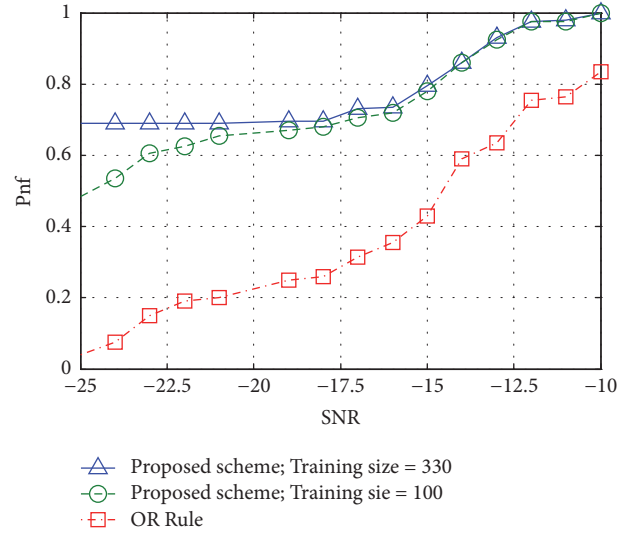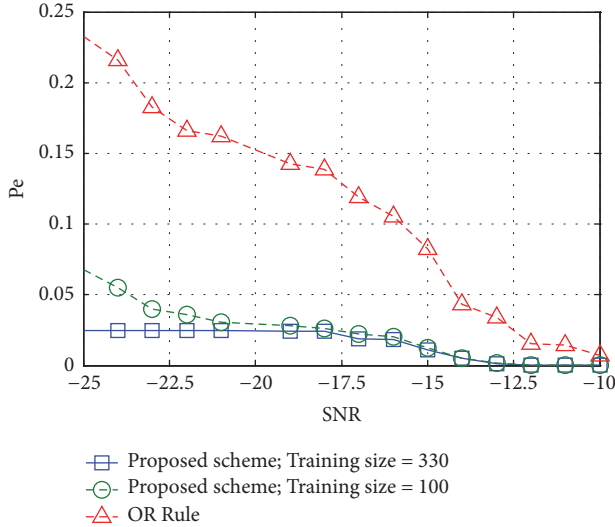FIGURE 6: System detection performance with nonfading channels.

FIGURE 7: System error performance with nonfading channels.

uses quantization. In machine learning technique, the performance of the proposed scheme is dependent upon the classification phase. In the simulations, the probability of detection is composed of those of both the training and classification phase. Similarly, training data in the proposed scheme is required to train the KNN classifier, and the performance of the classifier is depended on the training size of the data. The proposed scheme utilizes the majority rule to get training data. Since malicious users or anomalies are not considered in the paper, the majority rule works by majority voting and corresponding performance will be dependent upon local sensing decisions of the CR users. When the training phase is over, the classifier will have ample data available to the changing behavior of PU and will be trained.

Figure 6 shows the system detection performance in an AWGN channel. The proposed scheme with the larger training phase outperforms the other two schemes. The

FIGURE 8: System probability of exploiting spectral holes.

proposed scheme with a smaller training phase has the same detection performance as an OR rule in the low SNR regime. The reason is that the sensing reports in low SNR regimes do not have large distances from each other. The energies received under both hypotheses in the low SNR regime vary little from each other and thus, the scheme with fewer training instances fails to learn the environment more reliably. As the SNR improves, the proposed scheme with the smaller training phase results in more reliable spectrum sensing than conventional schemes. Figure 7 shows the error performance as calculated by (29). In this figure, it can also be seen that the proposed scheme with the larger training phase has a low probability of error even in the low SNR regime. The scheme with the smaller training phase converges to one with a larger training phase in better SNR conditions, which shows that even with a smaller training size the proposed scheme can result in more reliable spectrum sensing than conventional schemes.

Figure 8 shows the capability of the proposed scheme to exploit spectral holes which is defined by (28). Exploiting available opportunities for transmitting data is the highest priority from the perspective of a CR user. Even in bad SNR conditions our proposed scheme enables CR users to exploit data transmission opportunities. The proposed scheme with the smaller training phase lags behind the one with the larger training phase in bad SNR conditions but converges to the scheme with the larger training phase in good SNR regimes.

In the region of high SNR, the sensing reports which are formed are better reflections of the PU's activity. The sensing performance can be improved under the region of high SNR regimes since the PU signal will take larger portion of the received signal, compared to the added noise. That is to say, when SNR gets larger, a smaller number of training samples and further a smaller size of the training window are required to train the classifier. Therefore, when the SNR improves, a smaller training size results in the same performance. On the other hand, in the region of lower SNR, a larger training size
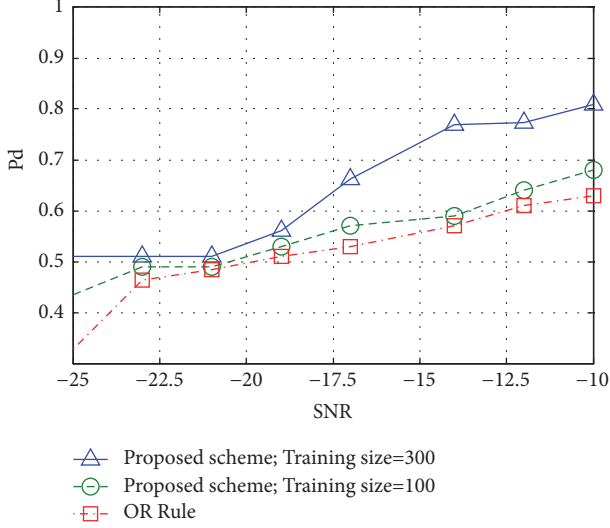
FIGURE 9: System detection performance with fading channels.
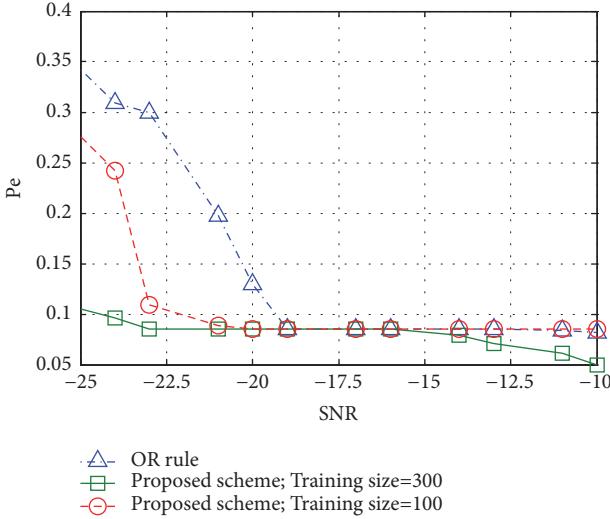

FIGURE 11: Effect of number of CR users.

FIGURE 10: System error performance with fading channels.

and a higher training size are needed to accurately reflect the PU's activity. All the three schemes show same performance trend but at different SNR levels. The OR rule has the best detection performance among conventional schemes, as it uses the most relaxed criteria for declaring, whether the PU is present or not out of all the conventional rules. However, this means that the OR rule cannot efficiently exploit data transmission opportunities. These figures show that our proposed scheme can protect PU data more effectively as well as provide more data transmission opportunities.

Figure 9 shows the detection performance of the proposed scheme in a fading environment. Fading affects the power of the received signal and thus the number of energy samples required to efficiently decide the status of the PU. In nonfading environment the amplitude gain of the channel is deterministic while in the fading channels the amplitude gain of the channel varies [17]. Thus the probability of

detection is dependent upon the instantaneous SNR. The effect of fading on performance of spectrum sensing was investigated in detail by [17]. Instead of following (2) and (3) for setting up a simulation environment, we have followed a path-loss model to incorporate fading as presented in [44]. We assume a path-loss model where the signal goes fading proportional to d^{α}, where d is the distance between the PU and the CR users and $\alpha = 3$. The average distance between the PU and CR users is assumed to be 20 m. The performance of our proposed scheme with the larger training phase outperforms the OR rule by 5% when the SNR is -23 dB, but when the SNR improves to -16 dB, the improvement is about 20%. The detection performance of the proposed scheme outperforms the OR rule by a larger margin when SNR conditions improve. As can be seen from the figure, the OR rule has a very poor detection performance in a fading environment despite the fact that it has the best detection performance among conventional fusion rules. Figure 10 shows the error performance of the proposed scheme in a fading environment. It can be seen that with increasing SNR, the error reduces. At -25 dB, the error probability is just above 0.1. Due to fading, the error probability of the OR rule is 0.35, which is very high compared to our proposed scheme.

Figure 11 shows the effect of the number of CR users on the performance of cooperative spectrum sensing under fading channels where some CR users undergo deep fading and thus have unreliable training data. To reflect the effect of increasing number of CR users fading conditions are required as in nonfading channels the performance with increasing the number of CR users remains the same because the training data of less CR users is also reliable and reflect the PU activity accurately. In the figure for each number of CR users the SNR is varied from -25 to -10 and then the mean of probabilities of detection is found. For instance, when the number of CR users is 6 the probability of detection for a multiple values of SNR varying between -25 and -15 is calculated and then the mean of the computed probabilities is the mean probability of detection. The mean probability of detection is represented by *Pmd*. As the values shown are mean values so the *Pmd*

cannot converge to 1. For each values of SNR the system is run 1,000 time for the proposed scheme having training size of 100 and 300 times for the proposed scheme having training size of 100. As can be seen as the number of CR users increases beyond a limit, in this case beyond 10 the improvement in mean probability of detection is not abrupt. That is because of the reasons explained in first paragraph of this section that to utilize the gain which can be introduced by increasing the number of CR users clusters need to be formed. When instead of cluster-heads the FC combines the sensing decisions of all CR users then the sensing decisions of many CR users may fall outside of the similarity distances range as calculated in Section 3.2.2 and thus their reports will be rejected. From Figure 11 it can be seen that the mean probability of detection of the proposed scheme with a larger training size surpasses the performance of the other schemes. A mean probability of detection when the number of users equals 20 reaches 0.8 which is target detection probability as we consider in this paper at SNR of -20 dB for nonfading channels when the number of CR users is 5 as we have considered in this paper. The proposed scheme reaches highest mean probability of detection of near 0.7 and the OR can achieve highest mean probability of detection of less than 0.6.

6. Conclusion

In this paper, a machine learning-based reliable spectrum sensing scheme is proposed. The proposed scheme learns from the environment by taking into account the true status of the PU. Sensing reports are stored in appropriate sensing classes and then the current sensing report is classified into one of the sensing classes. Based on the result of classification, the PU is declared present or absent. Local decisions are combined at the FC by a novel decision combination scheme that takes into account the reliability of the CR users. Mechanisms at both the CR level and the FC level ensure reliable spectrum sensing. Simulation results show that our proposed scheme has better detection performance and better spectral hole exploitation capability than the conventional OR rule. Fading affects detection performance, but our scheme detects successfully 80% of the times at -10 dB SNR even in a fading environment.

Data Availability

The simulations are carried out through Matlab.

Conflicts of Interest

The authors declare that there are no conflicts of interest regarding the publication of this paper.

Acknowledgments

References

[1] J. Mitola, *Cognitive Radio—An Integrated Agent Architecture for Software Defined Radio [Ph.D. thesis]*, KTH, Stockholm, Sweden, 2000.

[2] P. Kolodzy, "Spectrum policy task force," Rep. ET Docket 02-135, Federal Communications Commission, Washington, DC, USA, 2002.

[3] R. Fan and H. Jiang, "Optimal multi-channel cooperative sensing in cognitive radio networks," *IEEE Transactions on Wireless Communications*, vol. 9, no. 3, pp. 1128–1138, 2010.

[4] J. Ma, G. Zhao, and Y. Li, "Soft combination and detection for cooperative spectrum sensing in cognitive radio networks," *IEEE Transactions on Wireless Communications*, vol. 7, no. 11, pp. 4502–4507, 2008.

[5] S. Kyperountas, N. Correal, and Q. Shi, "A comparison of fusion rules for cooperative spectrum sensing in fading channels," *EMS Research, Motorola*, 2010.

[6] H. Guo, W. Jiang, and W. Luo, "Linear Soft Combination for Cooperative Spectrum Sensing in Cognitive Radio Networks," *IEEE Communications Letters*, vol. 21, no. 7, pp. 1573–1576, 2017.

[7] H. Sakran and M. Shokair, "Hard and softened combination for cooperative spectrum sensing over imperfect channels in cognitive radio networks," *Telecommunication Systems*, vol. 52, no. 1, pp. 61–71, 2013.

[8] H. A. Shah, M. Usman, and I. Koo, "Bioinformatics-inspired quantized hard combination-based abnormality detection for cooperative spectrum sensing in cognitive radio networks," *IEEE Sensors Journal*, vol. 15, no. 4, pp. 2324–2334, 2015.

[9] P. Kaligineedi and V. K. Bhargava, "Sensor allocation and quantization schemes for multi-band cognitive radio cooperative sensing system," *IEEE Transactions on Wireless Communications*, vol. 10, no. 1, pp. 284–293, 2011.

[10] R. Chen, J.-M. Park, and K. Bian, "Robust distributed spectrum sensing in cognitive radio networks," in *Proceedings of the 27th Conference on Computer Communications (INFOCOM '08)*, pp. 31–35, Phoenix, Ariz, USA, 2008.

[11] Z. Han, R. Zheng, and H. V. Poor, "Repeated auctions with Bayesian nonparametric learning for spectrum access in cognitive radio networks," *IEEE Transactions on Wireless Communications*, vol. 10, no. 3, pp. 890–900, 2011.

[12] J. Lundén, V. Koivunen, S. R. Kulkarni, and H. V. Poor, "Reinforcement learning based distributed multiagent sensing policy for cognitive radio networks," in *Proceedings of the 2011 IEEE International Symposium on Dynamic Spectrum Access Networks (DYSPAN)*, pp. 642–646, Aachen, Germany, 2011.

[13] M. Bkassiny, S. K. Jayaweera, and K. A. Avery, "Distributed Reinforcement Learning based MAC protocols for autonomous cognitive secondary users," in *Proceedings of the 20th Annual Wireless and Optical Communications Conference, (WOCC '11)*, Taiwan, 2011.

[14] A. Galindo-Serrano and L. Giupponi, "Distributed Q-learning for aggregated interference control in cognitive radio networks," *IEEE Transactions on Vehicular Technology*, vol. 59, no. 4, pp. 1823–1834, 2010.

[15] B. Y. Reddy, "Detecting Primary Signals for Efficient Utilization of Spectrum Using Q-Learning," in *Proceedings of the 2008 Fifth International Conference on Information Technology: New Generations (ITNG)*, pp. 360–365, Las Vegas, Nev, USA, 2008.

[16] Q. Zhu, Z. Han, and T. Başar, "No-Regret Learning in Collaborative Spectrum Sensing with Malicious Nodes," in *Proceedings of the 2010 IEEE International Conference on Communications*, pp. 1–6, Cape Town, South Africa, 2010.

[17] A. Ghasemi and E. S. Sousa, "Collaborative spectrum sensing for opportunistic access in fading environments," in *Proceedings of the 1st IEEE International Symposium on New Frontiers in Dynamic Spectrum Access Networks (DySPAN '05)*, pp. 131–136, Baltimore, Md, USA, November 2005.

[18] K. M. Thilina, K. W. Choi, N. Saquib, and E. Hossain, "Machine learning techniques for cooperative spectrum sensing in cognitive radio networks," *IEEE Journal on Selected Areas in Communications*, vol. 31, no. 11, pp. 2209–2221, 2013.

[19] M. Y. Kiang, "A comparative assessment of classification methods," *Decision Support Systems*, vol. 35, no. 4, pp. 441–454, 2003.

[20] K. M. Thilina, K. W. Choi, N. Saquib, and E. Hossain, "Pattern classification techniques for cooperative spectrum sensing in cognitive radio networks: SVM and W-KNN approaches," in *Proceedings of the 2012 IEEE Global Communications Conference, (GLOBECOM '12)*, pp. 1260–1265, Anaheim, Calif, USA, 2012.

[21] M. Tang, Z. Zheng, G. Ding, and Z. Xue, "Efficient TV white space database construction via spectrum sensing and spatial inference," in *Proceedings of the 34th IEEE International Performance Computing and Communications Conference, IPCCC 2015*, pp. 1–5, Nanjing, China, December 2015.

[22] A. M. Mikaeil, B. Guo, and Z. Wang, "Machine learning to data fusion approach for cooperative spectrum sensing," in *Proceedings of the 6th International Conference on Cyber-Enabled Distributed Computing and Knowledge Discovery, CyberC '14*, pp. 429–434, Shanghai, China, 2014.

[23] J. Kanti, G. S. Tomar, and A. Bagwari, "A novel multiple antennas based centralized spectrum sensing technique," in *Transactions on Computational Science*, vol. 10220 of *Lecture Notes in Computer Science*, pp. 64–85, Springer, Berlin, 2017.

[24] A. Bagwari, G. S. Tomar, and S. Verma, "Cooperative spectrum sensing based on two-stage detectors with multiple energy detectors and adaptive double threshold in cognitive radio networks," *Canadian Journal of Electrical and Computer Engineering*, vol. 36, no. 4, Article ID 6776586, pp. 172–180, 2013.

[25] J. Kanti, G. S. Tomar, and A. Bagwari, "An improved-two stage detection technique for IEEE 802.22 WRAN," *Optik - International Journal for Light and Electron Optics*, vol. 140, pp. 695–708, 2017.

[26] J. Kanti, G. S. Tomar, and D. Pham, "Improved sensing detector for wireless regional area networks," *Cogent Engineering*, vol. 4, no. 1, 2017.

[27] A. Samarah, G. S. Tomar, A. Bagwari, and J. Kanti, "Double Stage Energy Detectors for Sensing Spectrum in Cognitive Radio Networks," in *Proceedings of the 2015 Fifth International Conference on Communication Systems and Network Technologies (CSNT '15)*, pp. 181–184, Gwalior, India, 2015.

[28] A. Bagwari and G. S. Tomar, "Cooperative Spectrum Sensing with Multiple Antennas Using Adaptive Double-Threshold Based Energy Detector in Cognitive Radio Networks," *Journal of The Institution of Engineers (India): Series B*, vol. 95, no. 2, pp. 107–112, 2014.

[29] A. Bagwari and G. S. Tomar, "Comparison between Adaptive Double-Threshold Based Energy Detection and Cyclostationary Detection Technique for Cognitive Radio Networks," in *Proceedings of the 5th International Conference on Computational Intelligence and Communication Networks (CICN '13)*, pp. 182–185, Mathura, India, 2013.

[30] K. M. Thilina, K. W. Choi, N. Saquib, and E. Hossain, "Pattern classification techniques for cooperative spectrum sensing in cognitive radio networks: SVM and W-KNN approaches," in *Proceedings of the 2012 IEEE Global Communications Conference (GLOBECOM '12)*, pp. 1260–1265, Anaheim, Calif, USA, 2012.

[31] T. Mengyun, Z. Zheng, G. Ding, and Z. Xue, "Efficient TV white space database construction via spectrum sensing and spatial inference," in *Proceedings of the 2015 IEEE 34th International Performance Computing and Communications Conference (IPCCC '15)*, pp. 1–5, Nanjing, China, 2015.

[32] M. Jia, X. Gu, Q. Guo, W. Xiang, and N. Zhang, "Broadband hybrid satellite-terrestrial communication systems based on cognitive radio toward 5G," *IEEE Wireless Communications Magazine*, vol. 23, no. 6, pp. 96–106, 2016.

[33] M. Jia, X. Liu, X. Gu, and Q. Guo, "Joint cooperative spectrum sensing and channel selection optimization for satellite communication systems based on cognitive radio," *International Journal of Satellite Communications and Networking*, vol. 3, no. 2, pp. 139–150, 2015.

[34] M. Jia, X. Liu, Z. Yin, Q. Guo, and X. Gu, "Joint cooperative spectrum sensing and spectrum opportunity for satellite cluster communication networks," *Ad Hoc Networks*, vol. 58, pp. 231–238, 2017.

[35] W. Tan, M. Matthaiou, S. Jin, and X. Li, "Spectral Efficiency of DFT-Based Processing Hybrid Architectures in Massive MIMO," *IEEE Wireless Communications Letters*, vol. 6, no. 5, pp. 586–589, 2017.

[36] W. Tan, D. Xie, J. Xia, W. Tan, L. Fan, and S. Jin, "Spectral and Energy Efficiency of Massive MIMO for Hybrid Architectures Based on Phase Shifters," *IEEE Access*, vol. 6, pp. 11751–11759, 2018.

[37] Y.-C. Liang, Y. Zeng, E. Peh, and A. T. Hoang, "Sensing-throughput tradeoff for cognitive radio networks," *IEEE Transactions on Wireless Communications*, vol. 7, no. 4, pp. 1326–1337, 2008.

[38] K. Taniuchi, Y. Ohba, V. Fajardo et al., "IEEE 802.21: Media Independent Handover: Features, Applicability, and Realization," *IEEE Communications Magazine*, vol. 47, no. 1, pp. 112–120, 2009.

[39] T. F. Smith and M. S. Waterman, "Comparison of biosequences," *Advances in Applied Mathematics*, vol. 2, no. 4, pp. 482–489, 1981.

[40] M. Usman and K. Insoo, "Secure cooperative spectrum sensing via a novel user-classification scheme in cognitive radios for future communication technologies," *Symmetry*, vol. 7, no. 2, pp. 675–688, 2015.

[41] H. Birkan Yilmaz, T. Tugcu, and F. Alagoz, "Novel quantization-based spectrum sensing scheme under imperfect reporting channel and false reports," *International Journal of Communication Systems*, vol. 27, no. 10, pp. 1459–1475, 2014.

[42] H. Vu-Van and I. Koo, "A cluster-based sequential cooperative spectrum sensing scheme utilizing reporting framework for cognitive radios," *IEEJ Transactions on Electrical and Electronic Engineering*, vol. 9, no. 3, pp. 282–287, 2014.

[43] A. Ghasemi and E. S. Sousa, "Optimization of spectrum sensing for opportunistic spectrum access in cognitive radio networks," in *Proceedings of the 4th Annual IEEE Consumer Communications and Networking Conference*, pp. 1022–1026, Las Vegas, Nev, USA, 2007.

[44] F. Gabry, A. Zappone, R. Thobaben, E. A. Jorswieck, and M. Skoglund, "Energy Efficiency Analysis of Cooperative Jamming in Cognitive Radio Networks with Secrecy Constraints," *IEEE Wireless Communications Letters*, vol. 4, no. 4, pp. 437–440, 2015.

Research Article

Congestion-Optimal WiFi Offloading with User Mobility Management in Smart Communications

Bin Liu [iD],[1] **Qi Zhu** [iD],[1] **Weiqiang Tan**,[2] **and Hongbo Zhu** [iD] [1]

[1]*Jiangsu Key Laboratory of Wireless Communications, Nanjing University of Posts and Telecommunications, Nanjing 210003, China*
[2]*School of Computer Science and Educational Software, Guangzhou University, Guangzhou 510006, China*

Correspondence should be addressed to Hongbo Zhu; zhuhb@njupt.edu.cn

We study the WiFi offloading problem in smart communications and adaptively seek for the optimal offloading strategies with the consideration of the mobility management and the dynamical nature of network state. With users mobility management, we formulate the offloading ratio optimization problem based on Markov process. Then, we propose a novel Congestion-Optimal WiFi Offloading (COWO) algorithm based on subgradient method, which aims to obtain the optimal offloading ratio for each access point (AP) to maximize the throughput and minimize the network congestion. Due to the computational complexity of subgradient method, we further improve the COWO algorithm by the equivalent transformation. By viewing all the APs as one virtual WiFi network, we try to optimize the identical offloading ratio for virtual WiFi network and develop a Virtualized Congestion-Optimal WiFi Offloading (VCOWO) algorithm with lower complexity. Under the equivalent conditions, the performance of the VCOWO algorithm could well approximate the optimal results obtained by the COWO algorithm. It is found that the VCOWO algorithm could obtain the upper bound of multiple APs WiFi offloading performance. Moreover, we investigate the impacts of user mobility on the WiFi offloading performance. Simulation results show that the proposed algorithm could achieve higher throughput with lower network congestion compared with other current offloading schemes.

1. Introduction

With the proliferation of smart devices such as smartphones and tablets, cellular networks are facing an exponential growth of mobile data traffic. According to Cisco's forecast, global mobile data traffic is expected to grow to 49 megabytes per month by 2021, a sevenfold increase over 2016 [1–4]. With the limited licensed bandwidth, the cellular network capacity, however, can not keep up with the explosive data growth [5–9]. The mobile operators have been seeking for the cost-effective and timely solution to alleviate the cellular network. Thanks to the abundant unlicensed spectrum and large-scale WiFi deployment, Wireless Local Area Network (WLAN) has attracted much attention as a promising approach to offload data from the cellular network [10–13] and enhance network survivability and resilience in smart communications.

Previous works have demonstrated WiFi offloading prospects in leveraging traffic load [14–18]. The work in [18] proposed the on-the-spot offloading (OTSO) scheme

and showed that the OTSO offloading could leverage more than 65% traffic from the cellular network through an experiment in Seoul. Gass and Diot [19] further verified that the WiFi offloading is favorable even if the connecting time is insufficient. Much effort has also been seen in WiFi offloading schemes and performance analysis under the integrated cellular and WLAN networks framework [20]. The authors in [21] demonstrated that larger portions of cellular traffic could be offloaded to WiFi if the delay to wait for WiFi network is allowed during user movement. It presented the offloading scheme called Wiffler, which schedules the network access based on the historical access knowledge. By extracting typical users' mobility profiles, the work of [22] optimized the energy consumption in offloading. The authors in [23] studied the capacity of delayed offloading without prior knowledge of users' mobility patterns and proposed online scheduling policy to maximize the amount of offloaded data. By taking downloading cost and delay into the offloading decision, the delayed offloading scheme was

proposed in [24] to harvest maximum benefits from WiFi offloading. The optimal transmission deadline for delayed offloading was further derived in [25] and could achieve the maximum monetary incentive while maintaining the outage probability. The WiFi offloading and LTE WLAN Aggregation (LWA) was jointly considered in [26] to make the full use of the spectrum in the licensed and unlicensed carriers aggregation approach.

However, previously proposed schemes mainly focus on using WiFi offloading merely as a capacity-augment solution and try to offload as much data traffic to WiFi as possible, without systematically considering the dynamic nature of the network, which may result in the network congestion and degrade user's quality of experience (QoE). For instance, the OTSO scheme, which has been used as a default setting in most of the smartphones, enables users to handover and offload data through WiFi whenever users enter the network coverage. Rather than consider the load balance and network congestion in the WiFi network, this scheme simply decides the offloading by the availability of the network. It nevertheless increases the access conflicts and degrades the performance [27]. The network selection game was proposed in [28, 29] to analyze the offloading by jointly considering the network congestion and the cost of switching between different networks. The Pareto-efficiency of the equilibria in congestion game was proved in [30], and a client-centric network selection is further proposed to reduce the network congestion. Though the load balance and network congestion are considered, few of these works are involved in the optimal users offloading ratio during their movement or analyze the impacts of network congestion and user mobility on WiFi offloading.

In this paper, we investigate WiFi offloading with consideration of the network congestion and the user mobility management in smart communications and deduce the throughput and blocking probability based on Markov process. From the geometric deduction, the user flow equilibrium is observed, i.e., the rate of the users entering and leaving out of the network is equal, and thus we obtain the user flow rate between different networks. We optimize the ratio of users performing offloading when they move into the WiFi access points (APs), which aims to maximize the network throughput and minimize the network congestion. In this paper, the network congestion is characterized by the blocking probability. To obtain the optimal offloading ratio for each WiFi network, the Congestion-Optimal WiFi Offloading (COWO) algorithm is proposed based on the subgradient method. High computational complexity often occurs, especially in the dense APs deployed scenario. To this end, we make the nearly equivalent transformation and view all the WiFi networks as a virtual network. In this case, the Virtualized Congestion-Optimal WiFi Offloading (VCOWO) algorithm could well approximate to the optimal results under equivalent conditions. Moreover, the effects of users mobility on offloading effectiveness are demonstrated.

The rest of this paper is organized as follows. In Section 2, we describe the scenario of WiFi offloading in Section 2. We analyze the WiFi offloading performance and formulate the offloading optimization problem in Section 3. The

TABLE 1: Notations and definitions.

Notation	Definition
S_{tot}	Coverage of the cellular network
S_i	Coverage of the ith AP
M	The number of APs
D	Radius of cellular network coverage
d_i	Radius of ith AP coverage
λ	Total active users arriving rate
λ_c	Active users arriving rate in the cellular network
λ_i	Active users arriving rate in the ith AP
γ_c	Average user flow rate in the cellular network
γ_i	Average user flow rate in the ith AP
μ_c	Average service completing rate in the cellular network
μ_i	Average service completing rate in the ith AP
ω_c	Service arriving rate in the cellular network
ω_i	Service arriving rate in the ith AP
l_c	Service leaving rate in the cellular network
l_i	Service leaving rate in the ith AP
N_c	Average number of users in the cellular network
N_i	Average number of users in the ith AP
P_c^b	Blocking probability in the cellular network
P_i^b	Blocking probability in the ith AP
T_c	Throughput in the cellular network
T_i	Throughput in the ith AP
C_u	Total number of channels in the cellular network
C_i	Total number of channels in the ith AP
v	Average velocity of user mobility
p_i	Offloading probability in ith AP
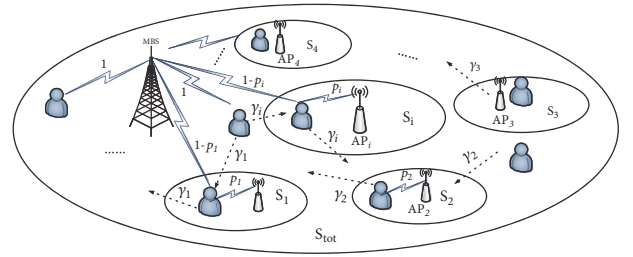
FIGURE 1: WiFi offloading scenario.

Congestion-Optimal WiFi Offloading algorithm is proposed in Section 4. With equivalent conditions, we develop the Virtualized Congestion-Optimal WiFi offloading algorithm in Section 5. We present the numerical results in Section 6 and draw conclusions in Section 7. The symbols used throughout the paper are summarized in Table 1.

2. System Model

We describe the WiFi offloading scenario under the integrated cellular and WLAN networks framework [31–34] in Figure 1, where the MO can tightly integrate the WiFi networks with the cellular networks through the recent IEEE and 3rd Generation Partnership Project (3GPP) standards.

For example, the network discovery and selection functionality (ANDSF) reports the network information related to the access network type, roaming consortium, and venue information through management frames to the macro base station (MBS) [28]. Then, the MBS decides and schedules the user offloading based on the reported information. In this paper, we consider that the MBS covers the whole scenario, with M WiFi APs randomly distributed in its coverage without overlapping with each other. The active users, defined as the users need network service at this moment, are assumed to have arriving rate λ with Poisson arrivals, and the active users follow the uniform distribution on the geometry coverage; i.e., the active user arriving rate for each network is proportional to their coverage, and the active user arriving rates for ith AP and cellular networks are λ_i, $i = 1, 2, \ldots, M$, and λ_c, respectively,

$$\lambda_i = \lambda \frac{S_i}{S_{tot}},$$

$$\lambda_c = \lambda \frac{S_{tot} - \sum_{i=1}^{N} S_i}{S_{tot}}, \tag{1}$$

where S_{tot} and S_i are the coverage area of the scenario and ith AP, respectively.

The user mobility management is considered, and the offloading ratio in user mobility is further investigated in this paper. With circular coverage, the user flow rates under fluid flow model and geometric angle mobility model were separately deduced in [35–38], and it is proved that the rate of the users entering and leaving the network is equal, which is called user flow equilibrium. With user mobility probability density function $f_V(v)$, we have the user flow rate as

$$\gamma = 2\rho d \int_{-\infty}^{+\infty} v f_V(v) \, dv = \frac{2NE(v)}{\pi d}, \tag{2}$$

where N is the number of users in the network, d is the radius of the network coverage, and $E(v)$ denotes the first moment of v. We start the analysis of user flow rate with the assumptions as follows:

(1) All the networks have circular geometric coverage.

(2) User moves within the coverage area with the random direction; i.e., the angle of direction is uniformly distributed in $[0, 2\pi]$.

(3) The user's mobility is in uniform linear motion; i.e., $E(v) = v$.

The user flow rate can be written as follows [37]:

$$\gamma = \frac{2NE(v)}{\pi d} = \frac{2Nv}{\pi d}. \tag{3}$$

To be specific, for the ith AP with radius d_i and MBS with radius D, we have the user flow rate separately:

$$\gamma_i = \frac{2N_i v}{\pi d_i},$$

$$\gamma_c = \frac{2N_c v}{\pi D}, \tag{4}$$
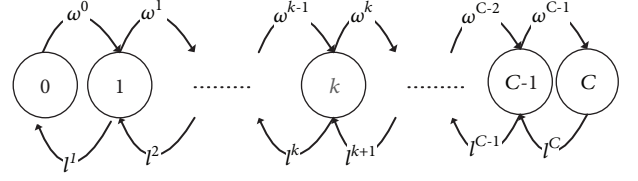
Figure 2: Markov state transition.

where N_i and N_c are the numbers of active user in ith AP and MBS.

We formulate the WiFi offloading model based on the discrete Markov process [39–41]. The occupation of network channel is described as a discrete Markov state, the service arriving means that the user enters the network service sequence, and service leaving means that the user cuts off the network service. Each user could access one channel at the same time. The maximum number of users served by the network is constrained by the number of channels C. Let ω^k denote the state transmission rate from the kth state to the $(k+1)$th state $0 \le k \le C - 1$, and l^u is the state transition rate of uth state to the $(u-1)$th state, $1 \le u \le C$, as shown in Figure 2. And we have the steady distribution as

$$\omega^{k-1}\pi^{k-1} + l^{k+1}\pi^{k+1} = \left(\omega^k + l^k\right)\pi^k, \quad 0 < k < C$$

$$\mu^{k+1}\pi^{k+1} = \omega^k\pi^k, \quad k = 0$$

$$\omega^{k-1}\pi^{k-1} = \mu^k\pi^k, \quad k = C \tag{5}$$

$$\sum_{k=0}^{C} \pi^k = 1,$$

where π^k is the steady-state probability distribution for the kth state, and

$$\pi^k = \frac{\left(\prod_{m=0}^{k-1}\omega^m / \prod_{x=1}^{k} l^x\right)}{\left(1 + \sum_{m=1}^{C}\left(\prod_{n=0}^{m-1}\omega^n / \prod_{x=1}^{m} l^x\right)\right)}. \tag{6}$$

We try to find the optimal offloading ratio p_i, aiming to maximize the network throughput and minimize the network congestion at both networks when the users enter into the ith AP's coverage area. With offloading ratio p_i, the serve arriving rates at ith AP ω_i and MBS ω_c are defined as

$$\omega_i = \lambda_i + p_i\gamma_i,$$

$$\omega_c = \lambda_c + \gamma_c, \tag{7}$$

where the first term denotes the newly active users in their own coverage, and the second term denotes the service increase by the users flow in their mobility. Note that only p_i of the users will be offloaded to the WiFi network when entering, while all the users moving out of the AP's coverage will be immediately handed over to the cellular network. Assume the average service completing rate in WiFi and

cellular network is μ_i and μ_c, respectively; the service leaving rates for ith AP l_i and MBS l_c are

$$l_i = N_i \mu_i + \gamma_i,$$

$$l_c = N_c \mu_c + \sum_{i=1}^{M} p_i \gamma_i, \tag{8}$$

where the first part is by the user finishing their transmission and turning to inactive, and the second part is by the user moving out of the network coverage, and handover to another network. Only p_i of the users could be accepted by the ith AP, i.e., only p_i of the users flowing out of the cellular network could leave the MBS service sequence, and the rest of users are still kept in service in the cellular network.

In this paper, we try to optimize the offloading ratio for multiple APs, which aims to increase the throughput and reduce the network congestion. On the one hand, it is an incentive to offload more user to leverage the cellular traffic load and to increase the throughput. On the other hand, the increase of offloading will nevertheless result in the conflicts and degrade the performance. Therefore, the offloading ratio should be carefully designed with the consideration of the network congestion and the user mobility.

3. Problem Formulation

In this section, we analyze the WiFi offloading performance from both cellular and WiFi network sides based on the Markov process and model the network congestion, which is characterized by the blocking probability. Then, we define the system utility as the function of throughput and blocking probability and formulate the offloading ratio optimization problem.

3.1. WiFi Network. First, we analyze the ith AP network with C_i channels in total. From (8), the steady-state probability distribution of ith AP is

$$\pi_i^j = \frac{\left(\sum_{m=0}^{C_i} \left((\xi_i)^m / m! \right) \right)^{-1} (\xi_i)^j}{j!}, \quad 0 \leq j \leq C_i, \tag{9}$$

where

$$\xi_i = \frac{\omega_i}{l_i / N_i} = \frac{\lambda_i + p_i \gamma_i}{\mu_i + \gamma_i / N_i} = \frac{\lambda_i + p_i \gamma_i}{\mu_i + 2v/(\pi d_i)}. \tag{10}$$

Thus, we have the number of users served by the ith AP N_i as the average queue length, and

$$N_i = N_i (\xi_i, C_i) = E(k \mid C_i) = \sum_{k=0}^{C_i} k \cdot \pi_i^k$$

$$= \xi_i \cdot \left\{ 1 - \frac{\left(\sum_{k=0}^{C_i} \left((\xi_i)^k / k! \right) \right)^{-1} (\xi_i)^{C_i}}{C_i!} \right\}. \tag{11}$$

In [42], the blocking probability P_i^b and nonblocking probability P_i^{ub} for the ith AP are defined as

$$P_i^b = 1 - P_i^{ub} = \frac{\left(\sum_{m=0}^{C_i} \left((\xi_i)^m / m! \right) \right)^{-1} (\xi_i)^{C_i}}{C_i!} = P(\xi_i), \tag{12}$$

where $P(\xi_i)$ denotes the fact that the blocking probability depends on the ratio of service arriving and leaving rate ξ_i in (10). Then, the average user number N_i can be rewritten as

$$N_i = N_i (\xi_i, C_i) = \xi_i \left(1 - P_i^b \right) = \xi_i P_i^{ub}. \tag{13}$$

With the average user number N_i in (13), the user flow rate can be expressed as

$$\gamma_i = \frac{2 N_i (\xi_i, C_i) v}{\pi d_i} = \frac{2 \xi_i v P_i^{ub}}{\pi d_i}$$

$$= \frac{2 v P_i^{ub}}{\pi d_i} \cdot \frac{\lambda_i + p_i \gamma_i}{\mu_i + 2v/(\pi d_i)}. \tag{14}$$

After modification, it is observed that the user flow rate γ_i is the function of blocking probability, which is denoted as $\phi(P_i^b)$, and we have

$$\gamma_i = \frac{2 v \lambda_i P_i^{ub}}{\pi d_i \mu_i + 2v \left(1 - p_i P_i^{ub} \right)} = \phi\left(P_i^b \right). \tag{15}$$

With the user flow rate in (15), we have the blocking probability P_i^b in its implicit function form $P_i^b = \varphi(P_i^b)$ as

$$P_i^b = P(\xi_i)\big|_{\xi_i = (\lambda_i + p_i \gamma_i)/(\mu_i + 2v/(\pi d_i))}$$

$$= \frac{\left(\left(\lambda_i + p_i \phi\left(P_i^b \right) \right) / \left(\mu_i + 2v/(\pi d_i) \right) \right)^{C_i} / C_i!}{\sum_{k=0}^{C_i} \left(\left(\left(\lambda_i + p_i \phi\left(P_i^b \right) \right) / \left(\mu_i + 2v/(\pi d_i) \right) \right)^k / k! \right)}, \tag{16}$$

where the second equation is denoted as $\varphi(P_i^b)$. Clearly, P_i^b is the root of $\psi(x)$ that holds

$$\psi(x) = x - \varphi(x) = x - P(\xi_i)\big|_{\xi_i = (\lambda_i + p_i \phi(x))/(\mu_i + 2v/(\pi d_i))}$$

$$= 0, \tag{17}$$

and it could be solved by the bisection method.

Proof. See Appendix A. □

From (16), it is also found that the P_i^b depends on the offloading ratio p_i, i.e., $P_i^b = h_i(p_i)$, and we thus have the user flow rate in the form of a function of p_i

$$\gamma_i = \frac{2 v \lambda_i \left(1 - h(p_i) \right)}{\pi d_i \mu_i + 2v \left(1 - p_i + p_i h(p_i) \right)} = \gamma_i(p_i). \tag{18}$$

Then, the throughput achieved under the offloading probability p_i in the ith AP is for simplicity; we normalize the achievable data rate of per channel in the ith AP network as R_i, and the throughput can be expressed as

$$T_i(p_i) = R_i N_i (\xi_i, C_i)$$

$$= R_i \left(1 - h_i(p_i) \right) \frac{\lambda_i + p_i \gamma_i(p_i)}{\mu_i + 2v/(\pi d_i)}. \tag{19}$$

3.2. Cellular Network.

The analysis of the cellular network follows the similar approaches in the WiFi network. Consider the cellular network with total C_u channels, and the steady-state probability distribution of the cellular network is expressed as

$$\pi_c^u = \frac{(\xi_c)^u}{\left(\sum_{m=0}^{C_u} \left((\xi_c)^m / m!\right)\right) u!}, \quad 0 \le u \le C_u, \quad (20)$$

where

$$\xi_c = \frac{\lambda_c + \gamma_c}{\mu_c + \sum_{i=1}^{M} (p_i \gamma_i / N_c)}. \quad (21)$$

The length of service queue is equal to the average number of users N_c served by the cellular network,

$$N_c(\xi_c) = E(u) = \sum_{u=0}^{C_u} u \cdot \pi_c^u$$

$$= \xi_c \left\{ 1 - \frac{\left(\sum_{m=0}^{C_u} \left((\xi_c)^m / m!\right)\right)^{-1} (\xi_c)^{C_u}}{C_u!} \right\} \quad (22)$$

$$= \xi_c \left(1 - P_c^b\right) = \xi_c P_c^{ub},$$

where P_c^b and P_c^{ub} are defined the blocking probability and nonblocking probability in the cellular network as (13):

$$P_c^b = 1 - P_c^{ub} = \frac{(\xi_c)^{C_u}}{\left(\sum_{m=0}^{C_u} \left((\xi_c)^m / m!\right)\right) C_u!} = P_c(\xi_c), \quad (23)$$

where $P(\xi_c)$ denotes that the blocking probability depending on the ratio of service arriving and leaving rate ξ_c.

Fixing the average user number N_c in (22), the user flow rate γ_c can be expressed as the function of blocking probability, which is denoted as $\phi_c(P_c^b)$,

$$\gamma_c = \frac{N_c(\xi_c) \nu}{\pi D} = \frac{2\nu \left(P_c^{ub} \lambda_c - \sum_{i=1}^{M} p_i \gamma_i\right)}{\left(\pi D \mu_c - 2 P_c^{ub} \nu\right)} = \phi_c\left(P_c^b\right). \quad (24)$$

With the user flow rate in (24), we have the blocking probability P_c^b in its implicit function form,

$$P_c^b = P_c(\xi_c)\big|_{\xi_c = (\lambda_i + \phi_c(P_c^b))/(\mu_c + \sum_{i=1}^{M} (p_i \gamma_i / N_c))} = \varphi_c\left(P_c^b\right). \quad (25)$$

Similar to (16), P_c^b could be obtained through solving (25) by the bisection method. From (25), it is also found that the P_c^b depends on the offloading ratio for each AP p_i, $i = 1, 2, M$; i.e., P_c^b is the function of vector composed by p_i, $P_c^b = g(\overrightarrow{\mathbf{p}})$, $\overrightarrow{\mathbf{p}} = [p_1, p_2, \ldots, p_i, \ldots, p_M]$. Thus, the user flow rate γ_c also has the formation of the function of offloading ratio vector $\overrightarrow{\mathbf{p}}$ as

$$\gamma_c = \frac{2\nu \left\{[1 - g(\overrightarrow{\mathbf{p}})] \lambda_c - \sum_{i=1}^{M} p_i \gamma_i\right\}}{\left[\pi D \mu_c - 2[1 - g(\overrightarrow{\mathbf{p}})] \nu\right]} = \gamma_c(\overrightarrow{\mathbf{p}}). \quad (26)$$

The throughput of the cellular network is similarly given:

$$T_c\left(\overrightarrow{\mathbf{p}}\right) = R_i\left(1 - g\left(\overrightarrow{\mathbf{p}}\right)\right)$$

$$\cdot \frac{\pi D \left\{\left(1 - g\left(\overrightarrow{\mathbf{p}}\right)\right) \lambda_c - \sum_{i=1}^{M} p_i \gamma_i\right\}}{\left(1 - g\left(\overrightarrow{\mathbf{p}}\right)\right) \cdot \left[\pi D \mu_c - 2\nu \left(1 - g\left(\overrightarrow{\mathbf{p}}\right)\right)\right]}, \quad (27)$$

where R_c is the normalized channel rate of the cellular network.

3.3. Congestion Optimization Problem.

In this paper, we seek for the optimal offloading ratio for multiple APs in user mobility, which aims to maximize the throughput and minimize the network congestion. The throughput is the sum of all networks, i.e., $T(\overrightarrow{\mathbf{p}}) = \sum_{i=1}^{M} T_i(p_i) + T_c(\overrightarrow{\mathbf{p}})$, and the network congestion is characterized by the blocking probability, i.e., $B(\overrightarrow{\mathbf{p}}) = \sum_{i=1}^{M} P_i^b + P_c^b$. Thus, we set the system utility function $Q(\overrightarrow{\mathbf{p}})$ so that it increases with the throughput and decreases with the network congestion, where the blocking probability acts as a penalty for network congestion. The constant β is defined as weight over the throughput and blocking probability, which embodies the s sensitivity to network congestion. The system utility function could be formulated as

$$\max_{\overrightarrow{\mathbf{p}}} \quad Q\left(\overrightarrow{\mathbf{p}}\right) = T\left(\overrightarrow{\mathbf{p}}\right) - \beta B\left(\overrightarrow{\mathbf{p}}\right)$$

$$= \sum_{i=1}^{M} R_i N_i\left(\xi_i, C_i\right) + R_c N_c\left(\xi_c\right)$$

$$- \beta \left(\sum_{i=1}^{M} P_i^b + P_c^b\right) \quad (28)$$

$$\text{s.t.} \quad \overrightarrow{\mathbf{p}} = [p_1, p_2 \ldots p_i \ldots p_M],$$

$$0 \le p_1 \ldots p_i \ldots p_M \le 1$$

4. Congestion-Optimal WiFi Offloading

In this section, we proposed the COWO algorithm to obtain the optimal offloading ratio p_i for each AP, which is based on subgradient method [43] and further reveal the impacts of user mobility on WiFi offloading performance.

4.1. Congestion-Optimal WiFi Offloading Algorithm.

The optimization problem in (28) is convex function with the convex feasible region. Thus, the subgradient method can be used to solve the optimization problem.

Proof. See Appendix B and Appendix C. □

The augmented Lagrangian function of optimization problem (28) is written as

$$\max \quad L\left(\overrightarrow{\mathbf{p}}, \nu\right)$$

$$= \sum_{i=1}^{M} \left[\left(1 - P_i^b\right) \frac{\lambda_i + p_i \gamma_i(p_i)}{\mu_i + 2\nu / (\pi d_i)} - \beta P_i^b\right]$$

$$+ \frac{\pi D \left(P_c^{ub} \lambda_c - \sum_{i=1}^{M} p_i \gamma_i \right)}{\pi D \mu_c - 2v P_c^{ub}} - \beta P_c^b$$

$$- \sum_{i=1}^{M} v_i \left(p_i - 1 \right)$$

$$\text{s.t.} \quad p_1 \ldots p_i \ldots p_M \geq 0,$$

$$v_i > 0, \tag{29}$$

where v_i is the Lagrange multiplier. The Lagrange problem in (29) could be solved in subgradient method, and the optimal $\overrightarrow{\mathbf{p}}$ satisfies

$$\frac{\partial L \left(\overrightarrow{\mathbf{p}}, \alpha \right)}{\partial \overrightarrow{\mathbf{p}}}$$

$$= \left[\frac{\partial L \left(\overrightarrow{\mathbf{p}}, \alpha \right)}{\partial p_1} \quad \frac{\partial L \left(\overrightarrow{\mathbf{p}}, \alpha \right)}{\partial p_2} \quad \cdots \quad \frac{\partial L \left(\overrightarrow{\mathbf{p}}, \alpha \right)}{\partial p_M} \right]^T \tag{30}$$

$$= \overrightarrow{\mathbf{0}},$$

where the ith element in the partial derivatives of p_i can be calculated as (31), as shown below.

$$\frac{\partial L \left(\overrightarrow{\mathbf{p}}, v \right)}{\partial p_i} = \left[R_i \left(1 - P_i^b \left(1 + C_i - \xi_i P_i^{ub} \right) \right) \right.$$

$$\left. - \frac{\beta_i P_i^b \left(C_i - \xi_i P_i^{ub} \right)}{\xi_i} \right] \frac{\partial \xi_i}{\partial p_i}$$

$$+ \left[R_i \left(1 - P_c^b \left(1 + C_u - \xi_c P_c^{ub} \right) \right) \right. \tag{31}$$

$$\left. - \frac{\beta_c P_c^b \left(C_u - \xi_c P_c^{ub} \right)}{\xi_c} \right] \frac{\partial \xi_c}{\partial p_i} + v_i.$$

Equation (30) is nonlinear. Thus, we make the transformation to simplify the calculation. The partial derivative of p_i is written as

$$\frac{\partial L \left(\overrightarrow{\mathbf{p}}, v \right)}{\partial p_i} = \gamma_i W^i - v_i \tag{32}$$

where

$$W^i = \frac{R_i}{\gamma_i} \frac{\partial N_i \left(\xi_i, C_i \right)}{\partial \xi_i} \frac{\partial \xi_i}{\partial p_i} + \frac{R_i \beta}{\gamma_i} \frac{\partial P_i^{ub}}{\partial \xi_i} \frac{\partial \xi_i}{\partial p_i}$$

$$+ \frac{R_c}{\gamma_i} \frac{\partial N_c \left(\xi_c \right)}{\partial \xi_c} \frac{\partial \xi_c}{\partial p_i} + \frac{R_c \beta}{\gamma_i} \frac{\partial P_c^{ub}}{\partial \xi_c} \frac{\partial \xi_c}{\partial p_i} > 0. \tag{33}$$

To achieve the identity $\partial L(\overrightarrow{\mathbf{p}}, v)/\partial \overrightarrow{\mathbf{p}} = \overrightarrow{\mathbf{0}}$, $v_i = \gamma_i W^i$ for $i = 1, 2 \ldots M$. Thus, we have

$$W^1 = \cdots = W^M = \chi, \tag{34}$$

where $\chi = v_i / \gamma_i$, and the augmented Lagrangian function in (28) can be written as

$$\max \quad L \left(\overrightarrow{\mathbf{p}}, \chi \right)$$

$$= \sum_{i=1}^{M} \left[\left(1 - P_i^b \right) \frac{\lambda_i + p_i \gamma_i \left(p_i \right)}{\mu_i + 2v / \left(\pi d_i \right)} - \beta_i P_i^b \right]$$

$$+ \frac{\pi D \left(P_c^{ub} \lambda_c - \sum_{i=1}^{M} p_i \gamma_i \right)}{\pi D \mu_c - 2v P_c^{ub}} - \beta_c P_c^b \tag{35}$$

$$- \chi \sum_{i=1}^{M} v_i \left(p_i - 1 \right) \quad \chi > 0$$

$$\text{s.t.} \quad p_1 \ldots p_i \ldots p_M \geq 0.$$

Then, χ could be updated with pace ϑ, and we have

$$\chi^{(k+1)} = \left[\chi^{(k)} + \vartheta_i^{(k)} \sum_{i=1}^{M} v_i \left(p_i - 1 \right) \right]^+. \tag{36}$$

The following parts give the update process in detail. For ith AP, the service arriving rate is $\omega_i = \lambda_i + p_i \gamma_i$, and $\lambda_i \leq \omega_i \leq \lambda_i + \gamma_i$. It is observed from (37) that W^i is dependent on ω_i, and thus we define the function $f_i(\omega_i)$

$$\frac{\partial L \left(\overrightarrow{\mathbf{p}}, \chi \right)}{\partial p_i} = \gamma_i \left(W^i - \chi \right) = f_i \left(\omega_i \right). \tag{37}$$

It can be proved that the $f_i(\omega_i)$ is a decreasing function of ω_i by the partial derivative deduction. Thus, if the zero point of $f_i(\omega_i)$ exists, it can be obtained by the bisection method. Let us denote the zero point of $f_i(\omega_i)$ as ω_i^*. If $f_i(\omega_i)$ does not have zero points, we modify it as

$$\omega_i^* = \begin{cases} \omega_i, & \exists \omega_i \in [\lambda_i, \lambda_i + \gamma_i] \cap f_i \left(\omega_i \right) = 0 \\ \lambda_i, & \forall \omega_i \in [\lambda_i, \lambda_i + \gamma_i] \cap f_i \left(\omega_i \right) > 0 \\ \lambda_i + \gamma_i, & \forall \omega_i \in [\lambda_i, \lambda_i + \gamma_i] \cap f_i \left(\omega_i \right) < 0. \end{cases} \tag{38}$$

If $\forall \omega_i \in [\lambda_i, \lambda_i + \gamma_i]$, $f_i(\omega_i) > 0$, the offloading ratio p_i is obtained by

$$p_i \gamma_i = \omega_i^* - \lambda_i, \quad i = 1, 2 \ldots M. \tag{39}$$

When $\forall \omega_i \in [\lambda_i, \lambda_i + \gamma_i]$, $f_i(\omega_i) < 0$, the offloading ratio is modified as

$$p_i^* = \begin{cases} p_i, & \exists p_i \in [0, 1] \cup \dfrac{\partial L \left(\overrightarrow{\mathbf{p}}, \alpha \right)}{\partial p_i} = 0 \\[2mm] 0, & \forall p_i \in [0, 1] \cup \dfrac{\partial L \left(\overrightarrow{\mathbf{p}}, \alpha \right)}{\partial p_i} > 0 \\[2mm] 1, & \forall p_i \in [0, 1] \cup \dfrac{\partial L \left(\overrightarrow{\mathbf{p}}, \alpha \right)}{\partial p_i} < 0. \end{cases} \tag{40}$$

Based on the subgradient method, the implementation of the proposed COWO algorithm is provided as in Algorithm 1.

1: Initialize: $\overrightarrow{\mathbf{p}}^{(0)} = [p_1^0, p_2^0 \ldots p_M^0] = [0, 0 \ldots 0] = \overrightarrow{\mathbf{0}}, \vartheta_i^{(0)} = 1, k = 0$
2: **while** $|\chi^{(k+1)} - \chi^k| \geq \varepsilon$ **do**
3:     Calculate P_i^b for $1 \leq i \leq M$ and P_c^b under the initial $\overrightarrow{\mathbf{p}}^{(k)}$ in the bisection method
4:     Get initial updating factor $\chi^{(0)} = \left[(1/M)\sum_{i=1}^M W^i\right]^+$
5:     Solve equation (37) and get ω_i^*
6:     Update ω_i by (38)
7:     Solve out $\overrightarrow{\mathbf{p}}^{(k)}$
8:     Set $k = k + 1$ and update $\chi^{(k+1)}$ according to (36)
9:     Iterate $\overrightarrow{\mathbf{p}}^{(k)}$ into $\overrightarrow{\mathbf{p}}^{(k+1)}$
10: **end while**
11: Set the optimal offload factor vector $\overrightarrow{\mathbf{p}}^* = \overrightarrow{\mathbf{p}}^{(k+1)}$

ALGORITHM 1: The proposed COWO algorithm.

4.2. Impacts of User Mobility on WiFi Offloading. In this section, we study the impacts of user mobility, mainly characterized by average velocity, on the WiFi offloading. First, we show its impacts on WiFi offloading throughput. The derivatives of throughput T_i with respect to v are

$$\frac{\partial T_i}{\partial v} = R_i \frac{\partial N_i(\xi_i, C_i)}{\partial v} = R_i \frac{\partial \xi_i}{\partial v}\left(1 - P_i^b - \xi_i \frac{\partial P_i^b}{\partial \xi_i}\right)$$
$$= R_i \frac{\partial \xi_i}{\partial v}\left(1 - P_i^b\left(C_i + 1 - \xi_i P_i^{ub}\right)\right). \tag{41}$$

From (10) and (11), ξ_i can be expressed as

$$\xi_i = \frac{\lambda_i + 2p_i N_i(\xi_i, C_i) v/(\pi d_i)}{\mu + 2v/(\pi d_i)}, \tag{42}$$

and we take the derivatives ξ_i of v, and we have

$$\frac{\partial \xi_i}{\partial v} = 2\frac{vp_i\left(\partial N_i(\xi_i, C_i)/\partial v\right) + p_i N_i(\xi_i, C_i)}{\pi d_i\left(\mu + 2v/\pi d_i\right)}$$
$$- \frac{\left(\lambda_i + 2p_i N_i(\xi_i, C_i) v/\pi d_i\right)\left(\mu + 2v/\pi d_i\right)^{-1}}{\pi d_i\left(\mu + 2v/\pi d_i\right)}. \tag{43}$$

Thus, the derivatives of throughput T_i with respect to v could be rewritten as

$$\frac{\partial T_i}{\partial v} = 2R_i\left(1\right.$$
$$- \left(1 - P_i^b\left(C_i + 1 - \xi_i P_i^{ub}\right)\right)\frac{2vp_i/(\pi d_i)}{\mu + 2v/(\pi d_i)}\right)^{-1} \tag{44}$$
$$\cdot \left.\left(\frac{p_i N_i(\xi_i, C_i) - \xi_i}{\pi d_i\left(\mu + 2v/(\pi d_i)\right)}\right)\left(1 - P_i^b\left(C_i + 1 - \xi_i P_i^{ub}\right)\right)\right),$$

where the details about the computation and the associated analysis can be found in the literature [44–46]. With the fact that $N_i(\xi_i, C_i) = \xi_i P_i^{ub} < \xi_i$ and the deduction in Appendix A and B, we have

$$0 < 1 - P_i^b\left(C_i + 1 - \xi_i P_i^{ub}\right) < 1. \tag{45}$$

Therefore, $\partial T_i/\partial v < 0$, which draws the conclusion that the average throughput for each network T_i is decreasing with the velocity v. It is also observed that ξ_i decreases with v. Furthermore, the blocking probability P_i^b has

$$\frac{\partial P_i^b}{\partial v} = \frac{P_i^b}{\xi_i}\left(C_i - \xi_i P_i^{ub}\right)\frac{\partial \xi_i}{\partial v} < 0 \tag{46}$$

Thus, P_i^b also decreases with the values of v. Similarly, the similar conclusions can be drawn in the cellular network. The blocking ratio P_c^b and throughput T_c all decrease with velocity. Therefore, the higher speed will degrade the capacity, but could lower the congestion. It could be explained by the fact that the increase of mobility rate in one hand enhances the handover opportunity, as well as the fairness for each user, since they have the more chance to access network; i.e., the increase of user mobility gives more opportunities to enter another network and enables some user who is always failing to connect to the AP to reconsider the network access. It could also lower the blocking probability in the congested situation but can not increase the system capacity.

5. Virtualized Congestion WiFi Offloading Algorithm

The COWO algorithm could obtain the optimal offloading ratio for each AP. However, it is based on the subgradient method, whose computational complexity will drastically increase with the number of networks [47, 48]. In this section, rather than optimize the independent offloading ratio for each AP, we view all the APs as one virtual WiFi network, and the channels and other resources in the WiFi networks will be jointly scheduled. Then, we proposed VCOWO algorithm, which could obtain the approximately optimal results under the equivalent conditions with much lower complexity. Though we did not get the separate offloading ratio, we can obtain some general results and useful insights from it.

Through observation, it is found that the offloading decision mainly depends on the service arriving ω and leaving rate l for given total channels in each network. As all the WiFi networks act as the capacity-augment utilities, it is reasonable

to view all the AP as one virtual WiFi network, where all the channels are centrally controlled. For simplicity, we consider the AP to have the same coverage, i.e., $d_i = d, i = 1, 2 \cdots M$, and same serving completing rate $\mu_i = \mu$. The virtual WiFi network satisfies the equivalent conditions as follows.

(1) The user flow rate of virtual WiFi network γ_a is the sum of user flow rate for each AP; i.e.,

$$\gamma_a = \sum_{i=1}^{M} \gamma_i = \sum_{i=1}^{M} \frac{2N_i \nu}{\pi d_i} = M \frac{2N_i \nu}{\pi d} = \frac{2N_i \nu}{\pi d_{eq}}, \quad (47)$$

where $d_{eq} = d/M$.

(2) The active users arriving rate of virtual WiFi network λ_a is equal to total active users arriving rate of all APs,

$$\lambda_a = \sum_{i=1}^{M} \lambda_i = \sum_{i=1}^{M} \lambda \frac{d_i^2}{D^2} = \lambda M \frac{d^2}{D^2}. \quad (48)$$

(3) All the channels in each AP are scheduled by the virtual WiFi network, i.e., the virtual WiFi network C_a has $C_a = \sum_{i=1}^{M} C_i$.

(4) The user serving rate in virtual WiFi network is $\mu_a = \mu$.

We try to find the optimal offloading ratio p_a for the virtual WiFi network. Thus, the steady-state distribution of virtual WiFi network can be expressed as

$$\pi_a^j = \frac{\left(\sum_{m=0}^{C_a} \left((\xi_a)^m / m! \right) \right)^{-1} (\xi_a)^j}{j!}, \quad 0 \le j \le C_a, \quad (49)$$

where

$$\xi_a = \frac{\lambda_a + p_a \gamma_a}{\mu_a + 2\nu / (\pi d_{eq})}. \quad (50)$$

Therefore, the number of users served by the virtual WiFi network N_a is the average queue length, and

$$N_a(\xi_a) = \sum_{k=0}^{C_a} k\pi_a^k$$

$$= \xi_a \left\{ 1 - \frac{(\xi_a)^{C_a}}{\left(\sum_{k=0}^{C_a} \left((\xi_a)^k / k! \right) \right) C_a!} \right\}. \quad (51)$$

Similarly, the blocking probability P_a^b and unblocking probability P_a^{ub} in virtual WiFi network are defined as

$$P_a^b = 1 - P_a^{ub} = \frac{\left(\sum_{m=0}^{C_a} \left((\xi_a)^m / m! \right) \right)^{-1} (\xi_a)^{C_a}}{C_a!}. \quad (52)$$

Then the users flow rate in virtual network γ_a is written as

$$\gamma_a = \frac{2N_a(\xi_a)\nu}{\pi d_{eq}} = \frac{2\xi_a \nu P_a^{ub}}{\pi d_{eq}}$$

$$= \frac{2\nu P_a^{ub}}{\pi d_{eq}} \cdot \frac{\lambda_a + p_a \gamma_a}{\mu_a + 2\nu / (\pi d_{eq})}. \quad (53)$$

After modification, it is observed that the user flow rate γ_a is the function of blocking probability, which is denoted as $\phi(P_a^b)$; i.e.,

$$\gamma_a = \frac{2\nu \lambda_a P_a^{ub}}{\pi \mu_a d_{eq} + 2\nu \left(1 - p P_a^{ub} \right)} = \phi \left(P_a^b \right). \quad (54)$$

Under the equivalent conditions, the analysis of offloading performance in the cellular network could be simplified. The users flowing rate in the cellular network is transformed as γ_c',

$$\gamma_c' = \frac{N_c(\xi_c')\nu}{\pi D} = \frac{2\xi_c \nu P_a^{ub}}{\pi D}$$

$$= \frac{2\nu P_c^{ub}}{\pi D} \cdot \frac{\lambda_c + \gamma_c'}{\mu_c + 2\nu p_a / (\pi D)}, \quad (55)$$

where

$$\xi_c' = \frac{\lambda_c + \gamma_c'}{\mu_c + 2\nu p / (\pi D)}. \quad (56)$$

The user flow rate γ_a can also be written as the function of blocking probability,

$$\gamma_c' = \frac{2\nu \lambda_c P_c^{ub}}{\pi D \mu_c + 2\nu \left(p_a - P_c^{ub} \right)} = \phi \left(P_c^b \right). \quad (57)$$

Similar to (17), the blocking probability could be solved in bisection method [49, 50]. Therefore, the optimization problem in (28) for all multiple APs could be transformed as follows:

$$\max \quad Q'(p_a)$$

$$= R_a N_a(\xi_c) + R_c N_c(\xi_c) - \beta \left(P_a^b + P_c^b \right) \quad (58)$$

$$\text{s.t.} \quad 0 \le p_a \le 1.$$

From (58), it is observed that the optimization is aimed at finding the optimal scalar p_a to maximize the throughput and minimize the blocking probability. The optimal scalar p_a could be solved by the golden section method, and we proposed the VCOWO algorithm as illustrated in Algorithm 2. The computational complexity in COWO is $\mathcal{O}(U + M)$, while the complexity is reduced to $\mathcal{O}(U + 1)$ in VCOWO algorithm, where U is the number of MBS, and $U = 1$ is assumed in this paper. It means the complexity of COWO algorithm increases with the number of APs M, while that of VCOWO algorithm is independent of M. The VCOWO algorithm could approach the optimal results under the equivalent conditions. To be more specific, the VCOWO could achieve the upper bound of the WiFi offloading performance achieved by COWO algorithm. Under the equivalent conditions, all WiFi networks are assumed to serve the users in a cooperation approach and could achieve higher throughput with lower blocking probability with the centralized control of WiFi channels allocation.

```
1: Calculate parameters in equivalent WiFi network
2: Initialize: p_0 = 0, k = 0
3: while |Q_{k+1} − Q_k| ≥ ε_2 do
4:     Calculate steady-state probability distribution π under given p_k
5:     Calculate utility function Q_k
6:     Update p_{k+1} according to golden section method
7: end while
8: Set the optimal offload factor vector p_a^* = p_{k+1}.
```

ALGORITHM 2: The proposed VCOWO.

TABLE 2: Simulation parameters.

Parameters	MBS	AP1	AP2	AP3	AP4
d_i/D(m)	1000	200	150	100	100
Channels	30	8	7	6	5
R_i/R_c (Mbps)	9.6	13.6	13.6	13.6	13.6
μ(links/s)			1/120		
v (m/s)			8		

6. Numerical Results

In this section, we evaluate the proposed algorithms with the OTSO scheme [18] in system utility as formulated in (28), blocking probability and throughput. The OTSO algorithm enables offloading user to a WiFi network whenever users enter into its coverage, which means the offloading ratio $p = 1$. Further, we show the approximation of VCOWO to COWO under equivalent conditions. Moreover, we verify the impacts of user mobility on WiFi offloading performance. In the simulation, we consider the scenario that contains one MBS $U = 1$ and multiple APs. Each AP is assumed to have no overlap with the others, and other parameters are shown in Table 2.

6.1. Performance Comparison. In this section, we compare the WiFi offloading performance with the multiple APs between COWO and OTSO under user arriving rate ranging from 0 to 0.5. First, Figure 3 illustrates that the system utility varies with the total active user arriving rate λ. When $\lambda <$ 0.3, it is found that the system utility grows with λ, and COWO algorithm has similar performance as the OTSO. It is because when the network is unsaturated and the congestion is small, the system utility increases by the throughput bought by the user arriving. The throughput increases since more users flow to the network and make the use of channels when unsaturated. However, it can be observed from Figure 3 that the utility in OTSO decreases with λ. Intuitively, when traffic load in the WiFi network is heavy, offloading data to WiFi network whenever possible will nevertheless incur higher blocking probability, which may degrade the utility function.

To further demonstrate the network congestion in WiFi offloading, we compare the blocking probability in Figure 4. It is obviously observed that the blocking probability in the proposed algorithm is much lower than the OTSO, especially when λ is larger. Without consideration of network congestion, the blocking probability grows rapidly with the
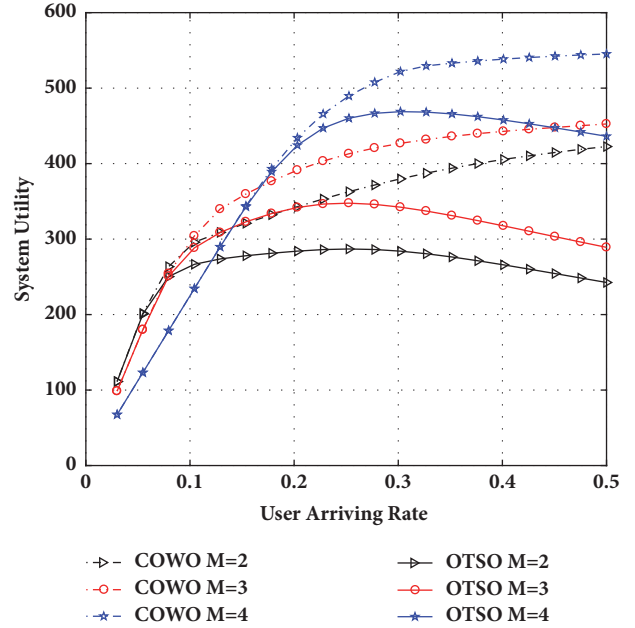

FIGURE 3: System utility varies with the users arriving rate.

active user arriving rate λ, which is also indicated in the decrease of system utility as shown in Figure 3.

Moreover, Figure 5 illustrates that the throughput varies with the user arriving rate λ. It can be observed that the throughput increases with λ. It is because the throughput increases with user arriving when the channels are not fully utilized. When λ is larger, the throughput does not change with the λ. Intuitively, when all the channels have been occupied, the increase of users will not bring higher throughput. Thus, it can be observed from Figure 5, constrained by the number of channels, that the throughput will not increase with the user arriving rate. The throughput is larger with
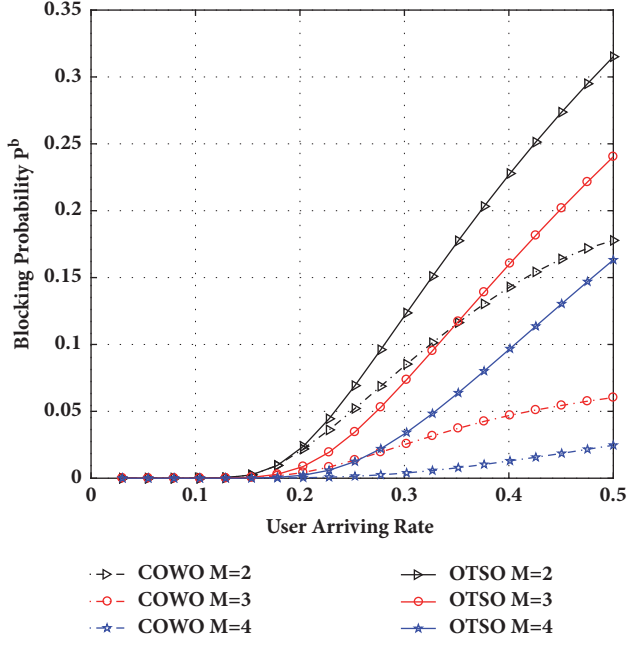
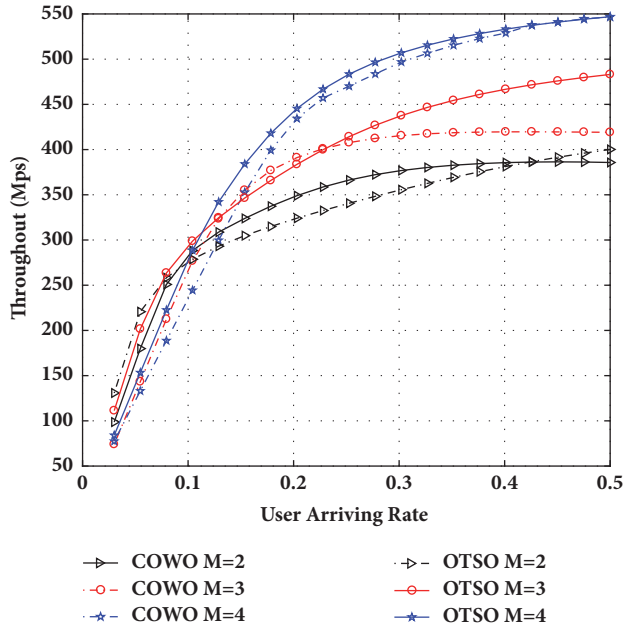FIGURE 4: Blocking probability varies with the users arriving rate.

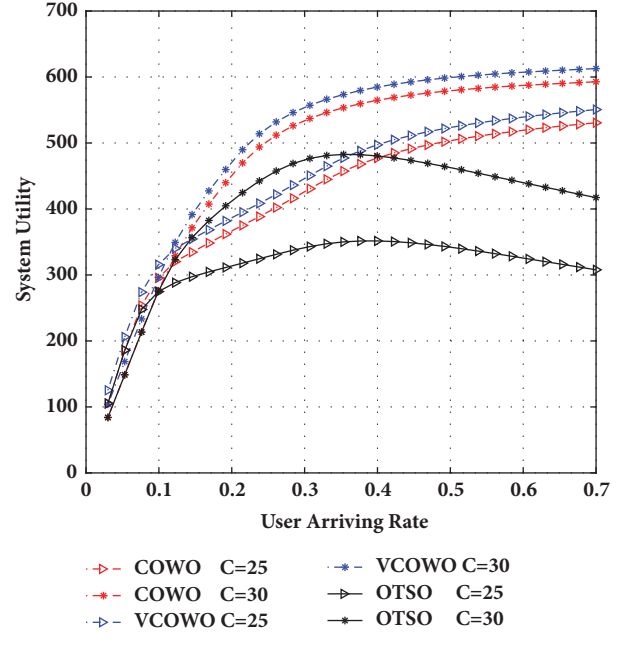FIGURE 5: Throughput varies with the users arriving rate.

FIGURE 6: System utility comparison varies with the users arriving rate.
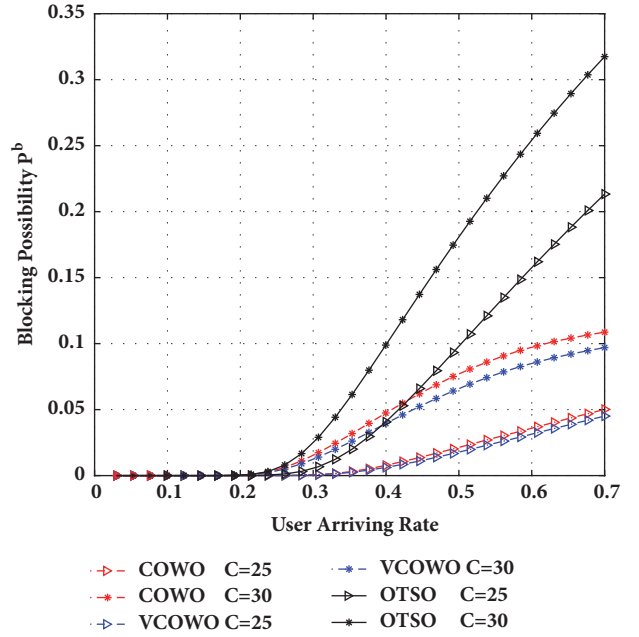
FIGURE 7: Blocking probability comparison varies with the active users arriving rate.

more WiFi APs, e.g., more available channels. To conclude, the proposed algorithm could maximize the throughput with lower blocking probability than OTSO algorithm.

6.2. Approximation Comparison. In this section, we evaluate the VCOWO algorithm under the equivalent conditions. We consider the 4 or 5 APs separately with equal coverage ($d = 150m$), and each with 5 channels, and it correspondingly has C = 20 or 25 channels for the virtual WiFi network. Assume the maximum user arriving rate λ range is 0.7. Other

parameters all satisfy the equivalent conditions in Section 5. In Figures 6–8, we compare the performance with OTSO under different channel numbers in WiFi network. Clearly, more channels offer service to more users and nevertheless could contribute to the larger system utility. It can be observed that the VCOWO achieves similar system utility, blocking probability and throughput to COWO algorithm. To be more specific, the performance in VCOWO is the

FIGURE 8: Throughput comparison varies with the user arriving rate.

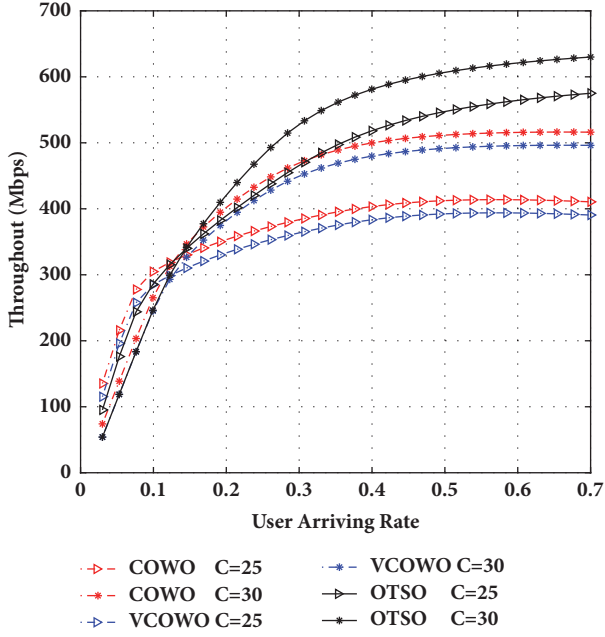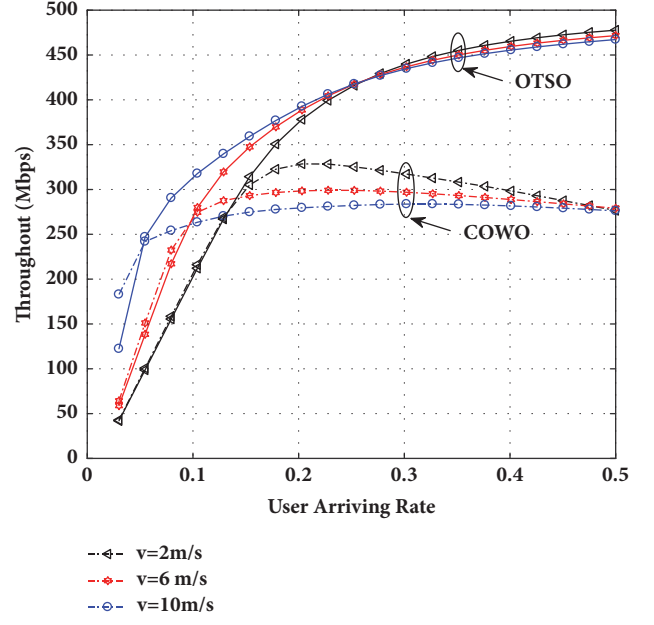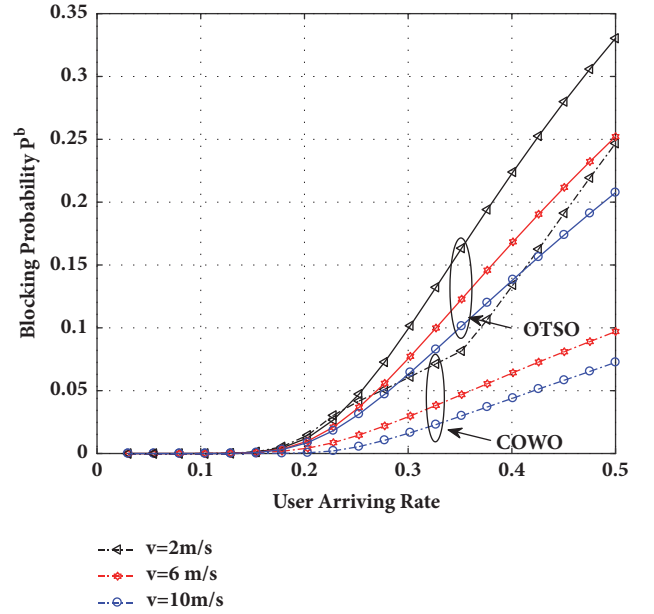FIGURE 9: Throughput evaluation under different mobility velocity v.

upper bound of COWO under the equivalent situation. Recall the equivalent assumption in Section 5; it is found that all the channels of different APs could be jointly scheduled in the virtual WiFi network. That is to say, all the APs serve the users with the association, rather than separately schedule the users' network access in COWO algorithm. Thus, VCOWO could give the tight upper bound of COWO algorithm performance with much lower complexity under the equivalent conditions.

6.3. User Mobility. In this section, we verify the impacts of user mobility on WiFi offloading as illustrated in Section 5. In Figures 9 and 10, the COWO and OTSO are evaluated under the different velocities with user arriving rate ranging from 0 to 0.5. It can be observed from Figure 9 that the throughput decreases with the velocity. Recall the fact that it was indicated in (41) that throughput T_i is the monotonically decreasing function about the velocity v. Intuitively, we deduce it in another way. At one-moment t, suppose that there are N users in ith AP; the users move with the average velocity v, and the $\xi_i = (\lambda_i + p_i \cdot 2N_i v/(\pi d_i))/(\mu_i + 2v/(\pi d_i))$. Then, for the next moment, $t + \Delta t$, with the increase of v, we have $\xi_i' = (\lambda_i + p_i \cdot 2N_i(v+\Delta v)/(\pi d_i))/(\mu_i + 2(v+\Delta v)/(\pi d_i))$, and $\xi_i > \xi_i'$. Therefore, the increase of v reduces the average number of users in the network and thus lowers the throughput and the blocking probability. The user mobility increases the opportunities to access, and could, to some extent, reduce the access blocking in the congested situation. The mobility only gives more users the chances to access the network. However, it can not guarantee the access success or improve the throughput. Actually, constrained by the number of total channels, the capacity will not increase. Even worse, the mobility impedes sustainable connection and nevertheless lowers the throughput in general.

FIGURE 10: Blocking probability evaluation under different user mobility velocity v.

7. Conclusion

In this paper, we studied WiFi offloading with user mobility management in smart communications. With consideration of the dynamic network nature, including the network congestion and the user mobility, we proposed the COWO algorithm to optimize the offloading ratio for each AP, which aims to maximize the throughput with lower blocking probability. By viewing all the APs as one virtual WiFi network, the VCOWO algorithm is proposed with

much lower complexity. Under equivalent conditions, the VCOWO algorithm could approximate optimal results by COWO algorithm and give an upper bound of offloading performance of COWO algorithm. Moreover, we investigated the impacts of user mobility on WiFi offloading. It is found that the increase of velocity in user mobility degrades the throughput performance, but could reduce the blocking in some way. For future work, it is an interesting direction for future research to consider other mobility models, especially the heavy-tailed distribution model, which was shown to be more accurate for modeling human mobility. It is promising to deal with the network congestion and load balance in smart communications through artificial intelligence technologies and wireless big data support, which could well predict the user random mobility patterns with statistical information of the possible user's trajectories and schedule the network access in a smarter way.

Appendix

A. Proof of the Bisection Method for Solving P_i^b

Due to P_i^b being the root of $\psi(P_i^b) = 0$, the derivation of $\psi(P_i^b)$ is

$$
\begin{aligned}
\psi'\left(P_i^b\right) &= 1 - \left.\frac{d\mathrm{P}\left(\xi_i\right)}{d\xi_i}\right|_{\xi_i = (\lambda_i + p\phi_i(P_i^b))/(\mu + 2\nu/(\pi d_i))} \cdot \frac{d\xi_i}{dP_i^b} \\
&= 1 \\
&\quad - \left.\frac{\phi'\left(P_i^b\right)}{\mu + 2\nu/\left(\pi d_i\right)} \frac{d\mathrm{P}\left(\xi_i\right)}{d\xi_i}\right|_{\xi_i = (\lambda_i + p_i\phi(P_i^b))/(\mu + 2\nu/(\pi d_i))}.
\end{aligned}
\tag{A.1}
$$

where

$$
\phi'\left(P_i^b\right) = \frac{-2\nu\left[\pi d_i\mu_i + 2\nu\left(1 - p_i + p_i P_i^b\right) + p_i\right]}{\left[\pi D\mu_i + 2\nu\left(1 - p_i + p_i P_i^b\right)\right]^2} \tag{A.2}
$$
$$
< 0,
$$

and

$$
\frac{d\mathrm{P}\left(\xi_i\right)}{d\xi_i} = \frac{P_i^b\left(C_i - \xi_i P_i^{ub}\right)}{\xi_i}. \tag{A.3}
$$

The maximum number of users served by the network will not be more than the channel number; i.e., $N(\xi_i) = \sum_{k=0}^{C_i} k\pi_i^k = \xi_i P_i^{ub} \leq C_i \sum_{i=0}^{C_i} \pi^i = C_i$, and thus we have $d\mathrm{P}(\xi_i)/d\xi_i \geq 0$. Overall, it is found that $\psi'(P_i^b) \geq 0$, and thus $\psi(P_i^b)$ is an increasing function of P_i^b. Moreover, $P_i^b \in [0, 1]$, $\psi(0) = -\varphi(0) < 0$, and $\psi(1) = 1 - \varphi(1) > 0$. Therefore, $\exists P_i^b \in [0, 1]$, $\psi(P_i^b) = 0$, and the bisection method can be used for the calculation of P_i^b.

B. Proof of Convex Optimization

The utility function can be divided into two parts:

$$
\begin{aligned}
Q\left(\overrightarrow{\mathbf{p}}\right) &= T\left(\overrightarrow{\mathbf{p}}\right) - \beta B\left(\overrightarrow{\mathbf{p}}\right) \\
&= \sum_{i=1}^{M} R_i N\left(\xi_i, C_i\right) + R_c N_c\left(\xi_c\right) \\
&\quad - \beta\left(\sum_{i=1}^{N} P_i^b + P_c^{\,b}\right) \\
&= \sum_{i=1}^{M}\left(R_i N\left(\xi_i, C_i\right) - \beta P_i^b\right) \\
&\quad + \left(R_c N_c\left(\xi_c\right) - \beta P_c^{\,b}\right) \\
&= \sum_{i=1}^{M} Q_i\left(p_i\right) + Q_c\left(\overrightarrow{\mathbf{p}}\right),
\end{aligned}
\tag{B.1}
$$

where the $Q_i(p_i)$ denotes the utility of ith WiFi network and $Q_c(\overrightarrow{\mathbf{p}})$ represents the cellular system utility.

The proof of convex optimization in (28) is equal to proving that the utility matrix $Q(\overrightarrow{\mathbf{p}})$ is a negative definite matrix. Hessian matrix $\partial^2 Q/\partial\overrightarrow{\mathbf{p}}^2$ is

$$
\frac{\partial^2 Q}{\partial\overrightarrow{\mathbf{p}}^2}
= \begin{bmatrix}
\dfrac{\partial^2 Q_1\left(p_1\right)}{\partial p_1^{\,2}} & 0 & \cdots & 0 \\
0 & \dfrac{\partial^2 Q_2\left(p_2\right)}{\partial p_2^{\,2}} & \cdots & 0 \\
\vdots & \vdots & \ddots & \vdots \\
0 & 0 & \cdots & \dfrac{\partial^2 Q_M\left(p_M\right)}{\partial p_M^{\,2}} \\
\dfrac{\partial^2 Q_c\left(\overrightarrow{\mathbf{p}}\right)}{\partial\overrightarrow{\mathbf{p}}\cdot\partial p_1} & \dfrac{\partial^2 Q_c\left(\overrightarrow{\mathbf{p}}\right)}{\partial\overrightarrow{\mathbf{p}}\cdot\partial p_2} & \cdots & \dfrac{\partial^2 Q_c\left(\overrightarrow{\mathbf{p}}\right)}{\partial\overrightarrow{\mathbf{p}}\cdot\partial p_M}
\end{bmatrix},
\tag{B.2}
$$

where

$$
\begin{aligned}
\frac{\partial^2 Q_c\left(\overrightarrow{\mathbf{p}}\right)}{\partial\overrightarrow{\mathbf{p}}\cdot\partial p_1} &= \frac{\partial^2 Q_c\left(\overrightarrow{\mathbf{p}}\right)}{\partial p_1^{\,2}} + \frac{\partial^2 Q_c\left(\overrightarrow{\mathbf{p}}\right)}{\partial p_2\cdot\partial p_1}\cdots \\
&\quad + \frac{\partial^2 Q_c\left(\overrightarrow{\mathbf{p}}\right)}{\partial p_M\cdot\partial p_1}.
\end{aligned}
\tag{B.3}
$$

Since $\partial^2 Q_c(\vec{\mathbf{p}})/(\partial p_i \cdot \partial p_j) = \partial^2 Q_c(\vec{\mathbf{p}})/(\partial p_j \cdot \partial p_i), i \neq j$, we have

$$\frac{\partial^2 Q}{\partial \vec{p}^2}$$

$$= \begin{bmatrix} \dfrac{\partial^2 Q_1(p_1)}{\partial p_1{}^2} & 0 & \cdots & 0 \\[2ex] 0 & \dfrac{\partial^2 Q_2(p_2)}{\partial p_2{}^2} & \cdots & 0 \\[1ex] \vdots & \vdots & \ddots & \vdots \\[1ex] 0 & 0 & \cdots & \dfrac{\partial^2 Q_M(p_M)}{\partial p_M{}^2} \\[2ex] 0 & 0 & \cdots & 0 \end{bmatrix}. \quad \text{(B.4)}$$

Then, the proof that the Hessian matrix is negative definite is equal to proving that its eigenvalue is nonnegative. That is,

$$\frac{\partial Q_i}{\partial p_i} = \frac{\partial Q_i}{\partial \xi_i} \frac{\partial \xi_i}{\partial p_i} \geq 0$$

$$\frac{\partial^2 Q_i}{\partial p_i{}^2} = \frac{\partial^2 Q_i}{\partial \xi_i{}^2} \left(\frac{\partial \xi_i}{\partial p_i}\right)^2 + \frac{\partial Q_i}{\partial \xi_i} \frac{\partial^2 \xi_i}{\partial p_i{}^2} \leq 0. \quad \text{(B.5)}$$

We assume that $\partial \xi_i/\partial p_i > 0$ and $\partial^2 \xi_i/\partial p_i{}^2 < 0$ hold, which has been proved in Appendix B with the bound of P_i^b. Thus, the convex optimization question is converted to prove $\partial Q_i/\partial \xi_i \geq 0$. The first-order and second-order partial derivative of Q_i are, respectively, given by

$$\frac{\partial Q_i}{\partial \xi_i} = 1 - P_i^b\left(1 + C_i - \xi_i P_i^{ub}\right) - \frac{P_i^b\left(C_i - \xi_i P_i^{ub}\right)}{\xi_i}. \quad \text{(B.6)}$$

and

$$\frac{\partial^2 Q_i}{\partial \xi_i{}^2}$$

$$= -\frac{P_i^b}{\xi_i}\left[\left(C_i - \xi_i P_i^{ub} + \xi_i P_i^b\right)\left(1 + C_i - \xi_i P_i^{ub}\right) - \xi_i\right] \quad \text{(B.7)}$$

$$- \frac{P_i^b}{\xi_i{}^2}\left[\left(C_i - \xi_i + 2\xi_i P_i^b\right)\left(C_i - \xi_i P_i^b\right) - C_i\right].$$

The lower and upper bound of P_i^b give the conditions [42]

$$P_i^b \leq \frac{\xi_i}{\xi_i\left(1 + C_i - \xi_i + P_i^{ub}\right) + C_i} \quad \text{(B.8)}$$

$$P_i^b \geq \frac{C_i + \xi_i{}^2}{\xi_i{}^2\left(1 + C_i - (\xi_i + 1)P_i^{ub}\right) + C_i\xi_i} - \frac{C_i - \xi P_i^{ub}}{\xi_i}, \quad \text{(B.9)}$$

and, thus, we have

$$0 \leq \frac{\partial Q_i}{\partial \xi_i} \leq 1$$

$$\frac{\partial^2 Q_i}{\partial \xi_i{}^2} \leq 0, \quad \text{(B.10)}$$

which completes the proof.

C. Proof of $\partial^2 \xi_i/\partial p_i{}^2 < 0$

We prove the $\partial \xi_i/\partial p_i > 0$ and $\partial^2 \xi_i/\partial p_i{}^2 < 0$ with the bound constraint in Appendix B. From (10), the derivative of ξ_i with p_i is

$$\frac{\partial \xi_i}{\partial p_i} = \frac{\gamma_i}{\mu_i + 2\nu/(\pi d_i)} + \frac{1}{\mu_i + 2\nu/(\pi d_i)}\frac{\partial \gamma_i}{\partial p_i}. \quad \text{(C.1)}$$

Then, the fist-order derivative of γ_i with p_i is calculated as

$$\frac{\partial \gamma_i}{\partial p_i} = \frac{-2\nu\lambda_i\left(\pi d_i\mu + 2\nu\right)}{\pi d_i\mu_i + 2\nu\left(1 - p_i P_i^{ub}\right)}\frac{\partial P_i^b}{\partial p_i}$$

$$+ \frac{\left(2\nu P_i^{ub}\right)^2 \lambda_i}{\left[\pi d_i\mu + 2\nu\left(1 - p_i P_i^{ub}\right)\right]^2}. \quad \text{(C.2)}$$

With (12), the derivative of P_i^b with p_i is

$$\frac{\partial P_i^b}{\partial p_i} = \frac{P_i^b\left(C_i - \xi_i P_i^{ub}\right)}{\xi_i}\frac{\partial \xi_i}{\partial p_i}. \quad \text{(C.3)}$$

With (C.1) and (C.3), the derivative of γ_i with p_i could be rewritten as

$$\frac{\partial \xi_i}{\partial p_i} = \frac{\gamma_i}{\mu_i + 2\nu/(\pi d_j)}\left[1 + \frac{2\nu p_i P_i^{ub}}{\pi d_i\mu + 2\nu\left(1 - p_i P_i^{ub}\right)}\right]$$

$$\cdot \left[1 + \frac{p_i}{\mu_i + 2\nu/(\pi d_j)}\right.$$

$$\left. \cdot \frac{2\nu\lambda_i P_i^b\left(\pi d_i\mu + 2\nu\right)\left(C_i - \xi_i P_i^{ub}\right)}{\left[\pi d_i\mu + 2\nu\left(1 - p_i P_i^{ub}\right)\right]\cdot \xi_i}\right]^{-1}. \quad \text{(C.4)}$$

Since the channel used in $\xi_i P_i^{ub}$ is less than the total channel in i-th AP, i.e., $C_i - \xi_i P_i^{ub} > 0$, thus, we have $\partial \xi_i/\partial p_i > 0$. Similarly, $\partial^2 \xi_i/\partial p_i{}^2 < 0$ can be proved.

Data Availability

The authors confirm that the data supporting the findings of this study are available within the article. All the simulation parameters and other experimental details are clearly shown in this article, which could be used to reproduce the experiment related to our findings.

Conflicts of Interest

The authors declare that there are no conflicts of interest regarding the publication of this paper.

Acknowledgments

References

[1] Cisco., "Cisco Visual Networking Global Mobile Data Traffic Forecast Update, 2016-2021 *White Paper*".

[2] B. Liu, Q. Zhu, and H. Zhu, "Delay-Aware LTE WLAN Aggregation for 5G Unlicensed Spectrum Usage," in *Proceedings of the 2017 IEEE 85th Vehicular Technology Conference (VTC Spring)*, pp. 1–7, Sydney, NSW, June 2017.

[3] W. Tan, D. Xie, J. Xia, W. Tan, L. Fan, and S. Jin, "Spectral and Energy Efficiency of Massive MIMO for Hybrid Architectures Based on Phase Shifters," *IEEE Access*, vol. 6, pp. 11751–11759, 2018.

[4] Y. Fang, G. Han, G. Cai, F. C. Lau, P. Chen, and Y. L. Guan, "Design Guidelines of Low-Density Parity-Check Codes for Magnetic Recording Systems," *IEEE Communications Surveys & Tutorials*, vol. 20, no. 2, pp. 1574–1606, 2018.

[5] F. Shi, W. Tan, J. Xia, D. Xie, L. Fan, and X. Liu, "Hybrid Cache Placement for Physical-Layer Security in Cooperative Networks," *IEEE Access*, vol. 6, pp. 8098–8108, 2018.

[6] F. Zhou, G. Luo, Y. Liu, Y. Wang, and L. Fan, "Coordinated beamforming for heterogeneous small-cell networks with a non-ideal backhaul," *IET Communications*, vol. 12, no. 5, pp. 595–602, 2018.

[7] W. Tan, S. Jin, C. Wen, and T. Jiang, "Spectral efficiency of multi-user millimeter wave systems under single path with uniform rectangular arrays," *EURASIP Journal on Wireless Communications and Networking*, vol. 2017, no. 1, 2017.

[8] L. Fan, X. Lei, N. Yang, T. Q. Duong, and G. K. Karagiannidis, "Secure Multiple Amplify-and-Forward Relaying with Cochannel Interference," *IEEE Journal of Selected Topics in Signal Processing*, vol. 10, no. 8, pp. 1494–1505, 2016.

[9] C. Li, S. Zhang, P. Liu, F. Sun, J. M. Cioffi, and L. Yang, "Overhearing protocol design exploiting intercell interference in cooperative green networks," *IEEE Transactions on Vehicular Technology*, vol. 65, no. 1, pp. 441–446, 2016.

[10] Z. Shi, S. Ma, G. Yang, K. Tam, and M. Xia, "Asymptotic outage analysis of HARQ-IR over time-correlated nakagami-m fading channels," *IEEE Transactions on Wireless Communications*, no. 99, article 1, 2017.

[11] C. Li, Y. Li, K. Song, and L. Yang, "Energy efficient design for multiuser downlink energy and uplink information transfer in 5G," *Science China Information Sciences*, vol. 59, no. 2, pp. 1–8, 2016.

[12] X. Lai, W. Zou, X. Li, and L. Fan, "Multiuser energy harvesting relaying system with direct links," *IET Communications*, vol. 11, no. 12, pp. 1846–1852, 2017.

[13] J. Xia, F. Zhou, X. Lai et al., "Cache aided decode-and-forward relaying networks: From the spatial view," *Wireless Communications and Mobile Computing*, vol. 2018, 9 pages, 2018.

[14] L. Fan, X. Lei, N. Yang, T. Q. Duong, and G. K. Karagiannidis, "Secrecy Cooperative Networks with Outdated Relay Selection over Correlated Fading Channels," *IEEE Transactions on Vehicular Technology*, vol. 66, no. 8, pp. 7599–7603, 2017.

[15] F. Shi, L. Fan, X. Liu, Z. Na, and Y. Liu, "Probabilistic caching placement in the presence of multiple eavesdroppers," *Wireless Communications and Mobile Computing*, vol. 2018, 2018.

[16] X. Wang, H. Zhang, L. Fan, and Y. Li, "Performance of Distributed Switch-and-Stay Combining for Cognitive Relay Networks with Primary Transceiver," *Wireless Personal Communications*, vol. 97, no. 2, pp. 3031–3042, 2017.

[17] R. Zhao, Y. Yuan, L. Fan, and Y.-C. He, "Secrecy Performance Analysis of Cognitive Decode-and-Forward Relay Networks in Nakagami-m Fading Channels," *IEEE Transactions on Communications*, vol. 65, no. 2, pp. 549–563, 2017.

[18] K. Lee, J. Lee, Y. Yi, I. Rhee, and S. Chong, "Mobile data offloading: how much can wifi deliver?" *IEEE/ACM Transactions on Networking*, vol. 21, no. 2, pp. 536–550, 2013.

[19] R. Gass and C. Diot, "An Experimental Performance Comparison of 3G and Wi-Fi," in *Passive and Active Measurement*, vol. 6032 of *Lecture Notes in Computer Science*, pp. 71–80, Springer, Berlin, Germany, 2010.

[20] D. Suh, H. Ko, and S. Pack, "Efficiency Analysis of WiFi Offloading Techniques," *IEEE Transactions on Vehicular Technology*, vol. 65, no. 5, pp. 3813–3817, 2016.

[21] B. Aruna, M. Ratul, and A. Venkataramani, "Augmenting mobile 3G using WiFi," in *Pro. Conf. Mobile Syst. Appl. Services*, pp. 209–222, 2010.

[22] W. Zhang, Y. Wen, and H.-H. Chen, "Toward transcoding as a service: Energy-efficient offloading policy for green mobile cloud," *IEEE Network*, vol. 28, no. 6, pp. 67–73, 2014.

[23] H. Deng and I.-H. Hou, "On the capacity-performance trade-off of online policy in delayed mobile offloading," *IEEE Transactions on Wireless Communications*, vol. 16, no. 1, pp. 526–537, 2017.

[24] M. H. Cheung and J. Huang, "DAWN: Delay-Aware Wi-Fi offloading and network selection," *IEEE Journal on Selected Areas in Communications*, vol. 33, no. 6, pp. 1214–1223, 2015.

[25] H. Ko, J. Lee, and S. Pack, "Performance Optimization of Delayed WiFi Offloading in Heterogeneous Networks," *IEEE Transactions on Vehicular Technology*, vol. 66, no. 10, pp. 9436–9447, 2017.

[26] B. Liu, Q. Zhu, and H. Zhu, "Delay-Aware LTE WLAN Aggregation in Heterogeneous Wireless Network," *IEEE Access*, vol. 6, pp. 14544–14559, 2018.

[27] Y. Li, B. Shen, J. Zhang, X. Gan, J. Wang, and X. Wang, "Offloading in HCNs: Congestion-Aware Network Selection and User Incentive Design," *IEEE Transactions on Wireless Communications*, vol. 16, no. 10, pp. 6479–6492, 2017.

[28] M. H. Cheung, F. Hou, J. Huang, and R. Southwell, "Congestion-aware DNS for integrated cellular and Wi-Fi networks," *IEEE Journal on Selected Areas in Communications*, vol. 35, no. 6, pp. 1269–1281, 2017.

[29] E. Aryafar, A. Keshavarz-Haddad, M. Wang, and M. Chiang, "RAT selection games in HetNets," in *Proceedings of the 32nd IEEE International Conference on Computer Communications (INFOCOM '13)*, pp. 998–1006, Turin, Italy, April 2013.

[30] A. Keshavarz-Haddad, E. Aryafar, M. Wang, and M. Chiang, "HetNets Selection by Clients: Convergence, Efficiency, and Practicality," *IEEE/ACM Transactions on Networking*, vol. 25, no. 1, pp. 406–419, 2017.

[31] M. Zhou, Y. Tang, W. Nie, L. Xie, and X. Yang, "GrassMA: graph-based semi-supervised manifold alignment for indoor WLAN localization," *IEEE Sensors Journal*, vol. 17, no. 21, pp. 7086–7095, 2017.

[32] M. Zhou, Y. Wei, Z. Tian, X. Yang, and L. Li, "Achieving cost-efficient indoor fingerprint localization on wlan platform: a hypothetical test approach," *IEEE Access*, vol. 5, pp. 15865–15874, 2017.

[33] Y. Fang, G. Han, P. Chen, F. C. M. Lau, G. Chen, and L. Wang, "A Survey on DCSK-Based Communication Systems and Their Application to UWB Scenarios," *IEEE Communications Surveys & Tutorials*, vol. 18, no. 3, pp. 1804–1837, 2016.

[34] J. Li, M. Wen, X. Jiang, and W. Duan, "Space-Time Multiple-Mode Orthogonal Frequency Division Multiplexing with Index Modulation," *IEEE Access*, vol. 5, pp. 23212–23222, 2017.

[35] S. Pattaramalai, V. A. Aalo, and G. P. Efthymoglou, "Evaluation of call performance in cellular networks with generalized cell dwell time and call-holding time distributions in the presence of channel fading," *IEEE Transactions on Vehicular Technology*, vol. 58, no. 6, pp. 3002–3013, 2009.

[36] G. Pan, H. Lei, Y. Deng, L. Fan, Y. Chen, and Z. Ding, "On secrecy outage of MISO SWIPT systems in the presence of imperfect CSI," in *Proceedings of the 2016 24th European Signal Processing Conference (EUSIPCO)*, pp. 818–822, Budapest, Hungary, August 2016.

[37] Z. Shi and Q. Zhu, "Throughput analysis and optimization based on mobility analysis and markov process for heterogeneous wireless networks," *Wireless Personal Communications*, vol. 77, no. 2, pp. 1091–1116, 2014.

[38] L. Wang and D. Binet, "Mobility-Based Network Selection Scheme in Heterogeneous Wireless Networks," in *Proceedings of the 2009 IEEE 69th Vehicular Technology Conference Spring*, pp. 1–5, Barcelona, Spain, April 2009.

[39] F. Zhou, L. Fan, X. Lei, G. Luo, H. Zhang, and J. Zhao, "Edge Caching With Transmission Schedule for Multiuser Multirelay Networks," *IEEE Communications Letters*, vol. 22, no. 4, pp. 776–779, 2018.

[40] X. Lai, W. Zou, D. Xie, and L. Fan, "DF relaying networks in randomly distributed interference environments," in *Proceedings of the 2017 9th International Conference on Wireless Communications and Signal Processing (WCSP)*, pp. 1–6, Nanjing, October 2017.

[41] F. Zhou, M. Du, Y. Wang, and G. Luo, "Joint source-channel coding for band-limited backhauls in coordinated multi-point systems," *IET Communications*, vol. 10, no. 13, pp. 1562–1570, 2016.

[42] Z. Shi and Q. Zhu, "Radio resource management scheme for heterogeneous wireless networks based on access proportion optimization," *Journal of Communications and Networks*, vol. 15, no. 5, pp. 527–537, 2013.

[43] I. Matei and J. S. Baras, "Performance evaluation of the consensus-based distributed subgradient method under random communication topologies," *IEEE Journal of Selected Topics in Signal Processing*, vol. 5, no. 4, pp. 754–771, 2011.

[44] F. Zhou, L. Fan, N. Wang, G. Luo, J. Tang, and W. Chen, "A Cache-Aided Communication Scheme for Downlink Coordinated Multipoint Transmission," *IEEE Access*, vol. 6, pp. 1416–1427, 2017.

[45] W. Tan, M. Matthaiou, S. Jin, and X. Li, "Spectral Efficiency of DFT-Based Processing Hybrid Architectures in Massive MIMO," *IEEE Wireless Communications Letters*, vol. 6, no. 5, pp. 586–589, 2017.

[46] D. D. Nguyen, Y. Liu, and Q. Chen, "On the Energy Efficient Multi-Pair Two-Way Massive MIMO AF Relaying With Imperfect CSI and Optimal Power Allocation," *IEEE Access*, vol. 6, pp. 2589–2603, 2018.

[47] Y. Liang, H. Wu, G. Huang, J. Yang, and H. Wang, "Thermal performance and service life of vacuum insulation panels with aerogel composite cores," *Energy and Buildings*, vol. 154, pp. 606–617, 2017.

[48] J. Li, X. Jiang, Y. Yan, W. Yu, S. Song, and M. H. Lee, "Low Complexity Detection for Quadrature Spatial Modulation Systems," *Wireless Personal Communications*, vol. 95, no. 4, pp. 4171–4183, 2017.

[49] J. Yang, H. Wu, S. He, and M. Wang, "Prediction of thermal conductivity of fiber/aerogel composites for optimal thermal insulation," *Journal of Porous Media*, vol. 18, no. 10, pp. 971–984, 2015.

[50] J. Yang, H. Wu, M. Wang, S. He, and H. Huang, "Prediction and optimization of radiative thermal properties of ultrafine fibrous insulations," *Applied Thermal Engineering*, vol. 104, pp. 394–402, 2016.

Research Article

Robust Heading Estimation for Indoor Pedestrian Navigation Using Unconstrained Smartphones

Zhian Deng ⓘ,[1] **Xin Liu** ⓘ,[2] **Zhiyu Qu** ⓘ,[1] **Changbo Hou,**[1] **and Weijian Si**[1]

[1]*College of Information and Communication Engineering, Harbin Engineering University, Harbin 150001, China*
[2]*School of Information and Communication Engineering, Dalian University of Technology, Dalian 116024, China*

Correspondence should be addressed to Xin Liu; liuxinstar1984@dlut.edu.cn

Heading estimation using inertial sensors built-in smartphones has been considered as a central problem for indoor pedestrian navigation. For practical daily lives, it is necessary for heading estimation to allow an unconstrained use of smartphones, which means the varying device carrying positions and orientations. As a result, three special human body motion states, namely, random hand movements, carrying position transitions, and user turns, are introduced. However, most existing heading estimation approaches neglect the three motion states, which may render large estimation errors. We propose a robust heading estimation system adapting to the unconstrained use of smartphones. A novel detection and classification method is developed to detect the three motion states timely and discriminate them accurately. For normal working, the user heading is estimated by a PCA-based approach. If a user turn occurs, it is estimated by adding horizontal heading change to previous user heading directly. If one of the other two motion states occurs, it is obtained by averaging estimation results of the adjacent normal walking steps. Finally, an outlier filtering algorithm is developed to smooth the estimation results. Experimental results show that our approach is capable of handling the unconstrained situation of smartphones and outperforms previous approaches in terms of accuracy and applicability.

1. Introduction

For Global Navigation Satellite Systems- (GNSS-) denied environments, various indoor pedestrian navigation solutions [1–5], such as wireless local area positioning systems, ultrawideband, and radio frequency identification, have been proposed. The usage of these infrastructure based solutions is limited to the space where special equipment or infrastructures are available. Pedestrian dead reckoning (PDR) [6–8] using inertial sensors built-in a smartphone may overcome this limitation, since the inertial sensors are continuously available. PDR achieves location estimation by combining step detection and step length estimation with user heading estimation. Once each user step is detected, the user position is updated by adding the current estimated relative displacement to the user position estimated at previous step. Recently, since smartphones are ubiquitous and carried almost everywhere we go, it is more and more practicable to deploy PDR approach in our daily lives.

User heading estimation is a central problem for PDR. Most existing heading estimation solutions deploy traditional attitude estimation based approaches [9, 10]. The user heading is estimated by adding a fixed user heading offset to the estimated device forward heading. This approach performs well if the device is constrained to a fixed carrying position and device orientation. However, for the smartphone in the trouser pocket or swinging in hand, the heading offset is changing all the time and hard to be estimated. Traditional attitude estimation based approaches may render a large heading estimation error due to the biased estimation of the heading offset.

To address the heading estimation problem with devices placed in the trouser pocket or swinging in hand, the uDirect approach [11], the PCA-based approach including conventional PCA approach [12], and our previous proposed RMPCA approach [13] combining rotation matrix (RM) and PCA have been proposed. The uDirect approach extracts local walking direction directly at a specific region, where the

forward acceleration dominates the acceleration in the horizontal plane. In contrast, PCA-based approach is more robust to the body locomotion dynamics, since all acceleration samples are exploited to extract the most variation of horizontal acceleration signals, which is assumed to be parallel with walking direction. Recently, to remove the restrictions on device carrying positions, we proposed a heading estimation approach independent of carrying position. The carrying position is recognized by a position classifier upon the distinguishable acceleration patterns, while assuming relatively stable device orientations under the same carrying positions.

To enable a really unconstrained use of smartphones for heading estimation, not only device carrying positions but also the varying device orientations should be considered. Thus, several critical problems still need to be solved to enhance the reliability and applicability of heading estimation.

Firstly, the current heading estimation solutions are sensitive and nonrobust to random hand movements. For PCA-based approach, the fundamental assumption is seriously corrupted by random hand movements, which make the maximum variance of the acceleration signals in the horizontal plane deviate from the walking direction.

Secondly, three motion states, namely, hand movements, carrying positions transitions, and user turns, and their impacts on heading estimations have been paid little attentions. Missed detection and confusion among the three motion states may render a large heading estimation error.

To solve the above problems, we propose a robust heading estimation system using unconstrained smartphones. The main idea is that we select the related optimal heading estimation strategy based on the detection and discrimination of three special motion states, namely, random hand movements, carrying position transitions, and user turns. A novel detection and classification method is developed to detect the three motion states timely and discriminate them accurately. If user turn occurs, the user heading is estimated by computing heading change in the horizontal plane directly. If the other two motion states occur, the user heading is assumed to be smooth and obtained by averaging estimation results of the normal neighbor walking steps.

The proposed estimation system deploys our previous RMPCA approach for heading estimation during normal walking. Finally, the estimation results are further smoothed by filtering outliers caused by hand movements undetected or hand movements misclassified as user turns. For simplicity, in this work, we only consider the two main pedestrian activities, namely, walking and standing, and assume that they have been already accurately recognized according to their different acceleration patterns [14, 15].

Experiments show that our heading estimation system outperforms existing approaches in terms of accuracy, reliability, and applicability under the unconstrained situations. In summary, our work makes the following contributions:

(i) We propose a robust heading estimation system independent of carrying positions and device orientations.

(ii) We point out that a large heading estimation error may be introduced by PCA-based approach, if the following three motion states cannot be detected and discriminated: random hand movements, carrying position transitions, and user turn.

(iii) We propose a novel detection and classification method to detect and discriminate the above three motion states.

(iv) We develop an outlier filtering algorithm to remove the outliers of user heading estimation results.

(v) We report the evaluation of the proposed detection and classification technique based on extensive samples collected from four participants and compare the accuracy performance of our heading estimation approach to existing approaches.

In the rest of this paper, we will firstly introduce an overview of the proposed robust heading estimation system using unconstrained smartphones in Section 2. Section 3 describes the detection and classification methods against the three special motion states in detail. Section 4 describes the robust user heading estimation approaches adapting the special motion states caused by unconstrained use of smartphones. The evaluations of experimental results are reported in Section 5. Conclusions are presented in the last section.

2. System Overview

Figure 1 shows an overview of the proposed robust user heading estimation system using unconstrained smartphones. The proposed system selects user heading estimation scheme based on continuous motion states detection and classification results. The basic idea of the motion state detection and discrimination method is to exploit their distinguishable acceleration and device attitude changing patterns. The attitude changing patterns include the accumulated pitch and roll angles, the horizontal device heading change angles, which can be derived from a continuous device attitude tracking model. For practical smartphone uses, we assume that position transition and user turn cannot occur simultaneously. Similar assumption is given to hand movement and user turn motion states. The assumptions are reasonable for the following two reasons. First, the probability of both motion states happening is rather low when the probability of each motion state is low. Second, requiring device carrying position transitions or significant hand movements when a user turn occurs is unnatural and also complicated for pedestrians.

For heading estimation scheme selection, during normal walking without any special motion state detected, we deploy our previous RMPCA approach, since the fundamental assumption of PCA-based approach still holds. If random hand movements or carrying position transitions are detected, the user heading is assumed to be smooth and calculated by averaging heading estimation results of the neighboring normal walking steps. If user turns are detected, the user heading is obtained by adding horizontal heading change to previous user heading. Besides, to avoid introducing estimation errors caused by undetected hand movements, the estimation results are further smoothed by an outlier filtering algorithm.

In order to describe the heading estimation problem, we define two coordinate systems, namely, global coordinate system (GCS) and device coordinate system (DCS). GCS is defined by three axes X_G, Y_G, and Z_G of the Earth coordinate system, which point east, north, and in the opposite direction of the gravity vector. User heading estimation problem can be considered as seeking walking direction expressions at GCS. All raw inertial signals including acceleration and angular velocity samples are initially measured at DCS. DCS is defined by axes X_D, Y_D, and Z_D. The axis X_D points rightward and Y_D points forward, while both axes are parallel with the device screen. The axis Z_D points outside of the screen and is the cross-product of X_D and Y_D.

In this work, we only investigate the most common four device carrying positions [17–20], namely, held in hand (hand-held), against ear during phone call (phone-call), placed in trouser pocket (in-pocket), and swinging in hand (swinging-hand). For pedestrian activities, we only consider two situations, namely, normal walking and standing, which may be easily recognized by their different acceleration patterns [14, 15]. For simplicity, we assume that the two activities are already accurately recognized.

3. Detection and Classification of the Three Special Motion States

Three special motion states, namely, hand movements, carrying position transitions, and user turns, may render the fundamental assumption of PCA-based approaches seriously corrupted. Therefore, we develop detection and classification method of the three motion states, as seen in Figure 2. We collect acceleration signals from an accelerometer and obtain the device attitude data from a continuous device attitude tracking model, which will be presented in Section 4.1. Then, the collected data are divided into small segments for subsequent detection and discrimination by a sliding window. We select a window twice the size of user walking step period, with 50% overlap between consecutive windows, which is appropriate for detecting and discriminating the motion states accurately and timely.

As shown in Figure 2, four parameters, namely, accumulated absolute acceleration change ΔAcc, device heading change ΔYaw, accumulated absolute pitch angle change ΔPitch, and accumulated absolute roll angle change ΔRoll, are calculated as follows:

$$\Delta\text{Acc} = \sum_{i=1}^{N_A-1} \left(\left| Acc_x\left(i+1\right) - Acc_x\left(i\right) \right| \right.$$
$$\left. + \left| Acc_y\left(i+1\right) - Acc_y\left(i\right) \right| \right. \tag{1}$$
$$\left. + \left| Acc_z\left(i+1\right) - Acc_z\left(i\right) \right| \right)$$

$$\Delta\text{Pitch} = \sum_{i=1}^{N_P-1} \left(\left| Pitch\left(i+1\right) - Pitch\left(i\right) \right| \right) \tag{2}$$

$$\Delta\text{Roll} = \sum_{i=1}^{N_R-1} \left(\left| Roll\left(i+1\right) - Roll\left(i\right) \right| \right) \tag{3}$$

$$\Delta\text{Yaw} = Yaw\left(EndTime\right) - Yaw\left(StartTime\right) \tag{4}$$

where $Acc_x(i)$, $Acc_y(i)$, $Acc_z(i)$ are the ith measured three dimensional acceleration signals at DCS; $Pitch(i)$ and $Roll(i)$ are the ith pitch and roll angle values of smartphone at GCS as seen in (13) in Section 4.1; and $Yaw(StartTime)$ and $Yaw(EndTime)$ are the yaw values of smartphone at GCS at the start time and end time of a sliding window as seen in (13).

After obtaining the four parameters, we start to deploy them to detect and discriminate the three special motion states by comparing the parameters with related threshold values. Firstly, we detect and recognize the position transition motion by exploiting the significant acceleration change patterns. Figure 3 shows a classical example of acceleration signals when position transitions occur during a pair of device carrying positions. Clearly, all kinds of position transitions consist of substantial acceleration change over three dimensions. Moreover, the acceleration changes are significantly larger than those of normal walking, user turn motion states, and most hand movements with a relatively small magnitude. This may be contributed to two reasons. First, position transitions involve significant relative displacement and subsequently introduce extra acceleration. Second, the subcomponents of the gravity vector added on the three axes are changing all the time due to the changing device attitude. Therefore, we set a threshold value for the accumulated absolute acceleration change ΔAcc, denoted as Th(ΔAcc). When the accumulated absolute acceleration change exceeds the threshold value, a position transition is assumed to occur. To avoid false detection, we deploy the Random Forest based carrying position classifier proposed in [16], to confirm if the carrying position is changed. The carrying position classifier selects statistics of mean, variance, maximum, and minimum over windowed acceleration samples as input features. For detailed information about the carrying position classifier, please see [16]. If a position transition does not occur and the carrying position is not in-pocket, hand movement with a large magnitude is detected.

Secondly, after excluding the position transition motion state, we detect and discriminate the remaining two motion states. We observe that the user turns only render device heading change in the horizontal plane, while most hand movements may introduce significant roll and pitch angle changes. Therefore, we set threshold values for the accumulated absolute pitch angle change ΔPitch and accumulated absolute roll angle change ΔRoll, denoted as Th(ΔPitch) and Th(ΔRoll), respectively. When the accumulated absolute pitch angle or roll angle change exceeds the related threshold values, respectively, and the carrying position is not in-pocket, a hand movement is assumed to occur.

Finally, if both carrying position transitions and hand movements are excluded, we may infer that a user turn occurs when the device heading change ΔYaw exceeds a predefined threshold value Th(ΔYaw). Otherwise, no special motion state is detected. The heading estimation is achieved by RMPCA approach. Generally, the choice of an appropriate threshold value is different for various device carrying positions. For in-pocket and swinging-hand positions, the threshold values are usually significantly larger than those
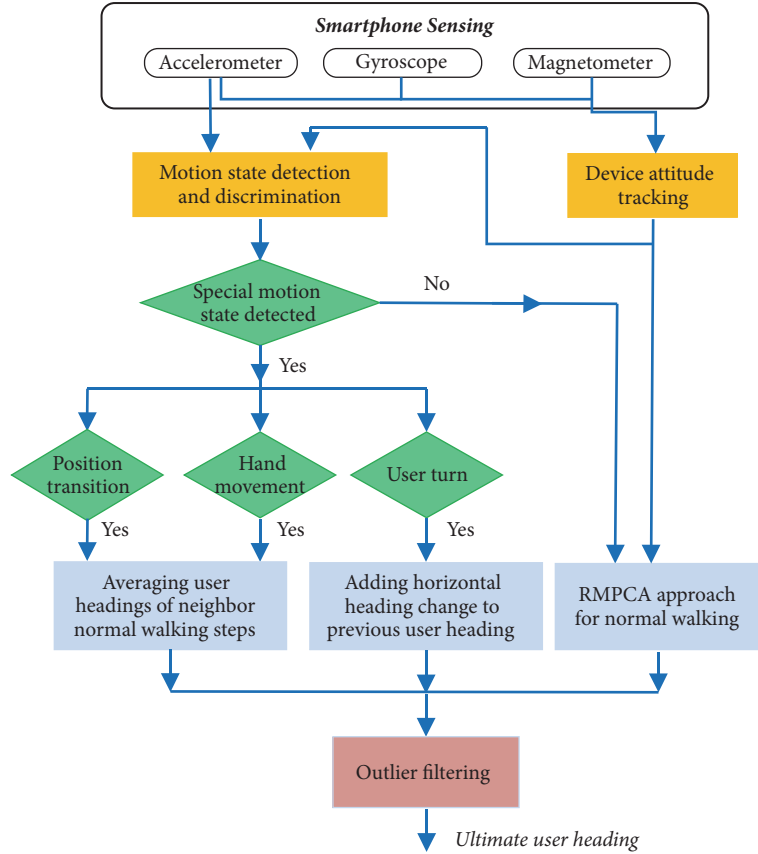
FIGURE 1: Architecture of the proposed robust heading estimation system.

of hand-held and phone-call positions, due to a stronger intensity of the body locomotion.

It should be noted that two false situations may happen, though their probabilities are rather low. One is that a hand movement may be missed, when it only introduces extra acceleration in the horizontal plane, and have little impacts on the pitch angles and yaw angles. Another false situation is that a hand movement may be misclassified as a user turn, when it only renders device heading change in the horizontal plane, and have little impacts on the pitch angles and yaw angles. Fortunately, large heading estimation errors caused by the two false situations may be avoided by an outlier filtering algorithm, which will be given in Section 4.3.

4. User Heading Estimation

The proposed user heading estimation approach consists of three strategies: an average of heading estimations of the neighboring normal walking steps, adding horizontal heading change to user heading of previous step, and RMPCA approach. Upon the detected and discrimination results of three special motion states, the most suitable strategy is selected for heading estimation, as seen in Figure 1. The first strategy is selected when hand movements or carrying position transitions are detected, while the second strategy is employed when user turns occur. During normal walking,

RMPCA approach is used as the last strategy. Besides, to avoid heading estimation errors caused by undetected hand movements, the estimation results of RMPCA are further smoothed by an outlier filtering algorithm.

Two basic assumptions are used for heading estimation. First, the initial heading offset between user heading and device forward heading is zero, since users need to hold device in hand and gaze at it when they start the localization application. Second, the initial user heading and related device attitude are assumed to be known a priori [21, 22], which can be obtained by Global Position System (GPS) tracking when the user enters a building, landmarks, or WiFi localization.

For both RMPCA approach and three special motion states detection, continuous device attitude information is required. Therefore, we firstly present the device attitude tracking model based on quaternions in Section 4.1. Then, we describe the heading estimation strategies in detail in Section 4.2. An outlier filtering algorithm is developed in Section 4.3.

4.1. Attitude Tracking Model. An Extended Kalman Filter (EKF) is employed to fuse the inertial sensors and magnetometer for device attitude tracking. We deploy the quaternion [23, 24] to describe device attitude tracking model, since it can avoid the singularity problems. The relationship
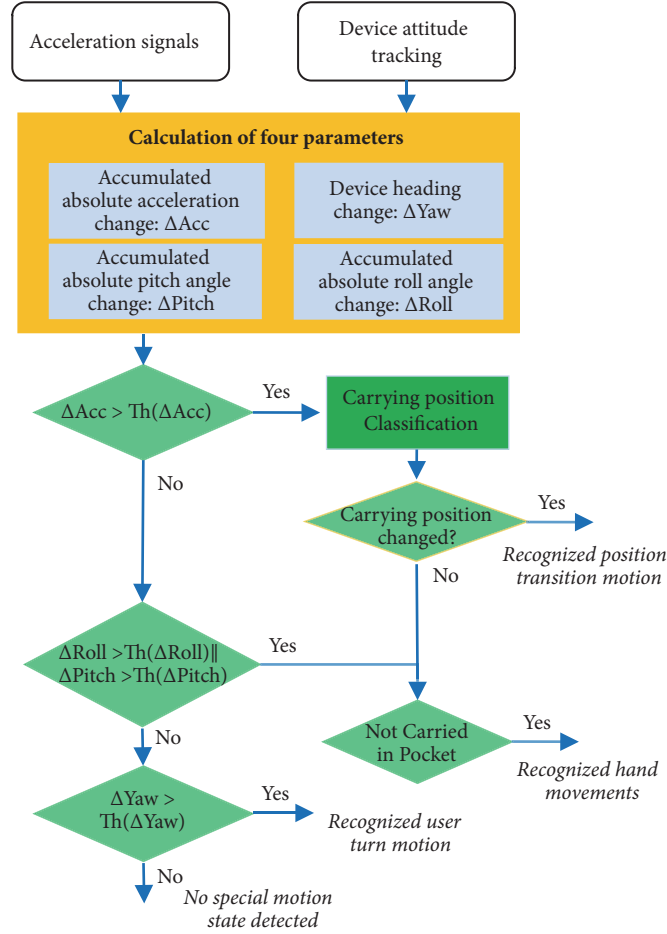
FIGURE 2: Flowchart of the proposed three motion states detection and classification method.

between GCS and real-time device attitude is constructed by the quaternion vector and related rotation matrix. The rotation matrix may transform any inertial signals represented at GCS into DCS as follows:

$$\mathbf{h}^{DCS}(t) = \left(\mathbf{R}_{GCS}^{DCS}(\mathbf{q}(t))\right)^T \mathbf{h}^{GCS}(t) \qquad (5)$$

where $\mathbf{R}_{GCS}^{DCS}(\mathbf{q}(t))$ is the rotation matrix of DCS corresponding to GCS at time t and $\mathbf{h}^{GCS}(t)$ and $\mathbf{h}^{DCS}(t)$ are the same 3×1 vectors represented at GCS and DCS, respectively. We may establish the one to one mapping relationship between rotation matrix and a quaternion vector:

$$\mathbf{R}_{GCS}^{DCS}(\mathbf{q})$$

$$= \begin{bmatrix} q_0^2 + q_1^2 - q_2^2 - q_3^2 & 2(q_1q_2 - q_0q_3) & 2(q_1q_3 + q_0q_2) \\ 2(q_1q_2 + q_0q_3) & q_0^2 - q_1^2 + q_2^2 - q_3^2 & 2(q_2q_3 - q_0q_1) \\ 2(q_1q_3 - q_0q_2) & 2(q_0q_1 + q_2q_3) & q_0^2 - q_1^2 - q_2^2 + q_3^2 \end{bmatrix} \qquad (6)$$

where $\mathbf{q} = \begin{bmatrix} q_0 & q_1 & q_2 & q_3 \end{bmatrix}^T$ is the normalized quaternion vector with the scalar part q_0 and the vector part $\begin{bmatrix} q_1 & q_2 & q_3 \end{bmatrix}^T$, and the parameter t is omitted for simplicity.

For device attitude estimation, we firstly construct the state equation of EKF. Based on the kinematic law of rigid

body [24], the discrete-time state model of quaternions is given by

$$\mathbf{q}_{k+1} = \exp\left(0.5 \times \Omega\left(\mathbf{w}_k T_s\right)\right) \mathbf{q}_k$$

$$= \left(\mathbf{I}\cos\left(0.5 \times \Delta\theta_k\right) + \frac{\Omega\left(\mathbf{w}_k T_s\right)\sin\left(0.5 \times \Delta\theta_k\right)}{\Delta\theta_k}\right)\mathbf{q}_k \qquad (7)$$

where $\mathbf{q}_k$ and $\mathbf{q}_{k+1}$ are the quaternion vectors at time instants kT_s and $(k + 1)T_s$, T_s is the time interval of state model, $\mathbf{w}_k = \begin{bmatrix} w_k^x & w_k^y & w_k^z \end{bmatrix}^T$ is the raw angular velocity vector measured at DCS, $\mathbf{I}$ is an 3×3 identity matrix, $\Delta\theta_k = T_s\sqrt{(w_k^x)^2 + (w_k^y)^2 + (w_k^z)^2}$, and $\Omega(\mathbf{w}_k T_s)$ is given by

$$\Omega\left(\mathbf{w}_k T_s\right) = T_s \begin{bmatrix} 0 & -w_k^x & -w_k^y & -w_k^z \\ w_k^x & 0 & w_k^z & -w_k^y \\ w_k^y & -w_k^z & 0 & w_k^x \\ w_k^z & w_k^y & -w_k^x & 0 \end{bmatrix}. \qquad (8)$$

In order to construct the state equation of EKF, we deploy a first order linearized approximation of the state model:

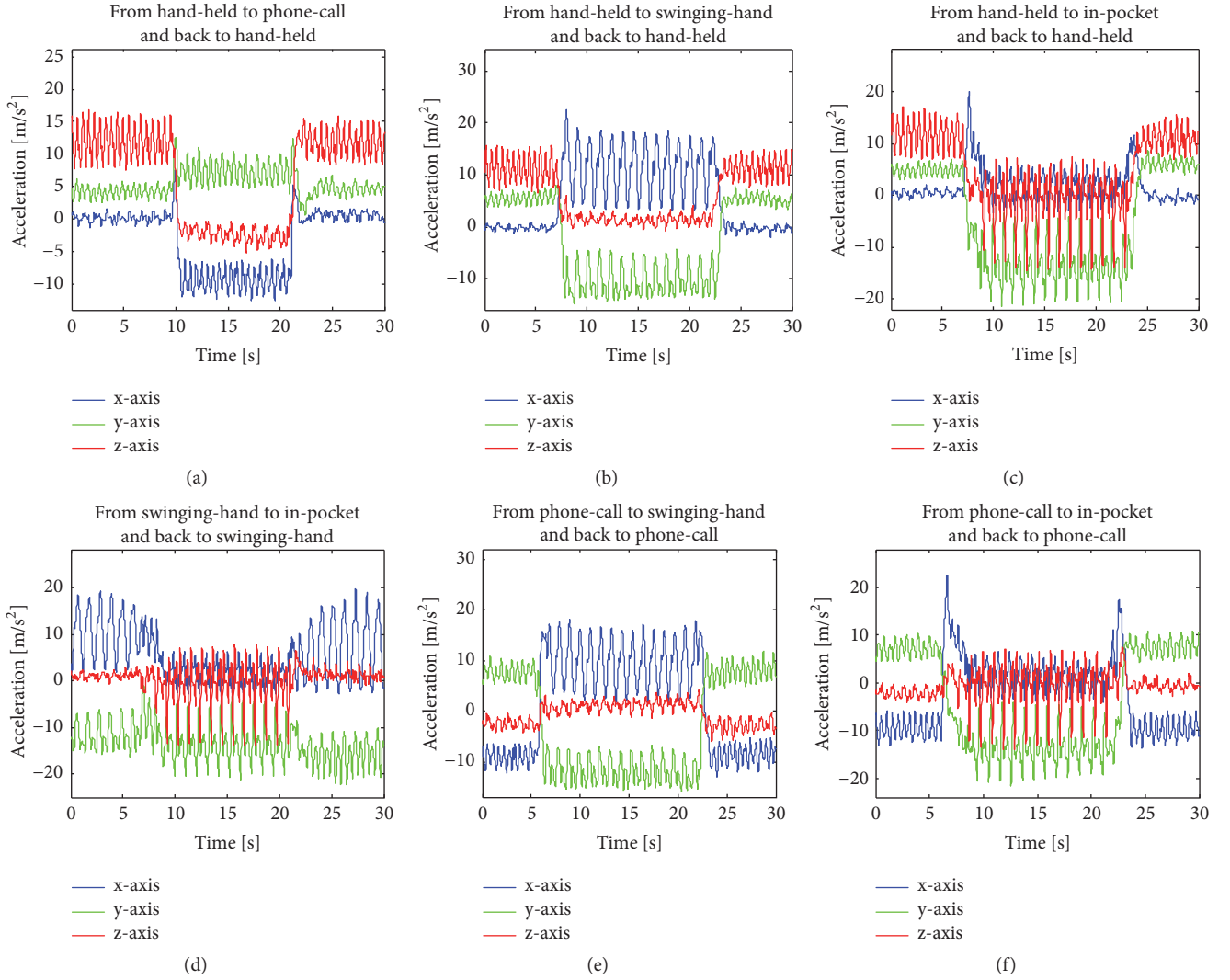$$\mathbf{q}_{k+1} = F_k\mathbf{q}_k + \mathbf{w}_k^q \qquad (9)$$

FIGURE 3: A typical example of acceleration signals when position transitions occur during a pair of device carrying positions: (a) hand-held and phone-call; (b) hand-held and swinging-hand; (c) hand-held and in-pocket; (d) swinging-hand and in-pocket; (e) phone-call and swinging-hand; (f) phone-call and in-pocket.

where the linearized transition matrix $F_k = \exp(0.5 \times \Omega(\mathbf{w}_k T_s))$, and

$$\mathbf{w}_k^q = \Xi_k \mathbf{w}_k^{gyro} = -\frac{T_s}{2} \begin{bmatrix} [\mathbf{e}_k \times] + q_0^k \mathbf{I} \\ -\mathbf{e}_k^T \end{bmatrix} \mathbf{w}_k^{gyro} \qquad (10)$$

where q_0^k and $\mathbf{e}_k = \begin{bmatrix} q_1^k & q_2^k & q_3^k \end{bmatrix}^T$ are the scalar and vector parts of the quaternion vector $\mathbf{q}_k$, $\mathbf{w}_k^{gyro}$ is the white Gaussian noise of gyroscope outputs, and $[\mathbf{e}_k \times]$ is a standard vector cross-product operator. The real-time quaternion vector is determined once the initial value of quaternion vector is known. Based on the two basic assumptions of our heading estimation approach, the related initial quaternion can be easily calculated by initial user heading and device attitude that are already known.

Then, we construct the measurement model of EKF based on the observed acceleration and magnetic field samples measured at DCS:

$$\mathbf{z}_{k+1} = \begin{bmatrix} \mathbf{a}_{k+1} \\ \mathbf{m}_{k+1} \end{bmatrix} = \phi(\mathbf{q}_{k+1}) + \mathbf{v}_{k+1}$$

$$= \begin{bmatrix} \left(\mathbf{R}_{GCS}^{DCS}(\mathbf{q}_{k+1})\right)^T & \mathbf{0} \\ \mathbf{0} & \left(\mathbf{R}_{GCS}^{DCS}(\mathbf{q}_{k+1})\right)^T \end{bmatrix} \begin{bmatrix} \mathbf{g} \\ \mathbf{h} \end{bmatrix} \qquad (11)$$

$$+ \begin{bmatrix} \mathbf{v}_{k+1}^a \\ \mathbf{v}_{k+1}^m \end{bmatrix}$$

where $\mathbf{a}_{k+1}$ and $\mathbf{g}$ are the observed acceleration sample at DCS and related gravity vector sample at GCS, $\mathbf{m}_{k+1}$ and $\mathbf{h}$ are the observed magnetic field sample at DCS and related magnetic

field sample at GCS, and $\mathbf{v}_{k+1}^a$ and $\mathbf{v}_{k+1}^m$ are the white Gaussian measurement noise of the acceleration and magnetic field values. The covariance matrices of the acceleration and magnetic field values are set according to [25], respectively.

In order to construct the measurement equation of EKF, we linearize the nonlinear function $\phi(\cdot)$ in (11) by computing the related Jacobian matrix:

$$H_{k+1} = \frac{\partial}{\partial \mathbf{q}_{k+1}} \phi \left(\mathbf{q}_{k+1} \right) \bigg|_{\mathbf{q}_{k+1} = \mathbf{q}_{k+1}^-} \tag{12}$$

where $\mathbf{q}_{k+1}^- = F_k \widehat{\mathbf{q}}_k$ is a priori state estimate of the unavailable true state $\mathbf{q}_{k+1}$ and $\widehat{\mathbf{q}}_k$ is the EKF estimation result of the state available at the previous time instant.

According to the state equation (9), measurement equation (11), and related parameters, the EKF model for estimating the real-time quaternion vector is constructed. Detailed procedures for executing the EKF model may be found in [26]. Therefore, the real-time device attitude tracking is achieved. We may calculate the real-time device yaw, pitch, and roll values at GCS as follows:

$$yaw = \arctan \left(\frac{2 \left(q_0 q_3 - q_1 q_2 \right)}{\left(q_0^2 - q_1^2 + q_2^2 - q_3^2 \right)} \right)$$

$$pitch = \arcsin \left(2 \left(q_2 q_3 + q_0 q_1 \right) \right) \tag{13}$$

$$roll = \arctan \left(\frac{2 \left(q_0 q_2 - q_1 q_3 \right)}{\left(q_0^2 - q_1^2 - q_2^2 + q_3^2 \right)} \right).$$

4.2. Heading Estimation Strategy Selection. During normal walking, we deploy RMPCA approach for heading estimation. User heading is estimated step by step. The walking steps are detected by a classic peak detection algorithm [27–29], which recognizes the peak acceleration caused by the unique heel strike during each walking step. We firstly project all acceleration within a walking step measured at DCS into GCS.

$$\mathbf{ACC}_{GCS} (t) = \mathbf{R}_{GCS}^{DCS} \left(\mathbf{q} (t) \right) \mathbf{ACC}_{DCS} (t) \tag{14}$$

where $\mathbf{ACC}_{GCS}(t) = \left[ACC_{GCS}^x (t) \ \ ACC_{GCS}^y (t) \ \ ACC_{GCS}^z (t) \right]^T$ is the acceleration sample represented at GCS at time t, $\mathbf{ACC}_{DCS}(t)$ is the related acceleration sample measured at DCS, and $\mathbf{R}_{GCS}^{DCS}(\mathbf{q}(t))$ is the related rotation matrix between GCS and DCS. All acceleration samples at GCS in the horizontal plane can be given as

$$\mathbf{HACC}_{GCS} (i) = \left[ACC_{GCS}^x (i) \ \ ACC_{GCS}^y (i) \right]^T,$$
$$i = 1, \ldots, N_{Acc} \tag{15}$$

where N_{Acc} is the number of acceleration samples within the walking step and $\mathbf{HACC}_{GCS}(i)$ is the ith acceleration sample in the horizontal plane. Then, we deploy PCA and extract the first eigenvector of the N_{Acc} acceleration samples in the horizontal plane as the ultimate global walking direction vector $\mathbf{WD}_{GCS} = \left[WD_{GCS}^x \ \ WD_{GCS}^y \right]^T$. The ambiguity problem of PCA [30] can be solved by exploiting the phase relationship

between the user walking direction and the vertical acceleration [13]. The ultimate user heading estimation ψ_{user} can be given as follows:

$$\psi_{user} = \arctan \left(\frac{WD_{GCS}^y}{WD_{GCS}^x} \right) - \frac{\pi}{2}. \tag{16}$$

For more details about RMPCA, we refer readers to our previous work [13].

When three special motion states are detected, extra acceleration may be introduced into the acceleration in the horizontal plane. Therefore, the principal component of the acceleration in the horizontal plane may deviate from the user walking direction. For example, when a hand movement occurs, the first eigenvector of PCA deviates from the walking direction and moves towards the hand movement direction. Similar observations may be seen when position transitions or user turns occur. Therefore, when hand movements or position transitions occur, instead of deploying RMPCA approach, we obtain the user heading by averaging user heading estimation of the neighbor K normal walking steps:

$$\psi_{user} (i) = \frac{\sum_{k=1}^{K/2} \left[\psi_{user} (i - k) + \psi_{user} (i + k) \right]}{K} \tag{17}$$

where $\psi_{user}(i)$ is the user heading of the ith walking step. Usually, without user turn, the user heading is smooth and setting K equal to four may obtain a reasonable heading estimation result.

When user turn occurs, we calculate the user heading of current walking step by adding user heading change to user heading of previous walking step. The horizontal device heading change is computed by the yaw angle change at GCS:

$$\delta\theta = \sum_{k=1}^{N_{gyro}} w_{GCS}^Z (k) T_{gyro} \tag{18}$$

where $\delta\theta$ is the horizontal device heading change within one walking step, $w_{GCS}^Z(k)$ is the kth angular velocity component rotating around Z_G at GCS, N_{gyro} is the total number of angular velocity samples within the step, T_{gyro} is the related sampling interval. The angular velocity sample at GCS can be obtained by angular velocity sample measured at DCS and the related rotation matrix as follows:

$$\mathbf{w}_{GCS} (t) = \mathbf{R}_{GCS}^{DCS} \left(\mathbf{q} (t) \right) \mathbf{w}_{DCS} (t) \tag{19}$$

where $\mathbf{w}_{GCS}(t)$ is the angular velocity sample vector with respect to GCS at time t, $\mathbf{w}_{DCS}(t)$ is the related sample at DCS, and $\mathbf{R}_{GCS}^{DCS}(\mathbf{q}(t))$ is the related rotation matrix.

4.3. Outlier Filtering for Heading Estimation Results. This section describes a postprocessing outlier filtering algorithm to remove the outliers caused by undetected hand movements. This fault situation can be divided into two classes. The first class is that a hand movement motion state is undetected and recognized as a normal walking state. The second class is that a hand movement state is misclassified as a user turn. During normal walking without significant user turns, the heading
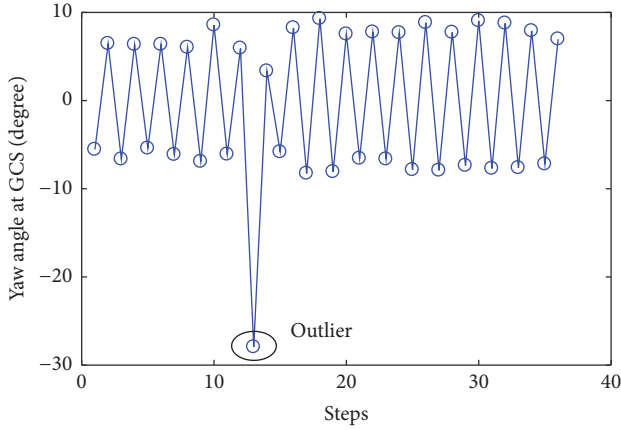
FIGURE 4: Illustration of an outlier among user heading estimations of RMPCA approach.
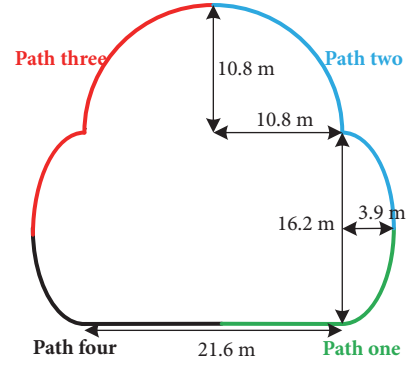

FIGURE 5: Walking path of test environment consists of one straight line, two symmetric parabolas, and a half circle and is divided into four subpaths by different colors. Figure 5 is reproduced from Deng, Z.A. et al. (2016) in [16] [under the Creative Commons Attribution License/public domain].

estimation results of RMPCA are smooth and do not change significantly compared with neighbor steps. If a user turn occurs, the user heading of current walking step may vary significantly from that of the previous step, being close to that of the next step without the user turn. In contrast, if an undetected hand movement occurs, the heading estimation result may vary significantly from the heading estimation results of both the previous step and the next step, as shown in Figure 4. Therefore, from the above observations, we develop an outlier filtering algorithm to detect the fault situation by comparing the difference values of heading estimation results between adjacent walking steps. If one heading estimation result is significantly larger (smaller) than previous walking step and smaller (larger) than the next walking step and the two difference values exceed related threshold values, an outlier is detected and removed. Then, we correct the user heading by averaging the estimation results of the adjacent normal walking steps.

5. Evaluation

5.1. Experimental Setup. We performed the user heading estimation experiments in indoor test environments, as seen in Figure 5. In order to test the heading estimation performance of both straight and nonstraight walking paths, the test environment consisted of two symmetric parabolas, one straight line and a half circle, whose total length was 76.9 m. Four subjects participated in the experiments with a smartphone. Before each experimental run, each subject initially held the phone in hand for few seconds to start the developed user heading estimation application. We also did all necessary calibrations to make the measurement outputs of all inertial sensors built in the smartphone as precise as possible. As in many other works [31, 32], we assume that the initial user heading was known. To label the ground truth, we also applied a camera to record the entire walking path of each subject. The user heading estimations were obtained and compared with the true values for each walking step.

In order to study the classification accuracy performance of the proposed detection and discrimination algorithm, each subject walked along the path with one hundred walking steps, including seventy steps for normal walking and the remaining steps for one of the three special motion states with an equal quantity. Each subject repeated the procedure ten times.

In order to study the effects of three special motion states on heading estimation accuracy individually, we compare the heading estimation errors between RMPCA and the proposed robust heading estimation approach when each special motion state occurs individually. For hand movements, various kinds of hand locomotion with different magnitudes were performed during walking steps. For carrying position transitions, we performed all twelve kinds of position transitions between four classic device carrying positions. For user turns, we performed user turns varying from 20 degrees to 180 degrees. Each special motion state was carried out one thousand times. We assume that each special motion state is surrounded by normal walking steps during practical pedestrian walking.

5.2. Classification Accuracy Results. Table 1 shows the classification results of the proposed three motion states detection and discrimination algorithm. The results show that the proposed detection and discrimination algorithm can classify all three special motion states with high accuracy. An averaged classification accuracy of 97.6% is obtained for the three special motion states. For hand movements, though the probability is rather low, some hand movements may involve small pitch and roll angle changes, while the yaw angle changes exceed the threshold. Therefore, this kind of hand movements may be misclassified as the user turns. Fortunately, these fault situations may not finally affect the user heading estimation performance, since the negative effects may be eliminated by the following outlier filtering algorithm of the proposed user heading estimation approach. For carrying position transitions, the accumulated absolute acceleration changes are always large enough to distinguish them from the other motion states. The confusion between position transitions and the other motion states can be neglected.

TABLE 1: Confusion table of the proposed motion states detection and discrimination algorithm.

	Hand movement	Position transition	User turn	Normal walking
Hand movement	0.952	0	0.018	0.03
Position transition	0.007	0.988	0.005	0
User turn	0	0.011	0.989	0
Normal walking	0.005	0	0	0.995
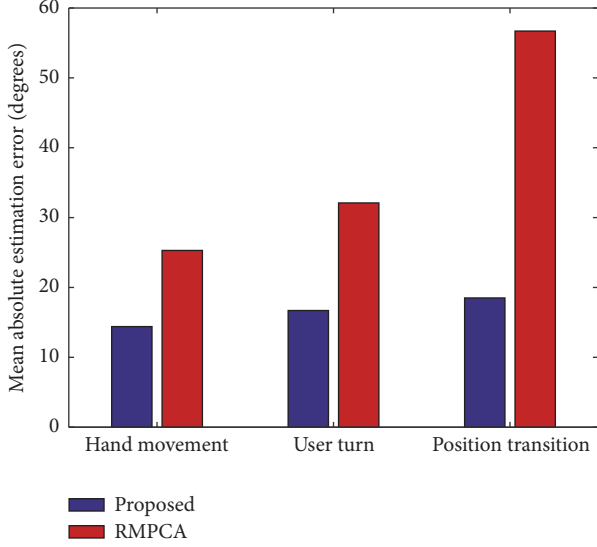
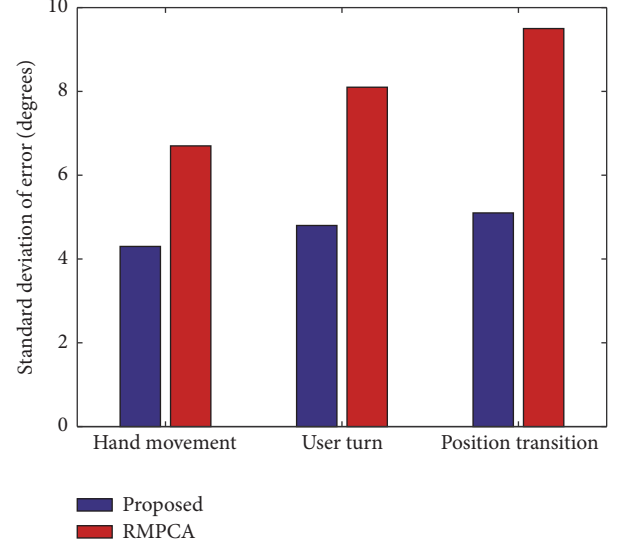FIGURE 6: Mean absolute heading estimation errors of the proposed approach and RMPCA when each special motion state occurs individually.

FIGURE 7: Standard deviation of absolute heading estimation errors of the proposed approach and RMPCA when each special motion state occurs individually.

5.3. Heading Estimation Results. Figures 6 and 7 show the mean and standard deviation of absolute estimation errors of RMPCA approach and the proposed approach. The heading estimation errors were calculated over the walking steps when the special motion states occurred. Compared with RMPCA approach, the proposed approach reduces the mean absolute estimation error by 43.1 percent (10.9 degrees), 48.0 percent (15.4 degrees), and 67.4 percent (38.2 degrees), for hand movement, user turn, and position transition motion states, respectively. Compared with RMPCA approach, the proposed approach reduces the standard deviation of absolute estimation error by 35.8 percent (2.4 degrees), 40.7 percent (3.3 degrees), and 46.3 percent (4.4 degrees), for hand movement, user turn, and position transition motion states, respectively. Significant absolute heading estimation error reduction can be achieved by the proposed robust heading estimation approach. Among three special motion states, the error reduction of the position transition motion state is the largest, since the extra acceleration signals introduced by a position transition motion are always significantly larger than those of the other two motion states. For the proposed robust heading estimation approach, when three special motion states are detected and accurately discriminated, an appropriate heading estimation scheme is selected rather than using RMPCA.

Furthermore, we study the overall heading estimation accuracy of the proposed robust heading estimation approach

with all three special motion states involved. The subject walked along the whole walking path, which is divided into four subpaths by different colors, as seen in Figure 5. The device carrying position was transited into another position of the remaining ones with equal probability once the subpath changed. The whole walking path required about 128 walking steps for each subject. Each subject consciously did random hand movements for fifteen times over the whole walking path. They repeated the procedure for twenty times. We performed user heading estimations over each walking step, and then a total number of more than ten thousand samples can be used. We also carried out and compared the proposed approach without outlier filtering, RMPCA approach [13], and uDirect approach [11].

Figure 8 shows the cumulative error distribution of the compared heading estimation approaches. As seen in Figure 8, the 75th percentile absolute error of the proposed approach is 13.8 degrees, while those of the proposed approach without outlier filtering, RMPCA, and uDirect are 14.2, 26.2, and 34.4 degrees, respectively. The 90th percentile absolute error of the proposed approach is 24.9 degrees, while those of the proposed approach without outlier filtering, RMPCA, and uDirect are 28.1, 42.7, and 54.9 degrees, respectively. As seen in Figure 9, compared with the proposed approach without outlier filtering, RMPCA approach, and uDirect approach, the proposed approach reduces the mean absolute estimation error by 13.9 percent (1.5 degrees), 46.9
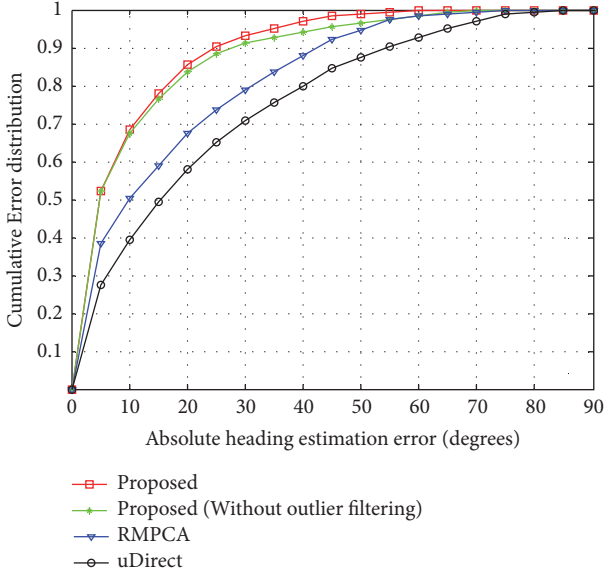
FIGURE 8: Comparisons of absolute heading estimation error distributions with all three special motion states involved in the experiments.
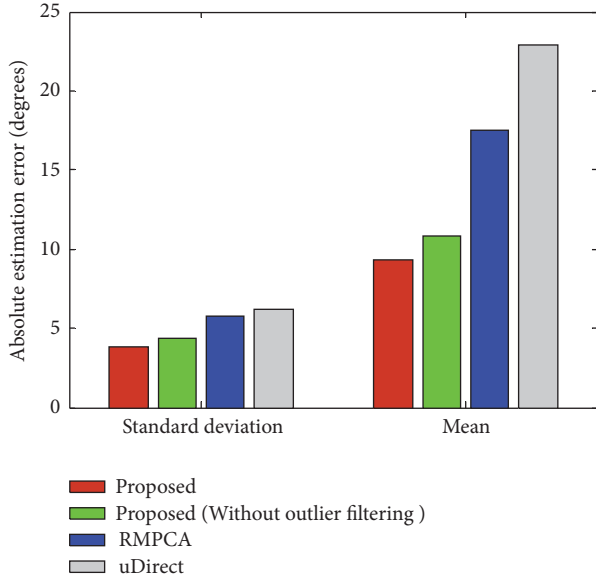

FIGURE 9: Comparisons of mean and standard deviation of absolute heading estimation errors with all three special motion states involved in the experiments.

percent (8.2 degrees), and 59.4 percent (13.6 degrees), respectively. For standard deviation of absolute estimation error, the proposed approach reduces it by 13.6 percent (0.6 degrees), 34.5 percent (2.0 degrees), and 38.7 percent (2.4 degrees), respectively.

The proposed approach achieves more significant heading estimation accuracy improvement than the compared approaches. This is because, when three special motion states occur, the proposed approach may detect and discriminate them accurately and timely and then select the related suitable heading estimation strategy. The traditional RMPCA and

uDirect approaches may render large heading estimation errors, since extra acceleration caused by irregular body locomotion may violate the fundamental assumptions of traditional approaches. However, these large heading estimation errors may be always avoided by the proposed approach. If one of the three special motion states is detected, related optimal heading estimation strategy will be carried out. For hand movements and position transitions, the user heading estimations are obtained by averaging heading estimation results of the neighboring normal walking steps. For user turns, the user headings are estimated by adding the yaw angle change to the user heading of the previous step. Besides, the outlier filtering algorithm may also improve the heading estimation accuracy slightly, since the outliers of heading estimations can be removed.

6. Conclusions

This paper proposes a robust user heading estimation approach adapting three special motion states, namely, rand hand movements, position transitions, and user turns. When these three motion states occur, the traditional approaches exploiting acceleration patterns may render large heading estimation errors. Therefore, we firstly develop the motion state detection and discrimination algorithm to determine the special motion state. Then, the most suitable strategy is selected for user heading estimation. Finally, an outlier filtering algorithm is developed to smooth the user heading estimation results. Experimental results show that the proposed robust heading estimation approach may improve the user heading estimation accuracy significantly. Compared with RMPCA and uDirect approaches, the proposed approach reduces the mean absolute user heading estimation error by 46.9 percent (8.2 degrees) and 59.4 percent (13.6 degrees), respectively.

Data Availability

The authors confirmed that the data supporting the findings of this study were available within the article.

Conflicts of Interest

The authors declare no conflicts of interest.

Acknowledgments

References

[1] M. Zhou, Y. Tang, Z. Tian, L. Xie, and W. Nie, "Robust neighborhood graphing for semi-supervised indoor localization with light-loaded location fingerprinting," *IEEE Internet of Things Journal*, 2017.

[2] Y. Sun, W. Meng, C. Li, N. Zhao, K. Zhao, and N. Zhang, "Human localization using multi-source heterogeneous data in indoor environments," *IEEE Access*, vol. 5, pp. 812–822, 2017.

[3] D. Zou, W. Meng, S. Han, K. He, and Z. Zhang, "Toward ubiquitous LBS: Multi-radio localization and seamless positioning," *IEEE Wireless Communications Magazine*, vol. 23, no. 6, pp. 107–113, 2016.

[4] M. Jia, X. Gu, Q. Guo, W. Xiang, and N. Zhang, "Broadband hybrid satellite-terrestrial communication systems based on cognitive radio toward 5G," *IEEE Wireless Communications Magazine*, vol. 23, no. 6, pp. 96–106, 2016.

[5] M. Zhou, Y. Tang, Z. Tian, and X. Geng, "Semi-supervised learning for indoor hybrid fingerprint database calibration with low effort," *IEEE Access*, vol. 5, no. 1, pp. 4388–4400, 2017.

[6] M. Zhou, Y. Tang, W. Nie, L. Xie, and X. Yang, "GrassMA: graph-based semi-supervised manifold alignment for indoor WLAN localization," *IEEE Sensors Journal*, vol. 17, no. 21, pp. 7086–7095, 2017.

[7] P. Zhang, Q. Zhao, Y. Li, X. Niu, Y. Zhuang, and J. Liu, "Collaborative WiFi fingerprinting using sensor-based navigation on smartphones," *Sensors*, vol. 15, no. 7, pp. 17534–17557, 2015.

[8] Z. Xiao, H. Wen, A. Markham, and N. Trigoni, "Robust indoor positioning with lifelong learning," *IEEE Journal on Selected Areas in Communications*, vol. 33, no. 11, pp. 2287–2301, 2015.

[9] H. Lee, J. Lee, J. Cho, and N. Chang, "Estimation of heading angle difference between user and smartphone utilizing gravitational acceleration extraction," *IEEE Sensors Journal*, vol. 16, no. 10, pp. 3746–3755, 2016.

[10] Z.-A. Deng, Y. Hu, J. Yu, and Z. Na, "Extended Kalman filter for real time indoor localization by fusing WiFi and smartphone inertial sensors," *Micromachines*, vol. 6, no. 4, pp. 523–543, 2015.

[11] S. A. Hoseinitabatabaei, A. Gluhak, R. Tafazolli, and W. Headley, "Design, realization, and evaluation of uDirect-An approach for pervasive observation of user facing direction on mobile phones," *IEEE Transactions on Mobile Computing*, vol. 13, no. 9, pp. 1981–1994, 2014.

[12] U. Steinhoff and B. Schiele, "Dead reckoning from the pocket - An experimental study," in *Proceedings of the 8th IEEE International Conference on Pervasive Computing and Communications (PerCom '10)*, vol. 60, pp. 162–170, April 2010.

[13] Z.-A. Deng, G. Wang, Y. Hu, and D. Wu, "Heading estimation for indoor pedestrian navigation using a smartphone in the pocket," *Sensors*, vol. 15, no. 9, pp. 21518–21536, 2015.

[14] S. Saeedi and N. El-Sheimy, "Activity recognition using fusion of low-cost sensors on a smartphone for mobile navigation application," *Micromachines*, vol. 6, no. 8, pp. 1100–1134, 2015.

[15] T. O. Oshin, S. Poslad, and Z. Zhang, "Energy-efficient real-time human mobility state classification using smartphones," *IEEE Transactions on Computers*, vol. 64, no. 6, pp. 1680–1693, 2015.

[16] Z.-A. Deng, G. Wang, Y. Hu, and Y. Cui, "Carrying position independent user heading estimation for indoor pedestrian navigation with smartphones," *Sensors*, vol. 16, no. 5, 2016.

[17] Y. Li, J. Georgy, X. Niu, Q. Li, and N. El-Sheimy, "Autonomous calibration of MEMS gyros in consumer portable devices," *IEEE Sensors Journal*, vol. 15, no. 7, pp. 4062–4072, 2015.

[18] J. Qian, L. Pei, J. Ma, R. Ying, and P. Liu, "Vector graph assisted pedestrian dead reckoning using an unconstrained smartphone," *Sensors*, vol. 15, no. 3, pp. 5032–5057, 2015.

[19] M. Kourogi and T. Kurata, "A method of pedestrian dead reckoning for smartphones using frequency domain analysis on patterns of acceleration and angular velocity," in *Proceedings of the IEEE/ION Position, Location and Navigation Symposium (PLANS '14)*, vol. 19, pp. 164–168, IEEE, May 2014.

[20] F. Ichikawa, J. Chipchase, and R. Grignani, "Where's the phone? A study of mobile phone location in public spaces," in *Proceedings of the 2nd International Conference on Mobile Technology, Applications and Systems*, pp. 1–8, IEEE, November 2005.

[21] F. Li, C. Zhao, G. Ding, J. Gong, C. Liu, and F. Zhao, "A Reliable and accurate indoor localization method using phone inertial sensors," in *Proceedings of the 14th International Conference on Ubiquitous Computing*, pp. 421–430, ACM, September 2012.

[22] Y. Kim, Y. Chon, and H. Cha, *Smartphone-Based Collaborative and Autonomous Radio Fingerprinting*, IEEE Press, 2012.

[23] A. M. Sabatini, "Quaternion-based extended kalman filter for determining orientation by inertial and magnetic sensing," *IEEE Transactions on Bio-Medical Engineering*, vol. 53, no. 7, 2006.

[24] J. C. K. Chou, "Quaternion kinematic and dynamic differential equations," *IEEE Transactions on Robotics and Automation*, vol. 8, no. 1, pp. 53–64, 1992.

[25] Z. Tian, X. Fang, M. Zhou, and L. Li, "Smartphone-based indoor integrated WiFi/MEMS positioning algorithm in a multi-floor environment," *Micromachines*, vol. 6, no. 3, pp. 347–363, 2015.

[26] Y. Bar-Shalom, X. Li, and T. Kirubarajan, *Estimation with Applications to Tracking and Navigation*, John Wiley & Sons, New York, NY, USA, 2001.

[27] A. Brajdic and R. Harle, "Walk detection and step counting on unconstrained smartphones," in *Proceedings of the ACM International Joint Conference on Pervasive and Ubiquitous Computing (UbiComp '13)*, pp. 225–234, September 2013.

[28] S. He and S. G. Chan, "Wi-Fi fingerprint-based indoor positioning: recent advances and comparisons," *IEEE Communications Surveys & Tutorials*, vol. 18, no. 1, pp. 466–490, 2016.

[29] Z. Yang, C. Wu, Z. Zhou, X. Zhang, X. Wang, and Y. Liu, "Mobility increases localizability: a survey on wireless indoor localization using inertial sensors," *ACM Computing Surveys*, vol. 47, no. 3, article 54, pp. 1–34, 2015.

[30] K. Kunze, P. Lukowicz, K. Partridge, and B. Begole, "Which way am I facing: inferring horizontal device orientation from an accelerometer signal," in *Proceedings of the International Symposium on Wearable Computers (ISWC '09)*, pp. 149-150, IEEE Computer Society, September 2009.

[31] N. Mohssen, R. Momtaz, H. Aly, and M. Youssef, "Humaine: a ubiquitous smartphone-based user heading estimation for mobile computing systems," *GeoInformatica*, vol. 21, no. 3, pp. 519–548, 2017.

[32] P. Nguyen, T. Akiyama, H. Ohashi, G. Nakahara, K. Yamasaki, and S. Hikaru, "User-friendly heading estimation for arbitrary smartphone orientations," in *Proceedings of the International Conference on Indoor Positioning and Indoor Navigation (IPIN '16)*, pp. 1–7, IEEE, October 2016.

Research Article

Device-Free Wireless Localization Using Artificial Neural Networks in Wireless Sensor Networks

Yongliang Sun [iD],[1,2] **Xuzhao Zhang,**[2] **Xiaocheng Wang** [iD],[2] **and Xinggan Zhang**[1]

[1]*School of Electronic Science and Engineering, Nanjing University, Nanjing 210023, China*
[2]*College of Computer Science and Technology, Nanjing Tech University, Nanjing 211816, China*

Correspondence should be addressed to Xiaocheng Wang; njutwxc@163.com

Currently, localization has been one of the research hot spots in Wireless Sensors Networks (WSNs). However, most localization methods focus on the device-based localization, which locates targets with terminal devices. This is not suitable for the application scenarios like the elder monitoring, life detection, and so on. In this paper, we propose a device-free wireless localization system using Artificial Neural Networks (ANNs). The system consists of two phases. In the off-line training phase, Received Signal Strength (RSS) difference matrices between the RSS matrices collected when the monitoring area is vacant and with a professional in the area are calculated. Some RSS difference values in the RSS difference matrices are selected. The RSS difference values and corresponding matrix indices are taken as the inputs of an ANN model and the known location coordinates are its outputs. Then a nonlinear function between the inputs and outputs can be approximated through training the ANN model. In the on-line localization phase, when a target is in the monitoring area, the RSS difference values and their matrix indices can be obtained and input into the trained ANN model, and then the localization coordinates can be computed. We verify the proposed device-free localization system with a WSN platform. The experimental results show that our proposed device-free wireless localization system is able to achieve a comparable localization performance without any terminal device.

1. Introduction

As Internet of Things (IoT) is becoming progressively popular, the related research areas that IoT involves have been well investigated, such as Wireless Sensors Networks (WSNs), Radio Frequency Identification (RFID), Micro-Electro-Mechanical System (MEMS), and mobile computing [1]. Among these, WSNs integrate various advanced technologies including sensor technology, wireless communication, and distributed information processing, so it has attracted great concerns in IoT [2, 3]. In a WSN, usually a number of sensor nodes are deployed in a monitoring area. These sensor nodes are connected through wireless communication to finish the tasks of sensing, recognizing, and monitoring in a cooperative manner. With the abilities of sensing, computing, and communicating, WSNs have been widely used in various fields, for example, indoor fire detection,

object tracking, survivor sensing, and building safety monitoring [4]. In these applications, localization in WSNs plays an essential and important role [5].

So far, various localization systems have been developed [6–9]. Satellite-based localization system is able to provide satisfactory Location Based Service (LBS) for users in outdoor environments [10]. Cellular-based system is able to calculate the locations of mobile phone users, but the cellular-based system usually suffers great localization errors [11]. Most localization systems using Wireless Local Area Networks (WLANs) are able to offer LBS for users when the users take WLAN terminal devices [12, 13]. Ultrawide Band (UWB) localization system needs users to take UWB tags for estimating their locations [6]. Smart phone sensors are also used for navigation and localization services [14]. Although infrared-based localization system does not need terminal devices, the performance can be easily affected by

surrounding environments [6]. In a word, most existing localization systems need users to carry terminal devices, which cannot be applied in some special scenarios like the elder monitoring, life detection, and so on. Device-free wireless localization in WSNs that makes use of Received Signal Strength (RSS) variations between sensor nodes is able to solve this problem. When a target goes into the monitoring area of a WSN, the presence of the target will reflect, scatter, and absorb the radio signals of the WSN [15]. Localization results can be calculated with the collected RSS variations. Therefore, device-free wireless localization that does not need any terminal device extends the application range of localization and it will have a promising prospect and increasing requirement.

However, one challenge of the device-free wireless localization in WSNs is the unpredictability of the RSS measurements in multipath environments, especially in the complex environments where people usually move. To deal with this problem, in this paper, we refer to the popular WLAN finger-printing localization method [6] and propose a device-free wireless localization system using Artificial Neural Networks (ANNs). In our proposed system, RSS difference values and corresponding matrix indices are fused as the inputs of an ANN model, whose outputs are location coordinates. Then a nonlinear function between the inputs and outputs can be approximated through training the ANN model. When we need to locate a target in the monitoring area, the trained ANN model is used to compute the localization coordinates of the target. The four contributions of this paper can be summarized as follows:

(1) We propose a device-free wireless localization system using an ANN model. The localization system consists of two phases: the off-line training and on-line localization. In the off-line phase, a professional stands at some selected locations with known location coordinates. RSS difference matrices between the RSS matrices collected when the monitoring area is vacant and with the professional in the area are computed. Some RSS difference values and corresponding matrix indices are used as the inputs, and the known location coordinates are used as the outputs for training the ANN model. In the on-line phase, when a target is in the monitoring area, the obtained RSS difference values and matrix indices are input into the trained ANN model for location coordinate estimation.

(2) We propose an ANN model for location coordinate estimation in our device-free wireless localization system. The proposed ANN model is not only used for nonlinear function approximation, but also used for data fusion. The model fuses the RSS difference values and corresponding matrix indices and then takes the fused data as the input vector of the ANN model. With the known location coordinates as the output vector, a nonlinear function can be approximated with the ANN model for computing the localization results.

(3) We build a hardware platform for the device-free wireless localization system with a ZigBee-based WSN. It consists of 16 sensor nodes, 1 sink node, and 1 localization server. Each sensor node sends the RSS data that are received from the other sensor nodes to the localization server through the sink node. The RSS data will be processed and then used to calculate localization results in the server.

(4) We verify the proposed localization system in a real indoor environment with our built hardware platform. We also try different system parameters for localization performance improvement and analyse the experimental results. The experimental results confirm that our proposed device-free wireless localization system is able to achieve a comparable localization performance.

The remainder of the paper is organized as follows. Related works about this research are reviewed in Section 2. In Section 3, the proposed device-free wireless localization system and ANN model for estimating localization results are given in detail. Section 4 describes the experimental hardware platform, experimental results, and analyses. Finally, conclusions are drawn and ideas for future works are presented in Section 5.

2. Related Works

So far, many device-free wireless localization methods have been proposed. Wilson and Patwari [16] presented a device-free localization method based on Radio Tomographic Imaging (RTI). RTI-based localization method imaged the RSS attenuation caused by targets with inexpensive and standard hardware [17]. They also proposed regularization methods to reduce noise and a statistical model relating variance to spatial locations of movement for motion image estimation [18]. Due to the comparable performance of this method, RTI-based device-free localization has been extensively researched. An RTI-based device-free localization using segmentation algorithm and connected component label algorithm for target tracking was proposed in [19]. Nannuru et al. [20] developed a model for multitarget tracking using RTI in indoor environments and successfully tracked three targets with the model. Bocca et al. [21] presented an RTI method that used RSS measurements on multiple frequency channels and combined them with a weighted average for real-time multitarget tracking. Alippi et al. [22] proposed an RTI method for locating people outdoors that achieved high localization accuracy and reduced the sensor energy consumption. Wang et al. [23–25] also have done solid works in this area and they applied saddle surface model, compressive sensing (CS), and Bayesian grid approach into device-free wireless localization. Savazzi et al. [26] proposed the uses of device-free localization methods and architectures to track a human worker in a human-robot industrial scenario. The proposed localization and detection algorithm was based on the jump linear Markovian and interactive multiple model. Wang et al. [15] introduced an energy-efficient framework for multitarget device-free localization. They applied CS to guarantee high localization performance with less RSS measurements.
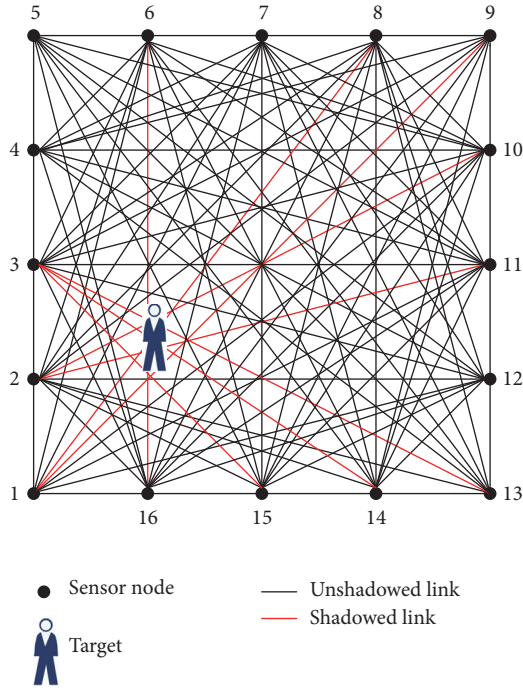
FIGURE 1: The device-free wireless localization system that consists of 16 sensor nodes.

Besides the aforementioned, similar to WLAN fingerprinting localization method, Zhang et al. [27] mounted some nodes on the ceiling and divided the tracking area into different subareas. For each subarea, they utilized the Support Vector Regression (SVR) model to estimate the localization coordinates. Youssef et al. [28] proposed a device-free wireless localization system based on radio-map. They calculated localization results with a probabilistic method. Then they proposed another device-free localization system with particle filtering [29]. Xu et al. [30] formulated the device-free localization problem with probabilistic classification approaches based on discriminant analysis and mitigated the errors caused by multipath effect. Because the fingerprinting localization method performs well in multipath environments, in this paper, we also refer to the fingerprinting localization method and propose a device-free localization system using an ANN model.

3. Proposed Device-Free Localization System

3.1. System Overview. The proposed device-free localization system is shown in Figure 1. The sensor nodes are evenly deployed on the edges of a square monitoring area. When a target goes into the monitoring area, some wireless links between sensor nodes will be shadowed. If we take Figure 1 as an example, the wireless links between sensor nodes 1 and 8, 1 and 9, 2 and 10, 2 and 11, 3 and 13, 3 and 14, 3 and 15, and 6 and 16 are shadowed, which cause RSS variations of these wireless links. When the target moves to a different location in the monitoring area, corresponding wireless links will be also shadowed. All the sensor nodes in the WSN measure the RSS data and send the data to a localization server through a

sink node. We assume L sensor nodes have been deployed in the monitoring area with known location coordinates (x_i, y_i), $i = 1, 2, \cdots, L$, then we can have $M = L(L-1)/2$ wireless links. The RSS data of these wireless links are sent to the sink node and then processed in the localization server. When the monitoring area is vacant, that is, no target is in the area, we collect the RSS data from the WSN and compile them into matrices. Then a professional stands at a number of selected locations with known location coordinates, and some wireless links are shadowed when the professional is at each location. We can also obtain the RSS matrices in the same manner and compute the RSS difference matrices. We establish a nonlinear function relationship between the RSS difference value information and location coordinates with an ANN model. This ANN model is used for calculating the location coordinates of the target in the monitoring area.

Based on the description above, more specifically, the proposed device-free wireless localization system consists of two phases: the off-line training and on-line localization. In the off-line training phase, we first collect the RSS data of the vacant monitoring area for a while. The RSS data of all the sensor nodes in the WSN are sent to the localization server through the sink node. The server will extract the RSS data and compile the data into RSS matrices. Then a number of specific locations are selected and their location coordinates are recorded. A professional stands at each location and the RSS data from all the sensor nodes are also collected and processed in the same manner in order to get the RSS matrices. The RSS difference matrices between the RSS matrices collected when the monitoring area is vacant and with the professional in the area are computed. Some RSS difference values are selected, and then these RSS difference values and their matrix indices are fused and input into the ANN model. Meanwhile, the known location coordinates of the selected locations are considered as the outputs of the ANN model. So the ANN model can be trained with these data and a nonlinear function is approximated for calculating localization coordinates. In the on-line localization phase, when a target goes into the monitoring area, some wireless links are shadowed. The localization server collects the RSS data from all the sensor nodes and compiles these RSS data into an RSS matrix. Then an RSS difference matrix is also computed. The same number of selected RSS difference values and their indices in the matrix are input into the trained ANN model, and therefore the location coordinates of the target can be calculated by the ANN model.

3.2. RSS Data Preprocessing. After the localization server collects enough broadcasted frames in the WSN that consist of RSS and Node Identification (NID) data, the RSS data can be extracted from these frames and compiled into an RSS matrix with dimensions of $L \times L$. The row of the RSS matrix represents the sensor node that receives the radio signals and the column of the RSS matrix represents the sensor node that transmits the radio signals. So the RSS matrix of the vacant monitoring area can be denoted by the following:

$$\mathbf{RSS} = \begin{bmatrix} 1 & RSS_{1,2} & \cdots & RSS_{1,L} \\ RSS_{2,1} & 2 & \cdots & RSS_{2,L} \\ \vdots & \vdots & \ddots & \vdots \\ RSS_{L,1} & RSS_{L,2} & \cdots & L \end{bmatrix}_{L\times L} \quad (1)$$

When a professional stands at ith location, the compiled RSS matrix can be denoted by the following:

$$\mathbf{rss}_i = \begin{bmatrix} 1 & rss_{1,2,i} & \cdots & rss_{1,L,i} \\ rss_{2,1,i} & 2 & \cdots & rss_{2,L,i} \\ \vdots & \vdots & \ddots & \vdots \\ rss_{L,1,i} & rss_{L,2,i} & \cdots & L \end{bmatrix}_{L\times L}, \quad (2)$$
$$i = 1, 2, \cdots, Q$$

where Q is the number of selected locations. So the RSS difference matrix $\Delta\mathbf{rss}_i$ between $\mathbf{RSS}$ and $\mathbf{rss}_i$ can be computed by the following:

$$\Delta\mathbf{rss}_i = \left|\mathbf{rss}_i - \mathbf{RSS}\right|, \quad i = 1, 2, \cdots, Q \quad (3)$$

As shown in Figure 1, there is one problem that should be considered that is the sensor nodes on the same edge of the monitoring area can also receive RSS data from each other. For instance, sensor node 1 can receive the RSS data from sensor node 5 and sensor node 13. Sometimes the RSS difference values between these sensor nodes on the same edge may vary greatly. Because this is not caused by the target in the monitoring area, if we take these RSS difference values into consideration and input the RSS difference values and their matrix indices into the ANN model, the localization errors might be significant. So we design a filtering matrix $\mathbf{m}$ to set the elements that represent the RSS difference values between the sensor nodes on the same edges of the monitoring area to be 0. This operation is able to remove the negative effect effectively. The final RSS difference matrix $\Delta\mathbf{rss}'_i$ after the filtering operation can be computed by the following:

$$\Delta\mathbf{rss}'_i = \Delta\mathbf{rss}_i \bullet \mathbf{m}, \quad i = 1, 2, \cdots, Q \quad (4)$$

3.3. Localization with ANN Model. In this paper, we apply a three-layer perceptron network for nonlinear function approximation and data fusion. The network has a basic network structure that consists of one input layer, one hidden

layer, and one output layer. The structure of the network is shown in Figure 2. Let the number of the neurons in the input layer, hidden layer, and output layer be $3K$, T, and 2, respectively. After the RSS data preprocessing, we can obtain the RSS difference matrix $\Delta\mathbf{rss}'_i$. We sort all the elements in matrix $\Delta\mathbf{rss}'_i$ in a descending order, then we select the first K maximum RSS difference values $\Delta rss'_{i,j}$, $j = 1, 2, \cdots, K$, and determine their indices in matrix $\Delta\mathbf{rss}'_i$ that are column $c_{i,j}$ and row $r_{i,j}$, $j = 1, 2, \cdots, K$. The RSS difference values and their indices are fused by the three-layer ANN model as the input vector of the ANN model denoted as $(\Delta rss'_{i,1}, c_{i,1}, r_{i,1}, \Delta rss'_{i,2}, c_{i,2}, r_{i,2}, \cdots, \Delta rss'_{i,K}, c_{i,K}, r_{i,K})$. Meanwhile, the outputs of the ANN model are the location coordinates (x_i, y_i) in X-axis and Y-axis, respectively. Then the nonlinear function between the inputs and outputs can be approximated and denoted by $F : \mathbb{R}^{3K} \to \mathbb{R}^2$ as follows:

$$(x_i, y_i) = F\left(\Delta rss'_{i,1}, c_{i,1}, r_{i,1}, \Delta rss'_{i,2}, c_{i,2}, r_{i,2}, \cdots, \Delta rss'_{i,K}, \right.$$
$$\left. c_{i,K}, r_{i,K}\right), \quad i = 1, 2, \cdots, Q \quad (5)$$

When we input the vector $(\Delta rss'_{i,1}, c_{i,1}, r_{i,1}, \Delta rss'_{i,2}, c_{i,2}, r_{i,2}, \cdots, \Delta rss'_{i,K}, c_{i,K}, r_{i,K})$ into the ANN model, the output $g_N^{(j)}$ of jth neuron in the Nth layer of the model can be calculated by the following:

$$g_N^{(j)} = f\left(u_N^{(j)}\right)$$
$$u_N^{(j)} = \sum_{i=1}^{I} \omega_{N-1,N}^{(i,j)} x_{N-1,N}^{(i,j)} - \theta_N^{(j)} \quad (6)$$
$$j = 1, 2, \cdots, T, \ I = 3K, \ N = 2; \ j = 1, 2, \ I = T, \ N = 3$$

where $x_{N-1,N}^{(i,j)}$ is the input from ith neuron in the $(N-1)$th layer to jth neuron in the Nth layer; $\omega_{N-1,N}^{(i,j)}$ is the weight from ith neuron in the $(N-1)$th layer to jth neuron in the Nth layer; $\theta_N^{(j)}$ is the threshold of jth neuron in the Nth layer; $f(\cdot)$ is the activation function of the ANN model.

We train the ANN model with the famous back propagation (BP) algorithm [31], which has been widely used for ANN training. The operation process of the algorithm is to propagate errors backwards and update the weights and thresholds of the network. The updating process will be suspended when one of the iteration termination conditions is achieved. The weights and thresholds of the ANN model can be updated by the following:

$$\omega_{N-1,N}^{(i,j)} = \omega_{N-1,N}^{(i,j)} + a\delta_N^{(j)} g_{N-1}^{(j)}$$
$$\theta_N^{(j)} = \theta_N^{(j)} - b\delta_N^{(j)}$$
$$\delta_N^{(j)} = \begin{cases} \sum_{m=1}^{2} \delta_{N+1}^{(m)} \omega_{N,N+1}^{(i,m)} f'\left(u_N^{(j)}\right), & N = 2 \\ \left[o^{(j)} - g_N^{(j)}\right] f'\left(u_N^{(j)}\right), & N = 3 \end{cases} \quad (7)$$

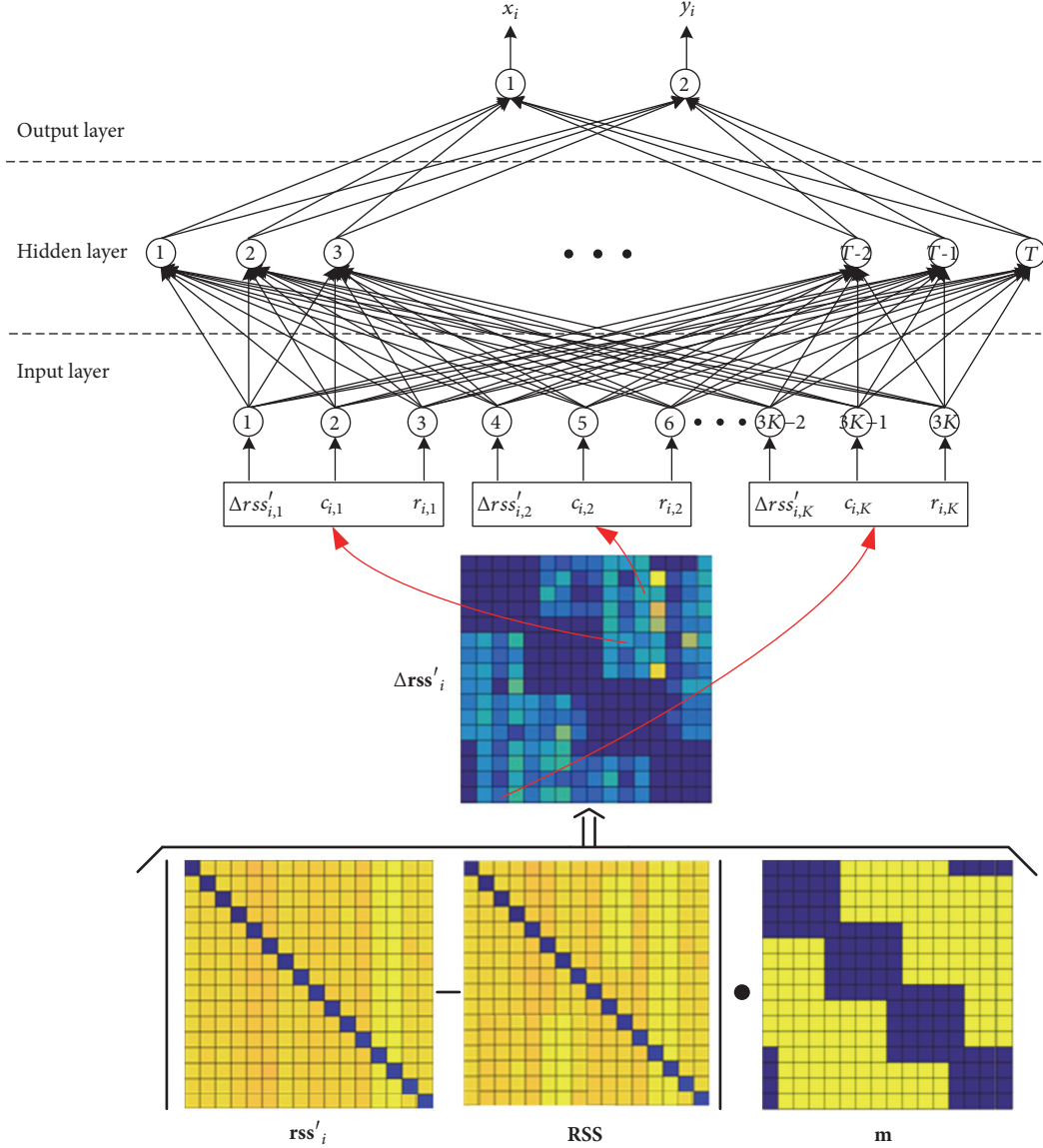$$i = 1, 2, \cdots, 3K, \ j = 1, 2, \cdots, T, \ N = 2; \ i = 1, 2, \cdots, T, \ j = 1, 2, \ N = 3$$

Figure 2: Proposed ANN structure and its inputs and outputs.

where $o^{(j)}$ is our expected output of jth neuron in the output layer; a and b are learning rates for adapting the stability and training time.

After finishing the ANN model training, when a target is in the monitoring area in the on-line localization phase, the shadowed RSS data of the WSN are collected and processed. Then the first K maximum RSS difference values and their matrix indices are fused as the input vector $(\Delta rss'_1, c_1, r_1, \Delta rss'_2, c_2, r_2, \cdots, \Delta rss'_K, c_K, r_K)$ and input into the trained ANN model. So the location coordinates $(\hat{x}, \hat{y})$ of the target can be estimated with the trained ANN model by the following:

$$(\hat{x}, \hat{y})$$
$$= F\left(\Delta rss'_1, c_1, r_1, \Delta rss'_2, c_2, r_2, \cdots, \Delta rss'_K, c_K, r_K\right) \quad (8)$$

4. Experimental Setup, Results, and Analyses

4.1. Experimental Setup. In this paper, we use CC2530 ZigBee nodes of Texas Instruments (TI) as the WSN nodes. This CC2530 ZigBee node has the advantages of low power cost, high controllability, and convenient networking. It operates on the 2.4 GHz ISM band and is also compatible with IEEE 802.15.4 protocol. When one sensor transmits radio signals, all the other sensor nodes in the network can receive the signals. In our experiment, the hardware platform consists of 16 sensor nodes, 1 sink node, and 1 localization server. The 16 sensor nodes measure the RSS data and transmit these RSS data in turn. The sink node is used to receive the RSS data from all the sensor nodes and also upload these data to the localization server.

In this experiment, we set that each sensor node is able to transmit radio signals and the other sensor nodes can

| Transmitting node NID | NID 1 | RSS 1 | …… | NID 16 | RSS 16 |

FIGURE 3: Structure of the transmitted frame

FIGURE 4: Photography of the experimental scenario.

receive these radio signals and measure the RSS data. To be more specific, a total of 16 sensor nodes are first evenly deployed on the edges of the square monitoring area. After the network start-up, one sensor node can broadcast its NID. The other 15 sensor nodes are able to receive the NID and measure the RSS data. The RSS and corresponding NID data are recorded in a frame and then the frame is also transmitted. The designed structure of the frame is shown in Figure 3. We set different time delays for different sensor nodes in order to avoid conflicts. When it is the turn of one sensor node to transmit its frame, the node will transmit its NID as well as the measured RSS data and corresponding NID information. After a while, every frame will contain the entire RSS data and NID information of all the nodes. The sink node can also receive all the frames in the WSN and upload these data to the localization server.

The real experimental scenario is shown in Figure 4. The monitoring area that is in a meeting room is a square area with dimensions of 7.2m×7.2m. There are three tables and some chairs in the monitoring area. The monitoring area plan is shown in Figure 5 and the chairs are not displayed in the plan for simplicity. The deployed 16 sensor nodes are on the edges of the monitoring area with 1.8m gaps and are also fixed on tripods with 1.2m height. The sink node and localization server are in the meeting room too, but they are not in the monitoring area. In the monitoring area, there are 52 locations are selected, which are marked with "×" in Figure 5. The RSS data that are collected for each location can be compiled into 20 RSS matrices. We divide these RSS matrices into two data sets. One set is used for training the ANN model and the other set is used as testing data.

4.2. Experimental Results and Analyses. In this experiment, we set the number of neurons in the hidden layer to be 35 and we train the ANN model with BP algorithm. We utilize 15 RSS matrices of each selected location to train the ANN model and the rest of 5 RSS matrices to test the trained model. We calculate the mean errors of the localization results with the number of first K maximum RSS difference values varying from 1 to 10. Figure 6 shows the mean errors with different parameter K. The maximum mean error is 1.31m when K equals 9 and the minimum one is 0.42m when K equals 6. The reason might be that when K is set to be too large, the
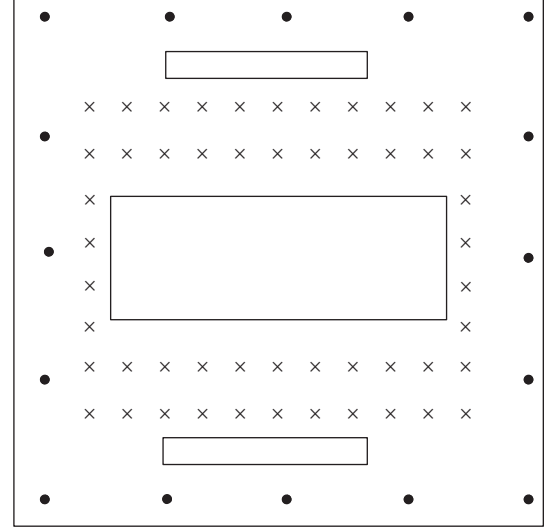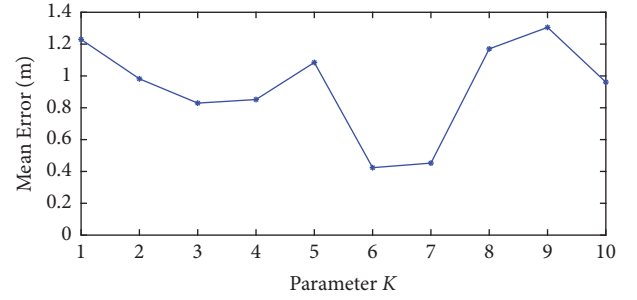

FIGURE 5: Monitoring area plan.

FIGURE 6: Mean errors with different parameter K.

number of inputs is $3K$, the performance of the ANN model decreases because there are only 35 neurons in the hidden layer. On the contrary, when K is set to be too small, the selected RSS difference values may be not caused by the target, so it is difficult to estimate the location coordinates of the target accurately. For example, when parameter K equals 2, only the first 2 maximum RSS difference values are selected. At this time, if it is not the target but some interference causes the RSS variations, then this will decrease the localization performance.

As presented in Table 1, the localization results with parameter K varying from 3 to 8 are compared. The error standard deviations with parameter K varying from 3 to 8 are 1.05, 1.15, 1.14, 1.08, 1.45, and 1.35, respectively. When parameter K increases to 7 or 8, the error standard deviation increases greatly. Meanwhile, the cumulative probabilities with parameter K varying from 3 to 8 within localization error of 1m are 75.4%, 76.4%, 60.4%, 83.5%, 79.2%, and 63.1%, respectively. The cumulative probabilities with parameter K varying from 3 to 8 within localization error of 2m are 91.5%, 88.1%, 83.5%, 90.0%, 87.7%, and 77.7%, respectively. The cumulative probabilities with different parameter K are also shown in Figure 7. Obviously, the localization performance of the proposed system when K equals 6 outperforms the others.

TABLE 1: Performance comparison with different parameter K.

K	Mean error (m)	Standard deviation (m)	Accuracy within 1m (%)	Accuracy within 2m (%)
3	0.83	1.05	75.4	91.5
4	0.85	1.15	76.4	88.1
5	1.08	1.14	60.4	83.5
6	0.42	1.08	83.5	90.0
7	0.45	1.45	79.2	87.7
8	1.17	1.35	63.1	77.7
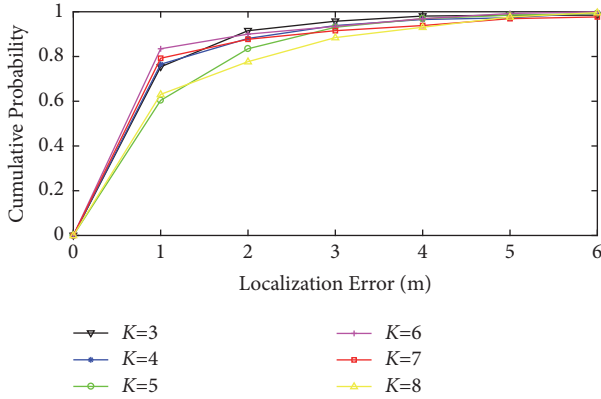
FIGURE 7: Cumulative probabilities with different parameter K.

5. Conclusions and Future Works

In this paper, a device-free wireless localization system using an ANN model is proposed. With the proposed localization system, location coordinates of a target can be estimated without any terminal device attached. We construct a WSN hardware platform with ZigBee nodes and RSS data of wireless links between the sensor nodes are collected. We compile the RSS data into RSS matrices and then compute the RSS difference matrices between the RSS matrices collected when the monitoring area is vacant and with a professional in the monitoring area. The first K maximum RSS difference values that are caused by the professional are selected. These RSS difference values and their matrix indices are taken as the inputs and the known location coordinates are used as the outputs to train the ANN model. In the on-line localization phase, when a target is in the monitoring area, the same number of RSS difference values and corresponding matrix indices can be obtained and input into the trained ANN model, then the localization coordinates can be calculated. The experimental results prove that our proposed device-free wireless localization system is able to achieve a comparable localization performance without any terminal device.

In the future, we will try to focus on the moving target or multitarget localization with the constructed hardware platform and the system parameter optimization for localization performance improvement. The nonlinear function approximation with other advanced machine learning algorithms will be investigated as well.

Data Availability

The data supporting the findings of this study are available within the article.

Conflicts of Interest

The authors declare that there are no conflicts of interest regarding the publication of this paper.

Acknowledgments

References

[1] R. Fantacci, T. Pecorella, R. Viti, and C. Carlini, "A network architecture solution for efficient IOT WSN backhauling: challenges and opportunities," *IEEE Wireless Communications Magazine*, vol. 21, no. 4, pp. 113–119, 2014.

[2] A. Zanella, N. Bui, A. P. Castellani, L. Vangelista, and M. Zorzi, "Internet of things for smart cities," *IEEE Internet of Things Journal*, vol. 1, no. 1, pp. 22–32, 2014.

[3] W. Lu, Y. Gong, X. Liu, J. Wu, and H. Peng, "Collaborative Energy and Information Transfer in Green Wireless Sensor Networks for Smart Cities," *IEEE Transactions on Industrial Informatics*, vol. 14, no. 4, pp. 1585–1593, 2018.

[4] J. Fan, Y. Hu, T. H. Luan, and M. Dong, "DisLoc: A Convex Partitioning Based Approach for Distributed 3-D Localization in Wireless Sensor Networks," *IEEE Sensors Journal*, vol. 17, no. 24, pp. 8412–8423, 2017.

[5] G. Han, J. Jiang, C. Zhang, T. Q. Duong, M. Guizani, and G. K. Karagiannidis, "A Survey on Mobile Anchor Node Assisted Localization in Wireless Sensor Networks," *IEEE Communications Surveys & Tutorials*, vol. 18, no. 3, pp. 2220–2243, 2016.

[6] Y. Gu, A. Lo, and I. Niemegeers, "A survey of indoor positioning systems for wireless personal networks," *IEEE Communications Surveys & Tutorials*, vol. 11, no. 1, pp. 13–32, 2009.

[7] M. Zhou, Y. Tang, Z. Tian, L. Xie, and W. Nie, "Robust Neighborhood Graphing for Semi-supervised Indoor Localization with Light-loaded Location Fingerprinting," *IEEE Internet of Things Journal*, 2017.

[8] M. Zhou, Y. Tang, Z. Tian, and X. Geng, "Semi-Supervised Learning for Indoor Hybrid Fingerprint Database Calibration with Low Effort," *IEEE Access*, vol. 5, pp. 4388–4400, 2017.

[9] Y.-L. Sun and Y.-B. Xu, "Error estimation method for matrix correlation-based Wi-Fi indoor localization," *KSII Transactions on Internet and Information Systems*, vol. 7, no. 11, pp. 2657–2675, 2013.

[10] D. Zou, W. Meng, S. Han, K. He, and Z. Zhang, "Toward ubiquitous LBS: Multi-radio localization and seamless positioning," *IEEE Wireless Communications Magazine*, vol. 23, no. 6, pp. 107–113, 2016.

[11] S.-H. Fang and T.-N. Lin, "Cooperative multi-radio localization in heterogeneous wireless networks," *IEEE Transactions on Wireless Communications*, vol. 9, no. 5, pp. 1547–1551, 2010.

[12] M. Zhou, Y. Tang, W. Nie, L. Xie, and X. Yang, "GrassMA: graph-based semi-supervised manifold alignment for indoor WLAN localization," *IEEE Sensors Journal*, vol. 17, no. 21, pp. 7086–7095, 2017.

[13] Y. Sun, W. Meng, C. Li, N. Zhao, K. Zhao, and N. Zhang, "Human localization using multi-source heterogeneous data in indoor environments," *IEEE Access*, vol. 5, pp. 812–822, 2017.

[14] Z. Deng, W. Si, Z. Qu, X. Liu, and Z. Na, "Heading estimation fusing inertial sensors and landmarks for indoor navigation using a smartphone in the pocket," *EURASIP Journal on Wireless Communications and Networking*, vol. 2017, no. 1, 2017.

[15] J. Wang, D. Fang, Z. Yang et al., "E-HIPA: an energy-efficient framework for high-precision multi-target-adaptive device-free localization," *IEEE Transactions on Mobile Computing*, vol. 16, no. 3, pp. 716–729, 2016.

[16] J. Wilson and N. Patwari, "Radio tomographic imaging with wireless networks," *IEEE Transactions on Mobile Computing*, vol. 9, no. 5, pp. 621–632, 2010.

[17] N. Patwari and J. Wilson, "RF sensor networks for device-free localization: measurements, models, and algorithms," *Proceedings of the IEEE*, vol. 98, no. 11, pp. 1961–1973, 2010.

[18] J. Wilson and N. Patwari, "See-through walls: motion tracking using variance-based radio tomography networks," *IEEE Transactions on Mobile Computing*, vol. 10, no. 5, pp. 612–621, 2011.

[19] V. Köster, A. Lewandowski, and C. Wietfeld, "A segmentation-based radio tomographic imaging approach for interference reduction in hostile industrial environments," in *Proceedings of the 2012 IEEE/ION Position, Location and Navigation Symposium, PLANS 2012*, pp. 1074–1081, usa, April 2012.

[20] S. Nannuru, Y. Li, Y. Zeng, M. Coates, and B. Yang, "Radio-frequency tomography for passive indoor multitarget tracking," *IEEE Transactions on Mobile Computing*, vol. 12, no. 12, pp. 2322–2333, 2013.

[21] M. Bocca, O. Kaltiokallio, N. Patwari, and S. Venkatasubramanian, "Multiple target tracking with rf sensor networks," *IEEE Transactions on Mobile Computing*, vol. 13, no. 8, pp. 1787–1800, 2014.

[22] C. Alippi, M. Bocca, G. Boracchi, N. Patwari, and M. Roveri, "RTI Goes Wild: Radio Tomographic Imaging for Outdoor People Detection and Localization," *IEEE Transactions on Mobile Computing*, vol. 15, no. 10, pp. 2585–2598, 2016.

[23] J. Wang, Q. Gao, M. Pan, X. Zhang, Y. Yu, and H. Wang, "Toward Accurate Device-Free Wireless Localization with a Saddle Surface Model," *IEEE Transactions on Vehicular Technology*, vol. 65, no. 8, pp. 6665–6677, 2016.

[24] J. Wang, Q. Gao, H. Wang, P. Cheng, and K. Xin, "Device-free localization with multidimensional wireless link information," *IEEE Transactions on Vehicular Technology*, vol. 64, no. 1, pp. 356–366, 2015.

[25] J. Wang, Q. Gao, P. Cheng, Y. Yu, K. Xin, and H. Wang, "Lightweight robust device-free localization in wireless networks," *IEEE Transactions on Industrial Electronics*, vol. 61, no. 10, pp. 5681–5689, 2014.

[26] S. Savazzi, V. Rampa, F. Vicentini, and M. Giussani, "Device-Free Human Sensing and Localization in Collaborative Human-Robot Workspaces: A Case Study," *IEEE Sensors Journal*, vol. 16, no. 5, pp. 1253–1264, 2016.

[27] D. Zhang, Y. Liu, and L. M. Ni, "RASS: a real-time, accurate and scalable system for tracking transceiver-free objects," in *Proceedings of the IEEE International Conference on Pervasive Computing and Communications (PerCom '11)*, pp. 197–204, Seattle, Wash, USA, March 2011.

[28] M. Youssef, M. Mah, and A. Agrawala, "Challenges: device-free passive localization for wireless environments," in *Proceedings of the 13th Annual ACM International Conference on Mobile Computing and Networking (MobiCom'07)*, pp. 222–229, September 2007.

[29] A. Saeed, A. E. Kosba, and M. Youssef, "Ichnaea: a low-overhead robust WLAN device-free passive localization system," *IEEE Journal of Selected Topics in Signal Processing*, vol. 8, no. 1, pp. 5–15, 2014.

[30] C. Xu, B. Firner, Y. Zhang, and R. E. Howard, "The Case for Efficient and Robust RF-Based Device-Free Localization," *IEEE Transactions on Mobile Computing*, vol. 15, no. 9, pp. 2362–2375, 2016.

[31] D. E. Rumelhart, G. E. Hinton, and R. J. Williams, "Learning representations by back-propagating errors," *Nature*, vol. 323, no. 6088, pp. 533–536, 1986.

Research Article

Speeding Up Exact Algorithms for Maximizing Lifetime of WSNs Using Multiple Cores

Pengyuan Cao [iD] [1,2,3] **and Xiaojun Zhu** [iD] [1,2,3]

[1]*College of Computer Science and Technology, Nanjing University of Aeronautics and Astronautics, Nanjing 211106, China*
[2]*State Key Laboratory for Novel Software Technology, Nanjing University, Nanjing 210023, China*
[3]*Collaborative Innovation Center of Novel Software Technology and Industrialization, Nanjing 210023, China*

Correspondence should be addressed to Xiaojun Zhu; xzhu@nuaa.edu.cn

Maximizing the lifetime of wireless sensor networks is NP-hard, and existing exact algorithms run in exponential time. These algorithms implicitly use only one CPU core. In this work, we propose to use multiple CPU cores to speed up the computation. The key is to decompose the problem into independent subproblems and then solve them on different cores simultaneously. We propose three decomposition approaches. Two of them are based on the notion that a tree does not contain cycles, and the third is based on the notion that, in any tree, a node has at most one parent. Simulations on an 8-core desktop computer show that our approach can speed up existing algorithms significantly.

1. Introduction

In wireless sensor networks, each sensor node has only a limited amount of energy. When a node sends or receives messages, it consumes the corresponding amount of energy. Thus, the amount of traffic of a node influences how long the node can work, which in turn determines the lifetime of the network. To this end, finding a routing tree to get longer lifetime is a key issue, which is known to be NP-hard [1]. Recall that algorithms that can guarantee finding the optimal routing tree are called *exact algorithms*. It is clear that, unless P=NP, all exact algorithms for the lifetime maximization problem are not polynomial time algorithms.

In fact, all existing exact algorithms run in exponential time [1–3]. A straightforward approach is to perform exhaustive search over the solution space (e.g., [2]). This process can be improved by dynamically eliminating suboptimal solutions in the search process [1], or integrating fast integer linear programming solvers [3]. However, these algorithms implicitly use only one CPU core and do not use the full potential of current multicore CPUs. Indeed, most

computers, even smartphones, are equipped with multiple cores.

In this work, instead of designing a new algorithm, we consider speeding up existing exact algorithms by using multicore CPUs to their full potential. The basic idea is to decompose the problem into independent subproblems and then solve them on different cores using existing exact algorithms. The challenge is how to decompose the problem. We propose three decomposition methods for different exact algorithms. The first is based on the fact that a tree does not contain (undirected) cycles, so we can break the network into subnetworks whenever we encounter an undirected cycle. This approach applies to all algorithms that consider the network as either an undirected graph or a directed graph. The second is based on directed cycle, and the network is divided whenever we find a directed cycle. The third is based on the fact that every node has only one parent node, so the network is divided according to different parent choices of a given node. The second and the third approaches apply to algorithms that consider the network as a directed graph.

Our contributions can be enumerated as follows:

 (1) We consider using the multicore of current computers to speed up existing algorithms. The proposed approaches are applicable to all exact algorithms based on one CPU core.

 (2) We propose three problem decomposition approaches. These approaches can decompose the problem into subproblems, which can be solved on different cores using any exact algorithm. We also propose a mechanism to expose information of solved subproblems to help solve other subproblems.

 (3) We implement our approach on an 8-core desktop computer and perform numerical simulations. The results suggest that, in general, the proposed approaches can reduce the empirical time of existing exact algorithms, especially when the problem size is large.

The rest of the paper is organized as follows. Section 2 reviews related work. Section 3 reviews the definition of the problem and proposes a solution framework. Section 4 proposes three decomposition approaches. Section 5 discusses several problems. Section 6 presents numerical simulation results. Finally, Section 7 concludes the paper.

2. Related Works

Finding routing paths of messages to maximize lifetime is a critical problem in wireless sensor networks (e.g., [1–3, 5–7]). Unfortunately, it is NP-hard in most scenarios when nodes can or cannot perform data aggregation. Researchers resort to polynomial-time approximation algorithms by sacrificing accuracy (e.g., [8]), or exponential-time exact algorithms by sacrificing running time (e.g., [1, 3]). While both algorithms have important applications, we focus on exact algorithms in this paper.

A simple method is to enumerate all spanning trees [2], which has a very poor running time. To improve the efficiency, [1] decomposes the underlying network graph into biconnected subgraphs to reduce problem size. A limitation is that the technique does not work when the graph is already biconnected. Reference [3] proposes to incorporate graph decomposition with integer linear programming. The basic idea is to decompose the graph into biconnected subgraphs and formulate the problem on each subgraph as an integer linear programming problem, which is solved by an integer linear programming solver. Besides routing, energy efficiency is also considered in other contexts such as compressive sensing-based encryption [9] and rechargeable sensor networks [10].

Contrary to these works, our work in this paper focuses on how to use the multiple cores in current computers to their full potential. The proposed approaches can be incorporated with existing exact algorithms. Though the idea of using multicores in wireless sensor networks is not new, existing works do not focus on our problem. For example, [11] uses the cores within a GPU to speed up lifetime simulation for sensor nodes, and [12] designs multicore sensor node hardware.

3. A Framework to Use Multicores

We first review the problem and then introduce the solution framework. A sensor network contains n sensors nodes v_1, $v_2, \ldots, v_n$ and a sink node v_0. Each sensor node senses the environment periodically, generating a data packet in each period. It needs to send the data packet to the sink node. The network can be represented as an undirected graph $G(V, E)$, where V is the set of nodes and E is the set of communication links. Sensor node v_i has initial energy e_i and the sink node has infinite initial energy; i.e., $e_0 = \infty$. The energy consumed for receiving a message is R_x and that for transmitting a message is T_x. For any tree $T \in G$ rooted at the sink, in each time period, the energy consumed by node v_i is $d_T(i)(R_x + T_x) + T_x$, where $d_T(i)$ is the number of descendants of node i in tree T. The lifetime of node v_i in tree T is the number of rounds it can support until it runs out of energy: $l(T, i) = e_i/(d_T(i)(R_x + T_x) + T_x)$. The lifetime of tree T is the smallest node lifetime; i.e., $l(T) = \min_{i=1,\ldots,n} l(T, i)$. Lifetime maximization problem is to find a tree that has the maximum lifetime. It has been proven to be NP-hard [1].

In this work, we assume that an operating system does not perform automatic multicore optimization; i.e., a single thread program can use at most one CPU core. To this end, we perform a simple experiment as follows. We run a dead loop program on two computers, one of which has 4 cores and the other has 8 cores. Both computers are equipped with the Windows operating system. The CPU utilization ratio is roughly 25% on the 4-core computer and is about 13% on the 8-core computer, which is consistent with our assumption. Note that if there are multiple threads, then the operating system will distribute the threads on different cores automatically.

3.1. Problem Decomposition Overview. We refer to the set of feasible solutions of a lifetime maximization problem as its solution space, i.e., the set of directed trees pointing to the sink. A subproblem is a lifetime maximization problem with smaller solution space. The basic idea is to find a set of subproblems whose solution space contains at least one optimal solution. A decomposition method is *feasible* if three conditions are satisfied.

 (i) Each subproblem is feasible; i.e., each subproblem contains at least one feasible solution.

 (ii) At least two subproblems are returned, unless the original problem has only one feasible solution; i.e., the original network graph is itself a tree.

 (iii) The union of the solution spaces of all subproblems contains at least one optimal solution to the original problem.

Figure 1 illustrates the basic idea. Given a problem, we apply a feasible decomposition method to get a set of subproblems. Then we solve these subproblems concurrently, compare the optimal solutions to subproblems, and select the best one, which is the optimal solution to the original problem.
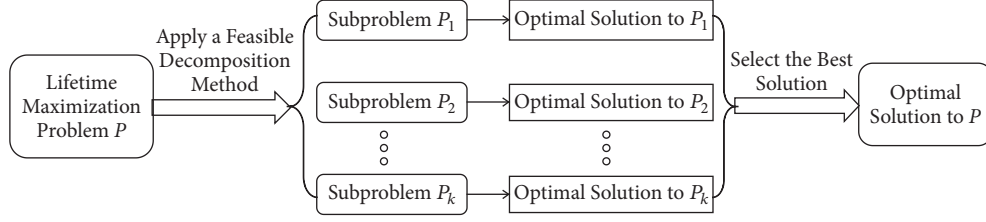
FIGURE 1: A problem decomposition framework.

```
Input: graph G, sink s, desired subproblem number t, a feasible decomposition method 𝒜
Output: a set of subproblems S
(1) S ← ∅;
(2) S′ ← apply 𝒜 on G;
(3) while |S ⋃ S′| < t ⋀ |S′| ≠ 0 do
(4)     let g be an arbitrary element of S′, remove g from S′;
(5)     S″ ← apply 𝒜 on g;
(6)     if |S″| = 1 then
            //g is a tree
(7)         add g to S;
(8)     else
(9)         S′ ← S′ ⋃ S″;
(10) S ← S′ ⋃ S;
(11) return S;
```

ALGORITHM 1: generate_sufficient_subproblems.

3.2. Generating a Sufficient Number of Subproblems. A challenge for the above framework is that a feasible decomposition method might not generate a sufficient number of subproblems. For example, a decomposition method may only give two subproblems. To this end, we observe that sequentially combining several feasible decomposition methods results in a feasible decomposition method.

Proposition 1. *Suppose 𝒜 and ℬ are two feasible decomposition methods. Apply 𝒜 on a problem P, and let the set of subproblems be H. If we apply ℬ on a subproblem h ∈ H and get subproblem set Q, then the union of solution spaces of subproblem set (H\{h}) ⋃ Q contains at least one optimal solution to problem P.*

Proof. Simply note that an optimal solution to subproblem h is contained in the solution space of Q, so it can be replaced by Q. □

Therefore, we can repeatedly apply a feasible decomposition method until the number of subproblems is sufficient. Algorithm 1 presents the detailed procedure.

In Algorithm 1, after initializing a variable S to store the final subproblem set in line (1), we apply the feasible decomposition method and get subproblem set S′ in line (2). We will ensure that S and S′ are disjoint throughout the algorithm, and S ⋃ S′ contains at least one optimal solution to the original problem. If the number of subproblems is insufficient, i.e., |S ⋃ S′| < t, we will remove one subproblem g from S′ in line (4) and apply 𝒜 to g to get another

subproblem set S″ in line (5). However, S″ may contain only one subproblem, e.g., when g is already a directed tree. In this case, we will insert g to S in line (7). Otherwise, we include S″ to S′. The above process is repeated until either the number of subproblems is sufficient or S′ is empty. Finally, we insert all elements remaining in S′ to S.

Theorem 2. *Algorithm 1 is a feasible decomposition method. It will call 𝒜 for at most 2t times where t is the desired number of subproblems. At termination, either |S| ≥ t or the solution space of each subproblem in S is simply a directed tree pointing to the sink.*

Proof. To see that Algorithm 1 is a feasible decomposition method, observe that all subproblems are obtained by sequentially applying 𝒜. The result follows from Proposition 1.

For the number of calls to 𝒜, consider the potential function $\phi = |S \bigcup S'| + |S|$. It is easy to see that $\phi \geq 0$ prior to the while loop, and $\phi \leq 2t$ at the last iteration. We claim that ϕ is increased by 1 in each iteration, indicating that the number of calls to 𝒜 is at most 2t.

To prove this claim, observe that each iteration of the while loop either increases $|S \bigcup S'|$ by at least one or increases $|S|$ by one. On the one hand, if line (9) is executed, then $|S''|$ is at least 2, so $|S \bigcup S'|$ is increased by at least one and $|S|$ is unchanged. On the other hand, if line (7) is executed, then $|S|$ is increased by one, so $|S \bigcup S'|$ is unchanged. Consequently, ϕ is increased by one. The claim is proved.
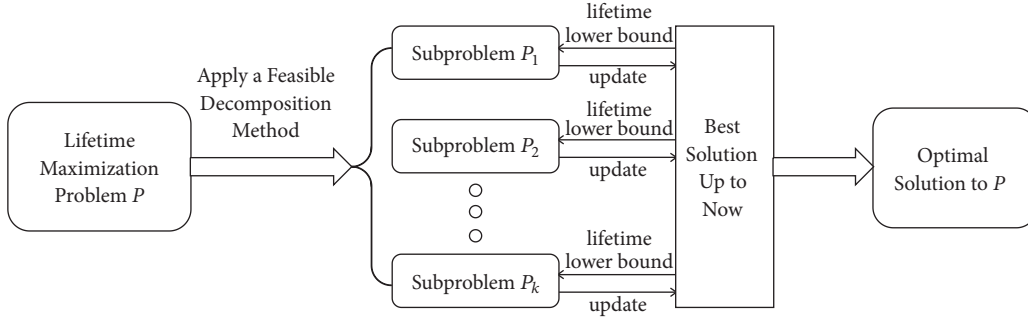
FIGURE 2: Incorporating feedback to the framework to reduce unnecessary computation. Solved subproblems can provide lifetime lower bound to unsolved subproblems.

For the last part, if $|S| \geq t$, then we are done. Otherwise, the while loop terminates with $|S'| = 0$. In this case, all elements in S are included in line (7), so these subproblems cannot be further divided, meaning that the solution space contains only one directed tree pointing to the sink. □

This theorem suggests that when t is a constant, Algorithm 1 has the same asymptotic running time as the given method $\mathcal{A}$. In Section 4, we will propose several feasible decomposition methods. These methods are used as subroutines of Algorithm 1 to generate a sufficient number of subproblems.

3.3. Solving Subproblems Concurrently on Multiple Cores. The straightforward method is to create threads whose number is equal to the number of subproblems. Each thread invokes an exact algorithm on a subproblem. Then the operating system will schedule the threads on available CPU cores automatically. Unfortunately, there are several drawbacks in this approach.

First, if the number of subproblems is greater than the number of cores, then there exists a core on which several threads are running. These threads compete in the core unnecessarily, wasting precious CPU time. Second, if the number of subproblems is required to be less than or equal to the number of cores, then some cores are wasted if their threads terminate early. Third, subproblems are solved independently, so that solving one subproblem cannot help solving the other problems. For example, if a solved subproblem has a solution with lifetime 100, then for the other unsolved subproblems, we should not waste time finding solutions with less lifetime.

To address these limitations, we create a thread for a core, so that l threads are created on a computer with l CPU cores. Each thread repeatedly performs the following three operations until all subproblems are solved.

  (i) Retrieve an unsolved problem and the best solution up to now.

 (ii) Invoke an exact algorithm on the unsolved subproblem with the best solution up to now as a lower bound.

(iii) Mark the subproblem as solved, and update the best solution up to now.

Figure 2 shows the change to the framework, where the solved subproblems provide feedback to unsolved subproblems. Instead of solving subproblems independently, we maintain the current best solution to reduce unnecessary recomputation in unsolved subproblems.

We can see that this approach does not have the above limitations. First, since the number of threads is equal to the number of cores, no two threads compete in the same core. Second, CPU cores are fully used, since they will keep running until all subproblems are solved. Third, when a thread attempts to solve a subproblem, it will retrieve the status of solved subproblems, e.g., the lifetime of the current best solution, which will help reduce unnecessary computation.

4. Three Feasible Decomposition Methods

We propose three decomposition methods based on different observations. First, a tree does not contain undirected cycles. Second, a tree does not contain directed cycles. Third, a node has only one parent in a directed tree.

4.1. Decomposition by Breaking Undirected Cycle. This approach applies to undirected graphs. Observe that a feasible solution to the lifetime maximization problem is a tree, so any feasible solution cannot contain a cycle. The basic idea of our approach is to find an undirected cycle and create subproblems by breaking the cycle, i.e., removing one edge at a time. Each decomposed subproblem contains one less edge than the original problem. Figure 3 gives an example. By breaking cycle $A - B - C - A$, we get three subproblems P_1, P_2, and P_3. Note that applying this method to directed graphs needs slight modifications.

One design issue is to decide which cycle to break. We propose to choose the cycle containing the minimum number of edges. The motivation is to generate a small number of subproblems at each time, so that the total number of subproblems can be controlled more easily when calling Algorithm 1. We will discuss this motivation in Section 5.

Algorithm 2 presents our approach. We first use the algorithm in [13] to find a minimum cycle in line (1). Then, in lines (2)-(5), we create subproblems whose number is equal

Input: graph $G(V, E)$, sink s
Output: subproblem set P
(1) find a cycle with minimum length by the MIN_CIRCUIT algorithm in [13], let C be the edges of the cycle;
(2) $i \leftarrow 1$;
(3) **foreach** $e \in C$ **do**
(4)   construct subproblem P_i with $G \setminus \{e\}$ as the network;
(5) $i \leftarrow i + 1$;
(6) $P \leftarrow \{P_1, P_2, \cdots\}$;
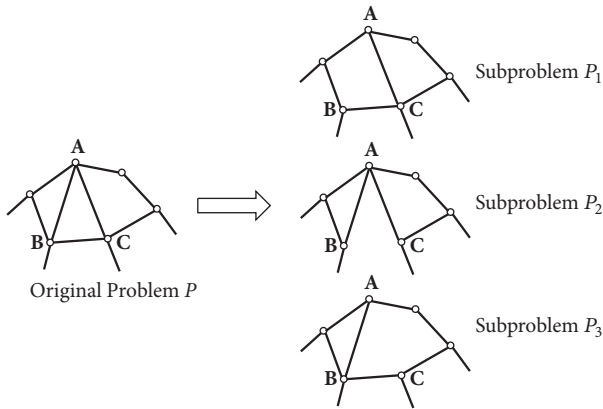
ALGORITHM 2: decompse_undirected_cycle.
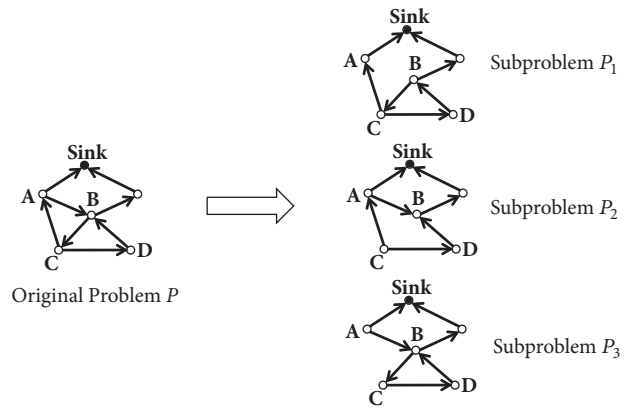

FIGURE 3: Breaking an undirected cycle to create three subproblems.

FIGURE 4: A directed network graph and three subproblems by breaking directed cycle ABCA.

to the number of edges in the cycle. Each subproblem is obtained by deleting one edge from the cycle.

Theorem 3. *Algorithm 2 is a feasible decomposition method. It runs in $O(mn)$ time, where m is the number of edges and n is the number of vertices.*

Proof. It is easy to verify that the first two conditions of a feasible decomposition method are satisfied, since a cycle contains at least three edges. For the third condition, let the original problem be P and the constructed subproblems be $P_1, P_2, \ldots, P_k$ with corresponding removed edges $e_1, e_2, \ldots, e_k$. Let $S(P)$ be the solution space of problem P. We claim a stronger result that

$$S(P) \subseteq \bigcup_{i=1}^{k} S(P_i). \qquad (1)$$

To prove this, consider an arbitrary feasible solution x to problem P, i.e., $x \in S(P)$. Because x is a tree, it cannot contain all edges in the cycle. Suppose it does not contain e_j. Then, $x \in S(P_j)$. The claim follows immediately.

For the running time, note that the algorithm in [13] runs in $O(mn)$ time. The found cycle contains at most $O(n)$ edges, so the for loop has at most $O(n)$ iterations. Since constructing a subproblem can be finished in $O(m)$ time, the for loop runs in $O(mn)$ time. The overall running time is $O(mn)$. □

4.2. Decomposition by Breaking Directed Cycle. When the network graph is directed, we can see that no solution contains a directed cycle. Thus, we first find a directed cycle and create a subproblem by removing one edge from the cycle. We choose the minimum cycle to create subproblems, so that the total number of subproblems can be better controlled. Figure 4 gives an example. In the problem, we can break cycle ABCA to get three subproblems.

One problem for this approach is that there may exist a subproblem that does not contain any feasible solution to the original problem. For example, in Figure 4, if we consider the cycle BCDB, then the subproblem by removing edge DB does not contain a feasible solution since no path connects D to the sink. To solve this problem, we check the feasibility of each subproblem and remove infeasible ones. If there is only one feasible subproblem, then we find directed cycles from the subproblem. Since one edge has been removed, the subproblem contains fewer edges than the original problem; the process will terminate.

Algorithm 3 presents the decomposition method. We first check whether the graph itself is a tree. If it is a tree, we return the graph immediately in line (1). Otherwise, we find a directed cycle with the minimum number of edges. If no directed cycle exists, then there exists at least one vertex with out degree larger than 1. We identify such a vertex and insert all its out edges into C in line (4). Then, we construct subproblems by removing one edge from C in lines (6)-(11).

```
Input: graph G(V, E), sink s
Output: subproblem set P
(1) return G if G is a tree;
(2) let C be the minimum directed cycle found by the DICIRCUIT algorithm in [13];
(3) if C = ∅ then // no cycle
(4)     find any vertex with out degree larger than 1, and
        insert its out edges into C;
(5) i ← 0;
(6) foreach e ∈ C do
(7)     G' ← G \ {e};
(8)     reverse the direction of edges in G', and perform a breadth-first search from the sink;
(9)     if all vertices are visited then
(10)        i ← i + 1;
(11)        construct subproblem P_i with G' as the network;
(12) if i = 1 then
(13)    C' ← graph of subproblem P_1;
(14)    return decomp_directed_cycle(G');
(15) else
(16)    return {P_1, P_2, ⋯ , P_i};
```

ALGORITHM 3: decomp_directed_cycle.

Different from Algorithm 2, we need to verify whether the constructed subproblem is feasible. This is done by reversing the directions of the edges and performing a breadth-first search from the sink in line (8). The subproblem is feasible if and only if all vertices are visited. If the subproblem is feasible, we store it in line (11). Finally, if we get only one feasible subproblem, then we recursively call Algorithm 3 to get subproblems in lines (13) and (14). Otherwise, we return in line (16).

Theorem 4. *Algorithm 3 is a feasible decomposition method. It runs in* $O(m^2 n)$ *time.*

Proof. Consider the recursion tree of Algorithm 3. If the last call to Algorithm 3 (i.e., the leaf node in the recursion tree) returns in line (1), then the original problem contains exactly one feasible solution. If it returns in line (16), then at least two feasible subproblems are returned. Similar to the proof of Theorem 3, the union of solution spaces of these subproblems contains at least one optimal solution to the original problem. So the algorithm is a feasible decomposition method.

For the running time, line (2) in Algorithm 3 runs in $O(mn)$ time. Observe that lines (3)-(11) run in $O(mn)$ time. So, except for the recursive call in line (14), the rest of the algorithm runs in $O(mn)$ time. Consider the recursion tree of the algorithm. Since each call to the algorithm will remove at least one edge from the input graph in line (7) and there are $O(m)$ edges, the depth of the recursion tree is $O(m)$. Therefore, the overall running time is $O(m^2 n)$. □

4.3. Decomposition by Fixing the Parent Node. Observe the fact that a node except for the sink has one parent in a directed tree. Thus, given a node, we can create subproblems by keeping one out edge to fix its parent and deleting other out edges. Figure 5 gives an example. Vertex A has three out
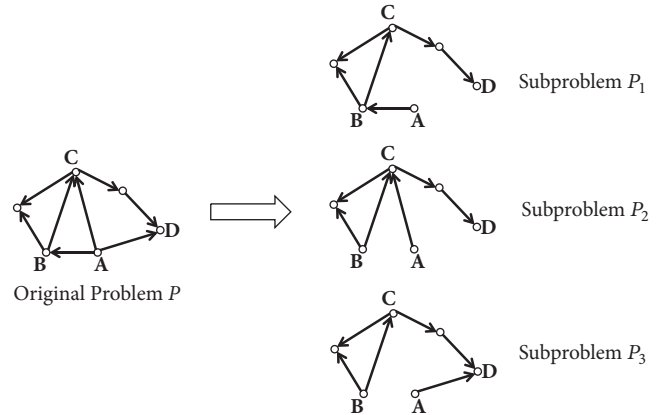
FIGURE 5: A directed network graph and three subproblems by fixing the parent node of vertex A.

edges pointing to nodes B, C, and D, so we can construct three subproblems P_1, P_2, and P_3, where the parent of A is fixed to B, C, and D, respectively.

Two issues need to be solved. First, a subproblem may not be feasible. This is similar to Section 4.2, and we can also introduce the verification step to remove infeasible subproblems. For the example in Figure 5, if D is the sink, then we cannot remove edge BC, since the resulting subproblem will be infeasible. Second, we need to consider which node to choose. We propose to choose the node with the minimum initial energy. This is based on the intuition that nodes with less energy are usually the bottleneck for the network's lifetime.

Algorithm 4 presents the method. We sort nodes in ascending order by their initial energy in line (2). We will consider nodes in this order one by one (lines (3)-(4)). For each node, we visit its out edges and construct a subproblem

```
Input: graph G(V, E), sink s
Output: subproblem set P
(1) P ← ∅;
(2) sort nodes in ascending order by initial energy, and let L be the sorted list;
(3) while L ≠ ∅ ∧ |P| ≤ 1 do
(4)     u ← L.removeFirst();
(5)     for uv ∈ G do
(6)         G' ← G \ {uw ∈ G | w ≠ v};
(7)         reverse the directions of edges in G' and perform a breadth-first search from the sink
(8)         if all vertices are visited then
(9)             construct subproblem P' with G' as the network;
(10)            include P' to P;
(11) return P;
```

ALGORITHM 4: decomp_fixing_parent.

by keeping one out edge and deleting others in line (6), which essentially fixes the node's parent in the routing tree. To check whether the resulting subproblem is feasible, we reverse the directions of the edges and perform a breadth-first search from the sink in line (7). The subproblem is feasible if and only if all vertices are visited. If the subproblem is feasible, we include it to subproblem set P in line (1). In either case, we continue to consider the next node until either L is empty or P contains at least two subproblems.

Theorem 5. *Algorithm 4 is a feasible decomposition method, and it runs in $O(m^2)$ time.*

Proof. Algorithm 4 terminates if either L is empty or P contains at least two feasible subproblems. In the first case, the original problem contains exactly one feasible solution. In the second case, at least two feasible subproblems are returned and it is easy to prove that the union of solution spaces of these subproblems contains at least one optimal solution to the original problem. So the algorithm is a feasible decomposition method.

For the running time, sorting nodes in line (2) runs in $O(n \log n)$ time. Observe that, in the worst case, each edge in G will be examined once in line (5), and lines (6)-(10) run in $O(m)$ times, so the while loop runs in $O(m^2)$ time. The overall running time is $O(m^2)$. □

5. Discussion

In this section, we analyze the overall running time of algorithms and discuss several related issues.

Lemma 6. *Suppose there are t subproblems and δ cores. Then, there exists a core that solves at most $\lfloor t/\delta \rfloor$ subproblems.*

Proof. It follows from the pigeonhole principle. □

Incorporating Algorithm 1 with the three decomposition methods, i.e., decomposition by breaking undirected cycle, decomposition by breaking directed cycle, and decomposition by fixing the parent, gives three algorithms, which are denoted by UnCycle, DCycle, and FixP.

Theorem 7. *Let $R(m, n)$ be the worst-case running time of an exact algorithm to solve a problem containing m directed edges and n vertices, t be the number of subproblems, and δ be the number of CPU cores. One has the following results.*

   (i) *UnCycle runs in $O(mnt) + (\lfloor t/\delta \rfloor + 1)R(m - 2, n)$ time.*

  (ii) *DCycle runs in $O(m^2nt) + (\lfloor t/\delta \rfloor + 1)R(m - 1, n)$ time.*

 (iii) *FixP runs in $O(m^2t) + (\lfloor t/\delta \rfloor + 1)R(m - 1, n)$ time.*

Proof. Observe that the running time of each algorithm consists of two parts, one of which is for dividing the problem into t subproblems and the other is for solving the subproblems. The first part is a single thread program, and, following Theorem 2, its running time is $2t$ times the running time of the corresponding decomposition method. Due to Theorems 3, 4, and 5, the first part running time for UnCycle is $O(mnt)$, that for DCycle is $O(m^2nt)$, and that for FixP is $O(m^2t)$.

The second part uses δ cores to solve the subproblems. By Lemma 6, there exists one core that solves at most $\lfloor t/\delta \rfloor$ subproblems. Consider this core. We can see that when this core finishes computing $\lfloor t/\delta \rfloor$ subproblems, there are no subproblems left. (Otherwise, this core should pick up another subproblem to solve.) This suggests that the other cores either already terminate or are computing the last subproblem. Thus, the running time is at most the time for computing $\lfloor t/\delta \rfloor + 1$ subproblems. Further note that each subproblem in UnCycle contains $m - 2$ edges, each subproblem in DCycle contains $m - 1$ edges, and each subproblem in FixP contains at most $m - 1$ edges. The theorem follows immediately. □

Note that this theorem studies the worst-case running time. Though FixP seems to have the same complexity with DCycle, the edges of each subproblem in FixP are usually less than $m - 1$.

Another concern for our approach is that the same tree may be produced by different subproblems, so that computations are wasted. This is indeed true for UnCycle and DCycle. However, this happens only if the two subproblems are being solved on different cores at the same time, because

if they are solved sequentially, then the solved subproblem provides feedback to the unsolved subproblem, eliminating redundant trees. This mechanism is shown in Figure 2. Since subproblems are smaller than the original problem, we find that using multiple cores does not increase the running time. In addition, the redundant computation problem does not exist for FixP. In different subproblems of FixP, at least one node has a different parent due to the decomposition method. Thus, it is not possible for two subproblems to produce the same tree.

In this paper, we consider constructing a single tree for the network. If multiple trees are allowed, i.e., the network uses a different routing tree after some time, then the overall lifetime can be further extended. The drawback of this approach is that sensor nodes need to perform complex operations, e.g., either to record multiple routing paths in memory to change parents periodically or to receive commands from the network periodically. We plan to extend our result to this scenario in the future.

Finally, we discuss the motivation for finding the minimum cycle in UnCycle and the minimum directed cycle in DCycle. There are several reasons. Ideally, we should find a cycle with length t so that we can break the problem into t subproblems, where t is provided by the user. However, this problem is NP-hard to solve. To see this, simply note that this problem contains the Hamiltonian path problem as a special case (when t=n). We cannot afford another exponential time algorithm to get the desired cycle. On the contrary, finding a minimum cycle or a cycle with arbitrary length can be done in polynomial time. To this end, we need to use Algorithm 1 to get the desired number of subproblems. If we decompose the graph by finding a cycle with arbitrary length (e.g., by performing a DFS search to get an arbitrary cycle), then it is probable that the number of subproblems may be much more than t. Instead, by finding a cycle with minimum length, we get small granularity in that each time we add a few subproblems to the set of subproblems. An additional benefit is that a resulting subproblem may be obtained by calling the decomposition method several times, so it has fewer edges.

6. Simulations

We compare our approach with previous single-thread approaches on randomly generated sensor networks. Sensors are uniformly and randomly distributed in a $100(m)\times100(m)$ square field, and the sink node is located at the center. Two nodes can receive messages from each other if and only if their distance is not greater than 20 meters. Thus, the graph is essentially a unit disk graph. Figure 6 shows one such network with 41 nodes. Each node has its initial energy uniformly drawn from $[1, 10]J$. The energy consumption for receiving and transmitting a message is $3.33 \times 10^{-4}J$ and $6.66 \times 10^{-4}J$, respectively. These settings are consistent with those in [1, 3]. We use Java language to program all algorithms and run them on a desktop computer with configuration listed in Table 1.

We implement the proposed decomposition methods to generate subproblems including decomposition by breaking undirected cycle (UnCycle), decomposition by breaking directed cycle (DCycle), and decomposition by fixing the
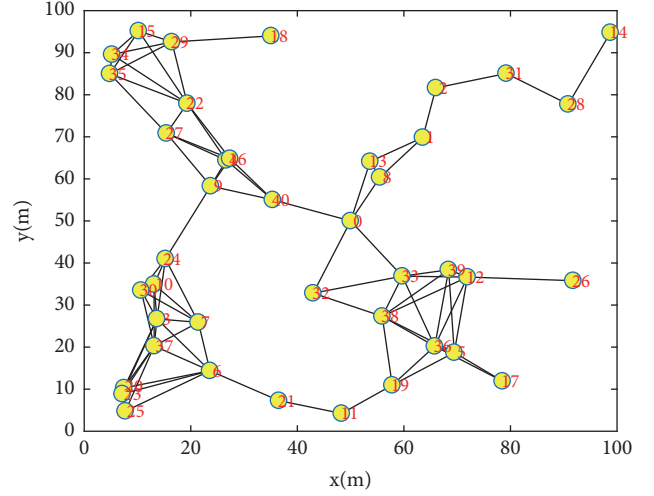

FIGURE 6: A randomly generated network consisting of 41 nodes.

TABLE 1: Desktop computer configuration.

Operating System	Windows 7 64 bit
CPU	Intel(R) Core(TM) i7-4770 Processor
Number of Cores	8
Memory	8GB
Java Runtime Environment	JRE 1.8.0
ILP Solver	lp_solve 5.5

parent (FixP). We consider networks with $30, 35, \ldots, 55$ nodes, and for each node number, we generate 20 network instances, so that there are 120 problem instances. We vary the number of subproblems from 8 to 20 with increments of 4. Note that if the number of subproblems is fixed to 1, then no decomposition is performed. We set the maximum allowed running time to 10 minutes, after which we terminate an algorithm and mark the network as fail for the algorithm. We implement two previous algorithms: ILP-B that uses integer linear programming with binary search [1] and ILP-BD that improves ILP-B by adding a procedure to decompose the network graph into biconnected subgraphs [3].

6.1. Performance Improvement on ILP-B. We study the improvement of our approach on ILP-B in terms of average running time. Figure 7 shows the results. When the number of subproblems is 1, our approach is not applied and the result corresponds to the original algorithm. Note that we do not take into account problem instances that no algorithm can solve within ten minutes. Other than these networks, we approximate the running time of an algorithm on a problem instance to ten minutes if it fails to get the optimal solution. We will also study the effect of this approximation.

We have two observations from the figure. First, our approach can significantly reduce the average running time. This is in line with intuition since all CPU cores are used. Second, when the number of subproblems is either small (8) or large (20), the average running time is not the smallest. We
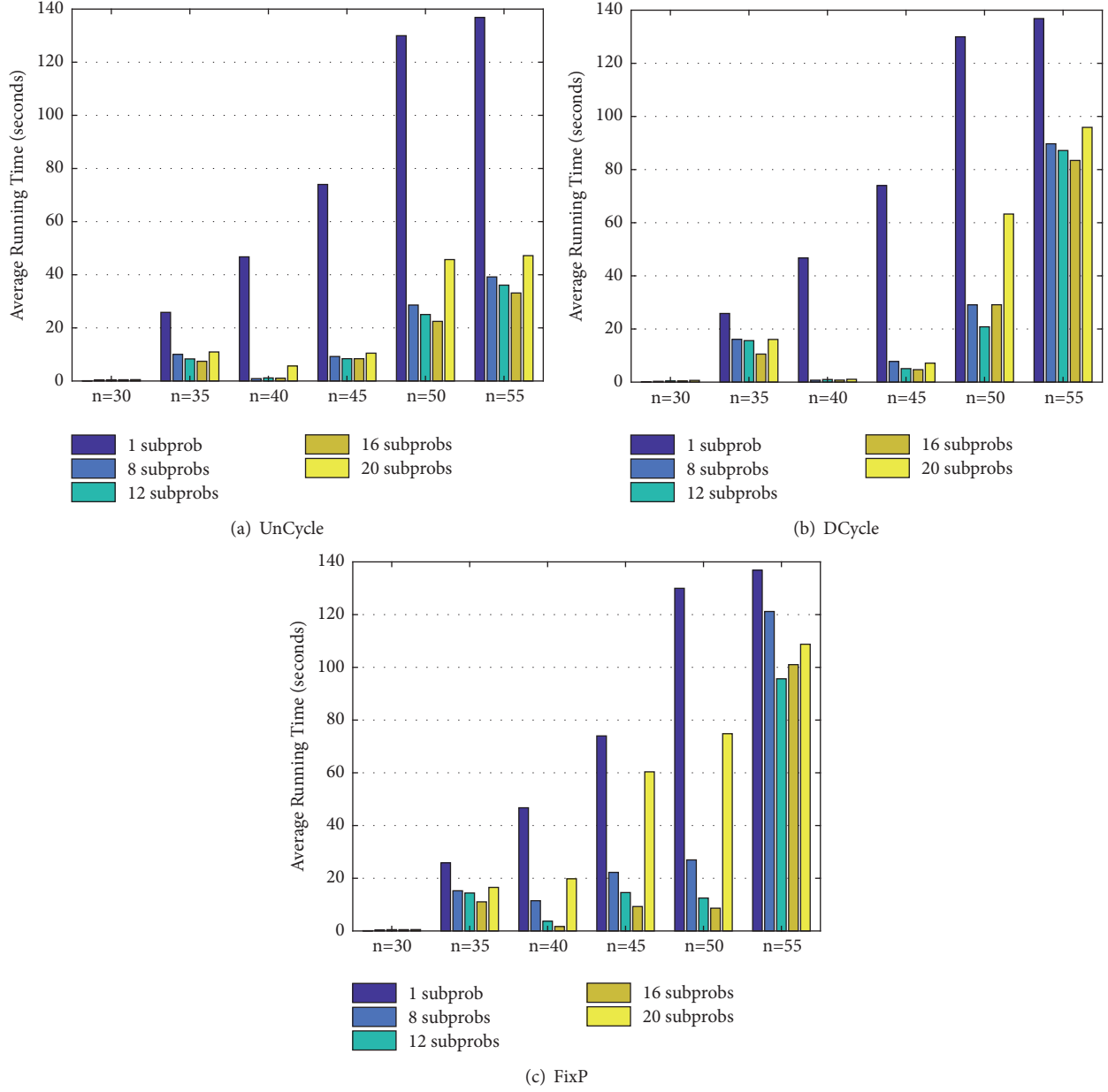
(a) UnCycle

(b) DCycle

(c) FixP

FIGURE 7: Average running time of ILP-B with three decomposition methods under different numbers of subproblems.

get smaller running time when the number of subproblems is 12 or 16. When the number of subproblems is small, most subproblems are still very similar to the original problem. But when we get too many subproblems, even though most subproblems are simpler, it is more likely that we encounter a difficult subproblem. Indeed, in lifetime maximization problem, small problem size is not a guarantee of less running time. Thus, we recommend to set the number of subproblems to within twice the number of CPU cores.

We show that the approximation of the running time of unsolved instance as ten minutes is reasonable in that the relationship of running time of different algorithms remains the same under this approximation. To this end, we vary the maximum allowed running time from 2 minutes to 10

minutes with increments of 2 minutes. Figure 9 shows the resulting average running time for networks containing 46 nodes. We can see that, with the increase of the maximum allowed running time, the average running time is increased since unsolved problem instances contribute more running time due to the approximation. However, the relationship between different algorithms remains the same; i.e., FixP has the smallest average running time in all cases, DCycle has the second smallest average running time, and so forth. Therefore, we believe the approximation is reasonable.

6.2. Performance Improvement on ILP-BD. We study the improvement on ILP-BD with the same problem instances in

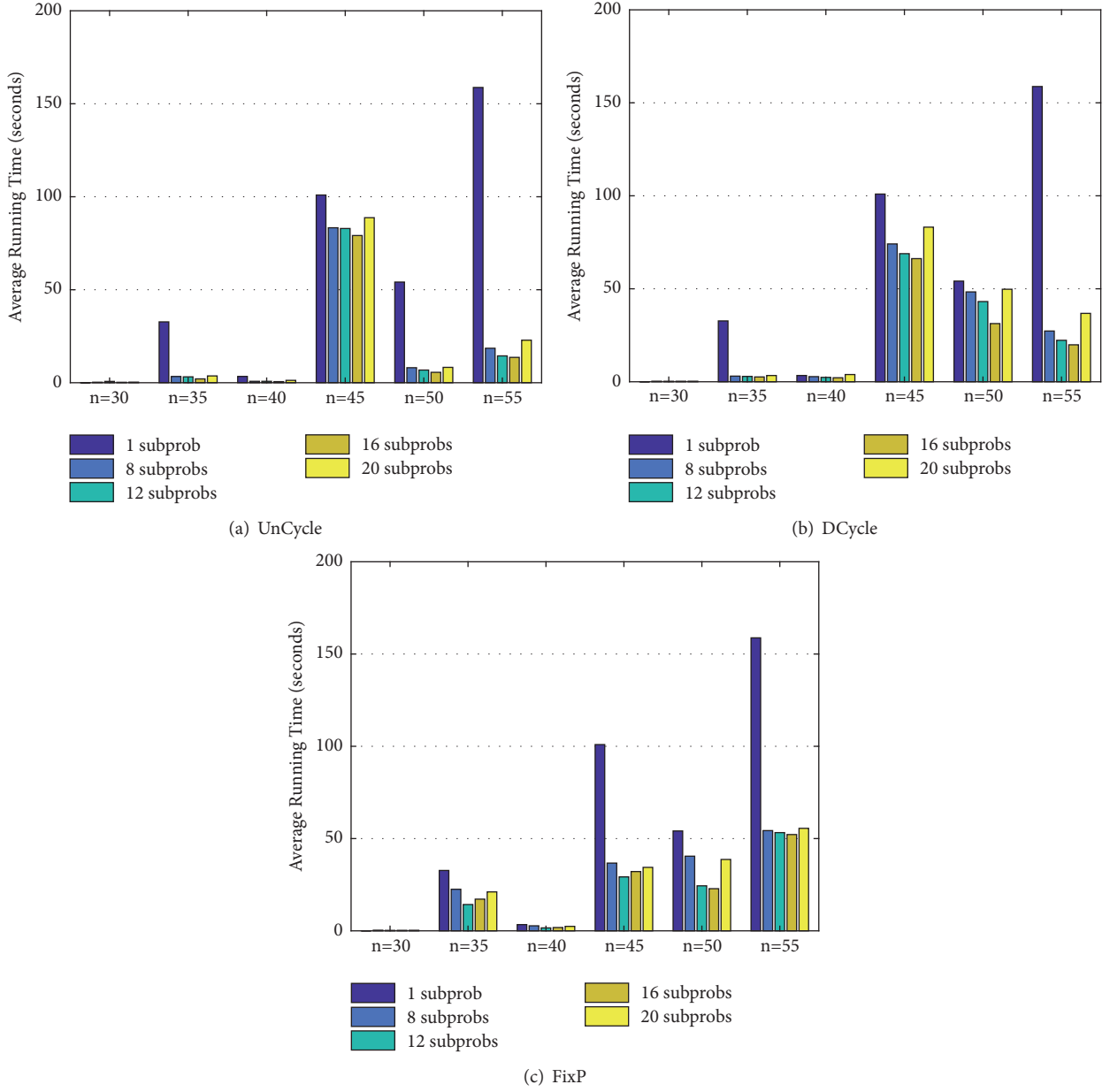(a) UnCycle

(b) DCycle

(c) FixP

FIGURE 8: Average running time of ILP-BD with three decomposition methods under different numbers of subproblems.

Section 6.1. We do not take a problem instance into account if all configurations cannot solve it. Figure 8 shows the results. The results are similar.

We can see again that our approach greatly reduces the average running time. The improvement is more significant when the number of nodes becomes larger. Setting the number of subproblems to 12 or 16 gives smaller running time than 8 or 20. Note that it is not fair to compare ILP-BD with ILP-B using Figures 7 and 8, because the problem instances used in average running time computation are different for the two approaches. In fact, ILP-BD can solve more problem instances in general, so some solved difficult problem instances increase the average running time.

6.3. Performance Improvements in the Number of Failed Networks. Besides average running time, we show that the number of failed networks is smaller for our approach. Figures 10 and 11 show the number of failed networks of each decomposition method on algorithms ILP-B and ILP-BD. Note that we omit the result for networks with 30 and 35 nodes, since all approaches can solve all problem instances within ten minutes. We can see that our methods can solve more networks than previous single-thread method. The improvement is more obvious when the network contains more nodes. In addition, ILP-BD can solve more problem instances than ILP-B, and our approach can further improve ILP-BD significantly.
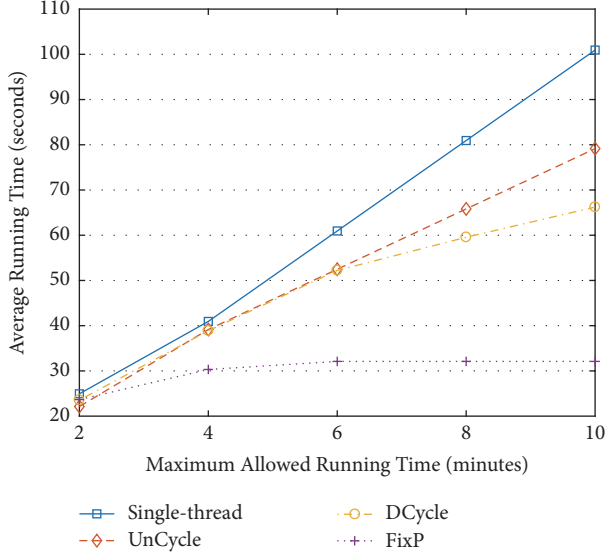
FIGURE 9: Impact of the maximum allowed running time on the computation of average running time.
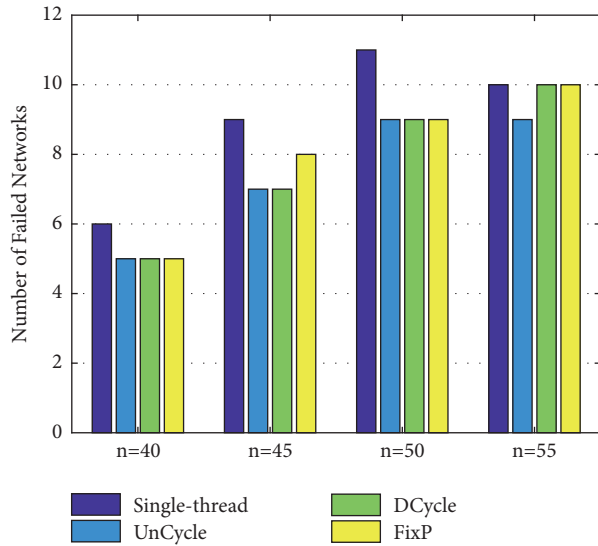

FIGURE 11: Number of failed networks of ILP-BD.

FIGURE 10: Number of failed networks of ILP-B.

FIGURE 12: A network with 49 nodes in [4]. Solid disk represents the sink. The distance between columns (and rows) is roughly 5 meters.

TABLE 2: Running time of each method on the network in [4].

Methods	Running time
Single-thread	175.285(s)
UnCycle	1.395(s)
DCycle	37.831(s)
FixP	0.746(s)

6.4. Performance on a Real Network. We test the algorithms on a real network reported in [4]. The network consists of 49 sensor nodes deployed on a 7×7 grid. The distance between adjacent columns is roughly 5 meters. Two nodes are connected by an edge if the received signal strength is at least -74db, giving a network topology in Figure 12. We run our algorithms with ILB-BD on the network and show the running time of each method in Table 2. We can see that using multiple cores can indeed reduce the running time. While the original single-thread program needs about 3 minutes, FixP terminates in less than 1 second.
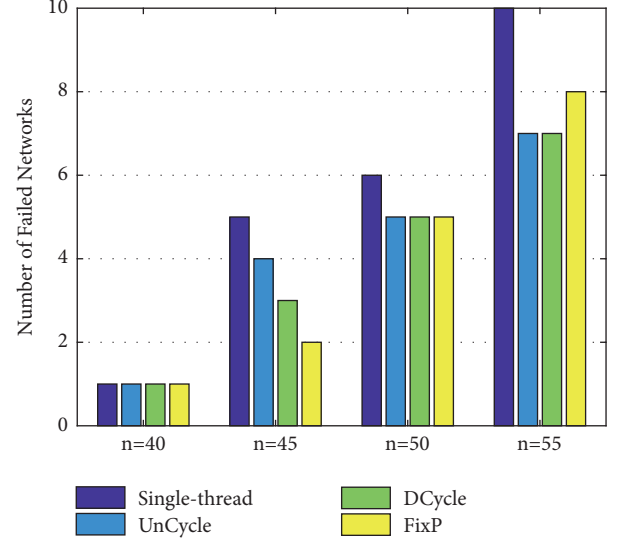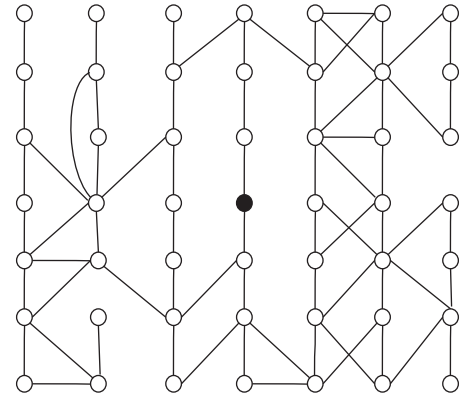
7. Conclusions

In this paper, we proposed to use multiple cores to speed up existing exact algorithms for finding optimal routing tree of wireless sensor networks. The basic idea is to decompose the original problem into multiple subproblems and run them on different CPU cores. We propose three decomposition methods and prove their correctness. Numerical results show that the three methods can speed up the calculation significantly

in terms of average running time and the number of solved problems.

Data Availability

The data used to support the findings of this study are available from the corresponding author upon request.

Conflicts of Interest

The authors declare that they have no conflicts of interest.

Acknowledgments

References

[1] X. Zhu, X. Wu, and G. Chen, "An exact algorithm for maximum lifetime data gathering tree without aggregation in wireless sensor networks," *Wireless Networks*, vol. 21, no. 1, pp. 281–295, 2015.

[2] Y. Wu, Z. Mao, S. Fahmy, and N. B. Shroff, "Constructing maximum-lifetime data-gathering forests in sensor networks," *IEEE/ACM Transactions on Networking*, vol. 18, no. 5, pp. 1571–1584, 2010.

[3] X. Ma, X. Zhu, and B. Chen, "Exact Algorithms for Maximizing Lifetime of WSNs Using Integer Linear Programming," in *Proceedings of the 2017 IEEE Wireless Communications and Networking Conference (WCNC)*, pp. 1–6, San Francisco, CA, USA, March 2017.

[4] Z. Zhong and T. He, "RSD: a metric for achieving range-free localization beyond connectivity," *IEEE Transactions on Parallel and Distributed Systems*, vol. 22, no. 11, pp. 1943–1951, 2011.

[5] M. Shan, G. Chen, D. Luo, X. Zhu, and X. Wu, "Building maximum lifetime shortest path data aggregation trees in wireless sensor networks," *ACM Transactions on Sensor Networks*, vol. 11, no. 1, 2014.

[6] H. Harb, A. Makhoul, D. Laiymani, and A. Jaber, "A distance-based data aggregation technique for periodic sensor networks," *ACM Transactions on Sensor Networks*, vol. 13, no. 4, 2017.

[7] L. Xu, X. Zhu, H. Dai, X. Wu, and G. Chen, "Towards energy-fairness for broadcast scheduling with minimum delay in low-duty-cycle sensor networks," *Computer Communications*, vol. 75, pp. 81–96, 2016.

[8] X. Zhu, G. Chen, S. Tang, X. Wu, and B. Chen, "Fast approximation algorithm for maximum lifetime aggregation trees in wireless sensor networks," *INFORMS Journal on Computing*, vol. 28, no. 3, pp. 417–431, 2016.

[9] J. Wu, Q. Liang, B. Zhang, and X. Wu, "On the Security of Wireless Sensor Networks via Compressive Sensing," in *The Proceedings of the Third International Conference on Communications, Signal Processing, and Systems*, vol. 322 of *Lecture Notes in Electrical Engineering*, pp. 69–77, Springer International Publishing, 2015.

[10] T. Liu, B. Wu, H. Wu, and J. Peng, "Low-Cost Collaborative Mobile Charging for Large-Scale Wireless Sensor Networks," *IEEE Transactions on Mobile Computing*, vol. 16, no. 8, pp. 2213–2227, 2017.

[11] M. Lounis, A. Bounceur, A. Laga, and B. Pottier, "GPU-based parallel computing of energy consumption in wireless sensor networks," in *Proceedings of the European Conference on Networks and Communications, (EuCNC '15)*, pp. 290–295, fra, July 2015.

[12] A. Munir, A. Gordon-Ross, and S. Ranka, "Multi-core embedded wireless sensor networks: Architecture and applications," *IEEE Transactions on Parallel and Distributed Systems*, vol. 25, no. 6, pp. 1553–1562, 2014.

[13] A. Itai and M. Rodeh, "Finding a minimum circuit in a graph," *SIAM Journal on Computing*, vol. 7, no. 4, pp. 413–423, 1978.

Research Article

Game-Theoretic Social-Aware Resource Allocation for Device-to-Device Communications Underlaying Cellular Network

Lei Wang ,[1,2] **Can Li,**[1] **Yanbin Zhang,**[1] **and Guan Gui** [1]

[1]*National and Local Joint Engineering Laboratory of RF Integration and Micro-Assembly Technology,*
 Nanjing University of Posts and Telecommunications, Nanjing, China
[2]*The State Key Laboratory of Integrated Services Networks, Xidian University, Xi'an, China*

Correspondence should be addressed to Guan Gui; guiguan@njupt.edu.cn

Academic Editor: Mu Zhou

Device-to-Device communication underlaying cellular network can increase the spectrum efficiency due to direct proximity communication and frequency reuse. However, such performance improvement is influenced by the power interference caused by spectrum sharing and social characteristics in each social community jointly. In this investigation, we present a dynamic game theory with complete information based D2D resource allocation scheme for D2D communication underlaying cellular network. In this resource allocation method, we quantify both the rate influence from the power interference caused by the D2D transmitter to cellular users and rate enhancement brought by the social relationships between mobile users. Then, the utility function maximization game is formulated to optimize the overall transmission rate performance of the network, which synthetically measures the final influence from both power interference and sociality enhancement. Simultaneously, we discuss the Nash Equilibrium of the proposed utility function maximization game from a theoretical point of view and further put forward a utility priority searching algorithm based resource allocation scheme. Simulation results show that our proposed scheme attains better performance compared with the other two advanced proposals.

1. Introduction

With the rapid spread of intelligence terminals and the explosive growth of communication capacity, local area services are considered as a popular issue. Traditional cellular networks can not meet the explosive demands for gigantic amount of mobile users in the following years. As Device-to-Device (D2D) communication enables direct communication between a pair of mobile users in proximity by occupying the cellular spectrum without traversing the BS or core network [1, 2], it becomes an important usage case through peer-to-peer scheme while nowadays mobile users in cellular networks need high-speed data service in which they could potentially be in range for direct communication [3–5]. For example, when friends close to each other want to exchange music, picture, or video via their own mobile phone, the D2D communication can provide a reasonable solution for the local media service as the same interested contents can be shared between mobile users. In this way, the throughput and spectral efficiency of the network can be highly increased [6–8].

In D2D communication underlaying cellular network, mobile users occupy the same licensed band of spectrum resource for cellular users to increase the system capacity. Hence, resource allocation becomes the key issue in D2D communication, and appropriate resource allocation schemes are imperative to be conducted to settle this issue [9]. Considering the fact that the D2D communication shares the uplink spectrum resource, Xu et al. utilize a reverse iterative combinatorial auction based mechanism to accomplish the resource allocation [10]. Ferdouse et al. propose a throughput efficient subcarrier allocation (TESA) proposal for multiclass cellular D2D systems [11]. Hoang et al. adopt graph-based approach to discuss the nonorthogonal dynamic spectrum sharing to maximize the weighted system sum rate [12].

Worth mentioning about the above studies [10–12] is that mobile users in social networks usually form stable social networks when communicating with others. They are grouped by social relationships or background to form different communities which have the same interested contents. Human beings in social communities share interested content through online social platforms, such as Weibo and WeChat. The more the interactions that take place in the community, the faster the transmission rate the community will consider. But these studies above all pay attention to improving the transmission rate in an overall perspective to restrict the interference cellular communication suffers [13]. The characteristics of high sociality may be able to improve the spectrum efficiency greatly; however, this has not been considered.

The sociality in D2D communication has been extensively studied for resource allocation optimization problem. Wang et al. model the strength of sociality of D2D links by counting contact time among mobile users [14]. The authors in [15] propose a social-aware resource allocation method based on two hops: communication with the BS (first hop) and extending communication with another device (second hop), but, with the iterations proceeding, the size of the master problem is also increasing. Li et al. quantitatively analyze the benefit taken by the incorporation of social features and propose a social-ware D2D communication framework by leveraging these social networking characteristics; this investigation has created the precedent for studying the problem of social-awareness based D2D resource allocation in [16].

The aforementioned works indicate that the rate performance of the network can be effectively improved by implementing proper interference control policy and fully using social networking characteristics. However, how to allocate cellular resource for each D2D pairs is much more complex. The difference of our work from all the works done by those predecessors is that we maximize the sum transmission rate of the system by jointly paying attention to the interference caused by the D2D transmitter to cellular user and rate performance enhanced by the social relationships between mobile users. Thus, we further design a priority searching algorithm based resource allocation scheme in D2D communications underlaying cellular network.

Generally, D2D pairs along with cellular users may be self-interested to maximize their own benefit through cooperation or competition in the underlaying D2D communication network. Consequently, it is needed to develop suitable solutions to the consideration we present above. At the same time, game theory is adopted for modeling and researching the resource allocation problem in recent works. Many kinds of game theory have been applied to the study of D2D resource allocation problems. In [17], a social-community utilization optimization game is proposed to optimize the utility of social community for each of the D2D pairs. But modeling the game in such a way seems quite a complex task. In [18], Stackelberg game has been applied to model the interactions between D2D users and cellular users. Since the Stackelberg game belongs to the category of cooperative game, its outcome is not social optimum. Further cooperative games such as Nash Bargaining Solution (NBS) are needed to improve the results. In [19], NBS is developed to tackle the

inefficiency of the scheme in [18] where the assumption is not reasonable in practical environment.

Despite the popularity of game theory in recent resource allocation related investigation, the most common idea of these papers is to verify that any strategy that deviates from the Nash Equilibrium (NE) can not improve the system performance any more. This one-side proof may be not convincing enough when applying to resource allocation problem between two disjoint sets influenced by mutual interference. Accordingly, the matching theory provides a distributed solution to resource matching problem between two disjoint sets. In [20], the matching theory was employed to match D2D pairs with cellular users to address the energy efficiency optimization problem in D2D enabled cellular networks. Besides, this work was extended to large-scale networks and acquired significant performance gains. In [21], a 3D iterative matching algorithm was proposed to maximize the sum rate of D2D pairs while guaranteeing the QoS requirement of both cellular communication and D2D communication. In [22], the matching theory was used to model the network as a one-to-one matching market and each secondary user (SU) can maximize its utility by selecting the most suitable primary user (PU). However, it is confirmed that sociality-interference joint resource allocation problem has not been considered from the perspective of matching theory.

In this paper, in order to jointly compare the influence of sociality between the mobile users within the same community and power interference caused by D2D communication, we discuss the main problem existing in current resource allocation scheme and propose a utility function maximization (UFM) game for D2D communication underlaying cellular network by utility function construction, game establishment, providing relative proof for the existence of Nash Equilibrium. Inspired by one-to-one matching theory, we propose a priority searching algorithm based resource allocation scheme to acquire the final resource allocation proposal for the UFM game. We perform extensive simulations under realistic social network to evaluate the rate performance of our proposed scheme. The result shows that our proposed scheme improves system performance obviously, in terms of increasing the overall transmission rate and decreasing the transmission time.

The remainder of this paper is organized as follows: we introduce the system model and formulate the problem in Section 2. UFM game is formulated in Section 3. Then, in Section 4, a priority searching based resource allocation algorithm is proposed, and, in Section 5, simulation result and analysis are given, and finally we make the conclusion of the paper in Section 6.

2. Problem Formulation

2.1. System Model. We consider the D2D communication underlaying cellular network in which D2D links occupy the spectrum resource of uplink cellular communication. The reason why we choose uplink one is that when the cellular users (CUs) are in downlink transmission they will suffer from sophisticated interference caused by D2D communication [23]. Otherwise, we divide the investigation of social-awareness based resource allocation for D2D communication
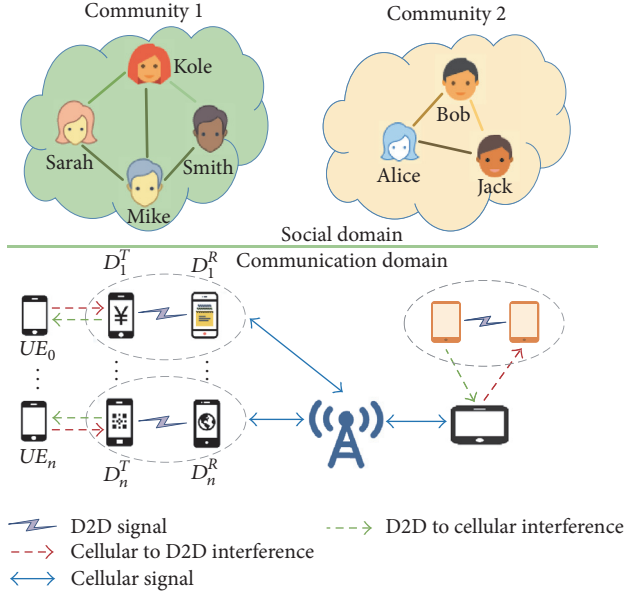
FIGURE 1: Illustration of social-aware D2D communications underlaying cellular network. In physical domain, wireless links are subject to the physical interference constraints, while social domain indicates the relationships between mobile users.

underlaying cellular networks into two domains in our work: physical domain and virtual social domain. More details about these are illustrated in Figure 1.

In the physical domain, the system contains N nodes labelled as the set of $\mathcal{N} = \{1, 2, \ldots, N\}$. Each node denotes a mobile user that can communicate with the BS or execute D2D communication with other users directly. For active mobile users, they can form $\mathcal{D} = \{1, 2, \ldots, D\}$ D2D pairs. The remaining, which is denoted by the set $\mathcal{C} = \{1, 2, \ldots, C\}$ can request for interested content toward BS via cellular communication. Those D2D pairs can choose to reuse the spectrum resource of any cellular users. But there exist physical constraints between mobile users, and only some of them can form D2D pairs (including D-Tx and D-Rx) [24].

In the social domain, for the reason that a community is combined by sophisticated relationship like friendship, kinship, or even classmates with each other [25], and they were physically in close proximity, we tend to make use of these characteristics to model the social relationship between the users. Users consider the strength of their social trust within a community and their properties of social trust between different communities, respectively, to make D2D communication more secure.

To ensure the practicality of our work, we set the channel scene as Rayleigh fading channel. Under the premise of the free space propagation model, the interference signal power level of cellular user which is introduced by D2D transmitter D-Tx sharing the same spectrum resource with cellular user can be expressed as follows according to Shannon theorem:

$$P_{\text{int},c} = P_d \cdot \zeta_{c,d}{}^{-\alpha} \cdot h_{c,d}^2, \tag{1}$$

while the interference signal of D2D receiver D-Rx is from the BS that establishes communication link with cellular users. Thus, the signal power can be expressed as

$$P_{\text{int},d} = P_B \cdot \zeta_{B,d}{}^{-\alpha} \cdot h_{B,d}^2, \tag{2}$$

where P_d and P_B are the transmitted power of BS and D2D transmitter, respectively. $\zeta_{c,d}$ denotes the distance between the D2D transmitter and cellular user and $\zeta_{B,d}$ denotes the distance between D2D receiver and the BS, α is the path loss exponent, and $h_{c,d}$ and $h_{B,d}$ are the complex Gaussian channel coefficients.

In our investigation, we assume there are one D2D pair and one cellular user within a single cell. By sharing cellular spectrum resource blocks with D2D pair, D2D communication and cellular communication can be conducted synchronously [26]. For the purpose of maximizing the overall system transmission rate, the Signal-to-Noise Ratio (SINR) of the two communication modes is regarded as important indicator. Based on (1) and (2), we can obtain the SINR of cellular user c and D2D receiver d as

$$\text{SINR}_{c,i} = \frac{p_c g_c}{P_{\text{int},c} + N_0},$$

$$\text{SINR}_{d,i} = \frac{p_d g_d}{P_{\text{int},d} + N_0} \tag{3}$$

p_c is the given transmission power of cellular user and p_d is the given transmission power of D2D transmitter; g_d and g_c are the channel gains of cellular link and D2D link, respectively. And N_0 is the noise power on each channel.

At the same time, we usually calculate the sum rate of the system to measure the quality of D2D communication underlaying cellular network. For uplink direction, let $R_{c,i}$ be the data transmission rate between the CU and the BS and $R_{d,i}$ be the data transmission rate between D-Tx and D-Rx. Since the transmission rate of each cellular link and D2D link can be determined by the Shannon capacity [27].

$$R_{c,i} = B_{c,i} \log_2 \left(\text{SINR}_{c,i} \right),$$

$$R_{d,i} = B_{d,i} \log_2 \left(\text{SINR}_{d,i} \right), \tag{4}$$

where $\text{SINR}_{d,i}$ and $\text{SINR}_{c,i}$ are the Signal-to-Noise Ratio (SINR) in D2D and cellular communication links and $B_{c,i}$ and $B_{d,i}$ are the allocated licensed band of resource for D2D and cellular communication. What is imperative to mention here is that we only consider the interference that occurred within a single cell and do not consider any influence from other microcells.

To describe reusing relationship of spectrum resource, we denote $x_{c,d} \in [0, 1]$ as the indicator matrix of the D2D pairs; that is, $x_{c,d} = 1$ when the D2D pair d occupies the licensed band of resource of the cellular user c; otherwise $x_{c,d} = 0$. Thus, we can acquire the transmission rate of D2D pair multiplying the indicator $x_{c,d}$ by $R_{d,i}$ as $R_{d,i} \cdot x_{c,d}$. The system performance can be represented by the sum of $R_{c,i}$ and $R_{d,i}$.

$$R = \sum_{i=1}^{\mathcal{D}} \left(R_{c,i} + R_{d,i} \cdot x_{c,d} \right). \tag{5}$$

We can improve the system performance by maximizing the sum rate to judge whether our proposed optimal social-aware resource allocation scheme is effective:

$$\max \quad \sum_{i=1}^{\mathscr{D}} R_{c,i} + R_{d,i} \cdot x_{c,d}$$

$$\text{s.t} \quad \sum_{d^i \in \mathscr{D}} x_{d^i}^{n^c} \le 1, \quad c \in \mathscr{C}, \ n^c \in \mathscr{C} \tag{6}$$

$$\sum_{n^c \in \mathscr{C}} x_{d^i}^{n^c} \le 1, \quad c \in \mathscr{C}, \ d^i \in \mathscr{D}.$$

2.2. Problem Description

2.2.1. Power Interference.
In D2D communication network, we assume the cellular users can share uplink resource with user equipment. During the D2D communication, it is inevitable that D2D transmitter interference will be introduced to others, especially to nearby CUs. And since we limit that each D2D pair can reuse the spectrum resource from at most one cellular user, by assuming there are D D2D pairs and C cellular users in the D2D underlaying communication cellular network, we can simplify the network as Figure 2.

In the simplified network we establish, besides the normal D2D communication, we only consider the effects of both the interference of a generic D2D transmitter introduced to others and all other interference caused to a D2D receiver. For instance, the base station (BS) introduces intratiers interference to the D2D receivers $D2D_1^R$ as shown in Figure 2. Meanwhile, due to the full frequency reuse, $D2D_1^T$ causes interference to CU_1. Considering the power interference caused by the transmitter of the D2D pairs to the nearby UE, we can give the definition that the interference introduced by D2D transmitter d to cellular users c is $I_{d \to c}, \ d \in \mathscr{D}, \ c \in \mathscr{C}$:

$$I_{d \to c} = g_{d,c} p_d, \tag{7}$$

where p_d denotes the transmission power of the corresponding D2D pairs $d, d \in \mathscr{D}$. $g_{d,c}$ denotes the gains of the channel between the transmitter of D2D pair d to cellular users c. Here, the terms c and $g_{d,c}$ are positive. Hence, all of the cellular users are assumed in the single cell and corresponding interference is introduced by prayer $d, \ d \in \mathscr{D}$, where the player d is called the generic D2D transmitter. Meanwhile, the transmission between player $c, c \in \mathscr{C}$, and the BS also introduces interference to D2D pair d, where we define the intratier interference from player c to player d as follows:

$$I_{c \to d} = g_{c,d} p_c, \tag{8}$$

where $g_{c,d}$ is the channel gain between the BS and the D2D pairs d. p_c is the transmission power of cellular user c. Here, we assume that orthogonal channels are used for different CUs, and we do not consider any power control policy at the macrocell layer. In our investigation, we pay attention to the power interference D2D transmitter introduced to the CUs, in other words, a new power control policy for the D2D transmitters.
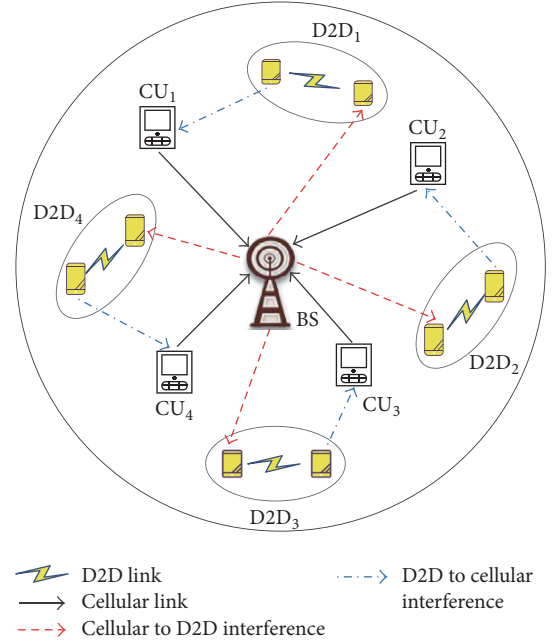

FIGURE 2: Interference model in the uplink.

2.2.2. Social Utilization.
In this part, we use a visualized social-network graph to analyze the social relationship between the mobile users and depict the social characteristic of the network. In the virtual social network, social ties are defined to qualitatively measure the strength of social relationship between D2D users and report the communication demands between users. Besides, social centrality plays a very important role in D2D data transmission; users with high centrality are more likely to hold high capacity in terms of data transmission volume and frequency. In that case, for the purpose of obtaining a visualization of the social characteristics existing in user's daily activities, we adopt the proximity social network derived from a real-world mobility dataset—Karate club. The network contains the social data of 34 members within a Karate club, documenting 78 pairwise links between members who interact inside or outside the club [28]. By analyzing the realistic dataset and the interaction behaviors among these members, we plot the social network formed by users visualized by the trace in Figure 3, where the magnitude of the node indicates the centrality of the specified user, and the label of the node indicates the strength of the social ties of corresponding links.

In the virtual social network, active mobile users in close relationship form certain community. In order to weigh the influence from the social relationship between the mobile users within the same community to our resource allocation scheme, we define the utility of social relationship by quantifying the social characteristic. Since we suppose mobile users in different communities have no social trust between each other, when cellular users download some content from the BS, cellular users belonging to the same community can deliver the content to other interested users directly instead of forwarding by the BS. And the amount of the content is
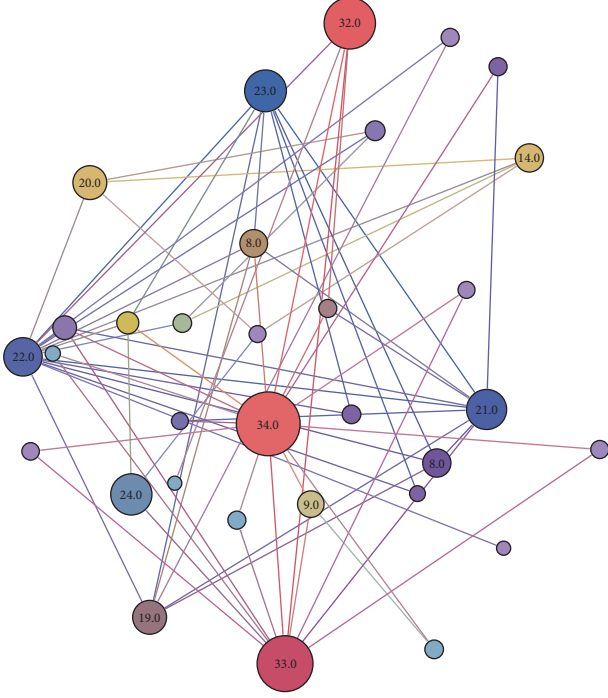
Figure 3: Social characteristics observed from social-network trace.

determined by the social closeness between the users. The more close social relationship the D2D users have, the more content they will exchange with each other [29].

Based on the analysis mentioned above, the social graph can be denoted by $G_s = (V_s, R_s)$. V_s and R_s stand for the set of all cellular users and D2D users and the set of relationships, respectively. To be mentioned, the matrix R_s demonstrates the strength of the relationship of V_s in the social network. Generally, we use the form of matrix described as $\omega_{d,r}$, $d, r = 1, 2, \ldots, D$, and $\xi_{d,c}$, $d = 1, 2, \ldots, D$, $c = 1, 2, \ldots, C$. $\omega_{d,r}$ denotes the intimacy coefficient between D2D users, and $\xi_{d,c}$ denotes the intimacy coefficient between the cellular users and D2D users. According to the definition in the dataset of Karate club, we plan to divide the closeness coefficient into two kinds: very close and a little close. The values of $\omega_{d,r}$ and $\xi_{d,c}$ follow the set of $[0, 1]$. For example, $\omega_{d,r} = 0$ implies a little close intimacy between the D2D users, and $\omega_{d,r} = 1$ naturally implies a very close intimacy. As illustrated in Figure 1, we construct a simple social network. In community 2, D2D users Jack and Alice have a very close intimacy, while Bob and Jack are unfamiliar with each other. Inspired by the analysis in Part A, the utility of D2D users can be represented as follows:

$$U_d = \log_2 \left(1 + \sum_{i=G_d^p \cap G_d^s} \mathrm{SINR}_{d,i} \right), \quad \forall d \in \mathcal{D}. \quad (9)$$

Approximately, the utility of cellular users can be represented as follows:

$$U_c = \log_2 \left(1 + \sum_{i=G_c^p \cap G_c^s} \mathrm{SINR}_{c,i} \right), \quad \forall c \in \mathcal{C}. \quad (10)$$

By the way, G^p and G^s denote the physical and social relationship of the system model mentioned above. Thus, G_c^p and G_c^s denote the set of cellular users that reuse the same frequency band of spectrum resource and maintain stable interaction with each other. G_d^p and G_d^s denotes the D2D users which reuse the same spectrum resource from cellular users and maintain stable interaction with the cellular users. U_d represents the influence of the social relationship to D2D communication and U_c represents the influence of the social relationship to cellular communication. To sum up, we can define the social-community utility function of D2D users d as follows:

$$U_d(X) = \sum_{r,d \in \mathcal{D}} \omega_{d,r} U_d + \sum_{c \in \mathcal{C}} \xi_{d,c} U_c. \quad (11)$$

X denotes the correlation matrix of $x_{c,d}$, and, in general, the degree of social utility enhancement involves two aspects: the weighted sum of social utility enhancement by D2D pairs having social connections with each other as $\sum_{r \in \mathcal{D}} \omega_{d,r} U_d$ and the weighted sum of utility enhancement between familiar cellular users and D2D pairs as $\sum_{c \in \mathcal{C}} \xi_{d,c} U_c$. In this way, the element of social relationship is considered in the investigation of resource allocation in D2D communication underlaying cellular network.

3. Game Theory-Based Framework for Resource Allocation

In our investigation, we tend to maximize the sum transmission rate of the system. For example, if D2D transmitter brings about higher-than-sociality interference to cellular users, the operator would remove the D2D link. So, we model the resource allocation issue between D2D links and cellular links as the utility maximization game.

3.1. Problem Formulation. The resource allocation policy of each of the D2D pairs d depends on the power interference introduced by D2D communication and social relationships between the mobile users. Compared to the physical relationship between mobile users, the social relationship is relatively less changeable. Thus, we need to consider the joint influence from social enhancement and power interference to the D2D pairs dynamically. By that, we tend to define the utility of a D2D link as the profits which are contributed by cellular users and D2D users using spectrum resources and D2D users using social characteristics. In this case, the utility function of the dth D2D links is defined as follows:

$$\Gamma_d(X) = \alpha \cdot R + \beta \cdot U_d(X) - \gamma \cdot B_{d,i} - \varepsilon \cdot I_{d \to c}$$
$$\text{iff } U_d(X) \geq I_{d \to c}. \quad (12)$$

α and β are the charging price of unit data rate supported by the spectrum resource and the social network. γ and ε are the cost function of a D2D occupied resource and power

interference. With respect to γ, a pricing function from (12) is adopted, which can be expressed as follows:

$$\gamma = n + s \cdot \left(B_{d,1} + \cdots + B_{d,i}\right)^{\tau}, \quad i = 1, 2, \ldots, m. \quad (13)$$

n, s, and τ denote nonnegative constants and $\tau \geq 1$ to guarantee that the cost function is convex. In order to improve the applicability, we suppose

$$\left[N_0 + g_d P_{d,r}\right] = \frac{p}{B_{d,i}}, \quad (14)$$

where p is a nonnegative constant [30]; then

$$\Gamma_d(X) = \alpha \cdot B_{d,i} \log_2\left(1 + \text{SINR}_{d,i}\right) + \beta \cdot \sum_{j \in \mathscr{D}} \omega_{d,r} U_d$$

$$+ \sum_{c \in \mathscr{C}} \xi_{d,c} U_c - \left[n + s \cdot \sum_{i=1}^{m} B_{d,i}\right] B_{d,i} - \varepsilon \cdot I_{i \rightarrow u}, \quad (15)$$

$$\text{iff } U_d(X) \geq I_{d \rightarrow c}.$$

In the proposed problem in (15), each D2D pair is aimed at integrating every aspect of influence and then maximizing its own utility. As the distribution of mobile equipment is changing all the time, the features of the network are varying instantaneously. So, for the purpose of exact comparison, we should implement some effective method to eliminate this kind of dilemma.

Dynamic game with complete information can model certain dynamic situation under the premise that the participant knows the type of the action it will take and the information needed for every decision of the action. It can be applied into our proposed model as every D2D pair can get to know the social utility and power interference and get the real-time $\Gamma_d(X)$ when D2D communication is in progress. So, the problem above can be regarded as a dynamic game with complete social information as well as sophisticated interference information. In this way, we can propose a dynamic game based scheme to optimize the overall performance of the D2D communication network due to the two-sides' competition.

3.2. UFM Game Formulation. From the analysis above, we derive the information from two-sides' action needed in our game theory. And, for the optimization problem, we usually utilize the game theory to solve it. Firstly, we define corresponding strategy adopted by each D2D user d in a certain point of history as $a_d, a_d \in A_d$, where A_d is the set of all available strategies of the D2D pair d. The choice of strategies of all the other participants, that is, all the other D2D pairs in our work, can be defined as $a_{-d} = \{a_1, \ldots, a_{d-1}, a_{d+1}, \ldots, a_D\}$. If the above assumption for the UFM game theory is perfect, there must exist a strategy $a_d \in A_d$ to maximize its own utility function:

$$\max_{a_d \in A_d} \quad \Gamma_d(a_d, a_{-d}), \quad \forall d \in \mathscr{D}. \quad (16)$$

The UFM game for the resource allocation thinking from the perspective of utility function is defined by quadruple $\Phi = \{\mathscr{D}, \{A_d\}_{d \in \mathscr{D}}, \{\Gamma_d\}_{d \in \mathscr{D}}, \{I_{d \rightarrow c}\}_{d \in \mathscr{D}, c \in \mathscr{C}}\}$, where $\mathscr{D}$ denotes the

D2D pairs. X_d denotes all of the resource allocation strategies D2D pairs set $\mathscr{D}$ can take. Γ_d denotes the utility function of each of the D2D pairs d, and $I_{d \rightarrow c}$ denotes the interference introduced by D2D pairs d to cellular user c.

3.3. Nash Equilibrium. Nash Equilibrium is a very important terminology in game theory [31, 32]. It represents a set of strategies which are combined by all optimal choices taken by each participant which reflect the optimal reaction each participant adopts against the other participant's strategies. According to this, if the choices chosen by all the D2D pairs are optimal, the system sum rate of the D2D communication underlaying cellular network will reach the extreme one. The following part will discuss the existence of Nash Equilibrium in UFM game theory and provide proof for it.

Generally, the UFM game $\Phi = \{\mathscr{D}, \{A_d\}_{d \in \mathscr{D}}, \{\Gamma_d\}_{d \in \mathscr{D}}, \{I_{d \rightarrow c}\}_{d \in \mathscr{D}, c \in \mathscr{C}}\}$ can reach the Nash Equilibrium if each of the D2D pairs has the only optimal response to the other D2D pair's strategy:

$$a_d^* = \arg\max_{a_d \in A_d} \quad \Gamma_d(a_{-d}, a_d), \quad \forall d \in \mathscr{D} \quad (17)$$

and $a^* = \{a_1^*, a_2^*, \ldots, a_D^*\}$ denotes the Nash Equilibrium.

Because of the same incentive of changing their strategy for all the D2D pair, we refer to the potential game theory to demonstrate the existence of NE for the UFM game. In [33], Monderer and Shapley propose the definition of potential game and elaborate the idea in detail, too. In the field of wireless resource allocation games, game theory has been applied in a few of authors' papers, for example, [34–36]. In potential game theory, the change in individual player's gain can be mapped to the global function, which is called the potential function. By this way, we can conclude if there is any change that occurred on individual player, the potential function will change equally in the strict potential game. Γ denotes an exact potential function if and only if $\exists F(I) : I \rightarrow U, \; \forall i, j, \; \forall I_i, I_j, \; U_i \in I_i$, and $U_j \in I_j$.

$$\Gamma_i\left(I_i, U_{-i}\right) - \Gamma_j\left(I_j, U_{-j}\right) = F\left(I_i, U_{-i}\right) - F\left(I_j, U_{-j}\right). \quad (18)$$

In the D2D communication system we have modeled, the change of power interference and social utility caused by D2D links would change the utility function of the game, which is consistent with the principle of potential function. On the other hand, potential game has the following inherent properties, which are described in [33]: (1) There must exist a pure-strategy NE and a solution for it. (2) The Nash Equilibrium corresponds to the maxima of the potential function Γ. (3) Generally, the convergence to Nash Equilibrium would be reached in finite improvement or searching path according to sequential best-response dynamics.

For the condition of a single band frequency channel, the potential game is formulated by utilizing the following utility-maximizing function:

$$\Gamma_i = -\left(\text{Total utility function generated by } i \right.$$
$$\left. + \text{Total utility function experienced by } i\right). \quad (19)$$

Based on the potential game theory, we can demonstrate the existence of the Nash Equilibrium of our proposed UFM game. For Γ for every $d \in \mathscr{D}$ and for every $a_{-d} \in A_{-d}$

$$P(d) = \Gamma_d(a_{-d}, a_d) - \Gamma_d(a_{-d}, a_d').$$ (20)

Theorem 1. *In certain history point t, function P(d) derived from UFM game is subgame perfect.*

Proof. We suppose strategy a_d denotes occupying the spectrum resource of cellular user c which is taken by D2D pairs d initially. Therefore, the initial indicator is $x_{c,d}$. Once D2D pair d change its strategy and make a request for the spectrum resource of cellular user c', the indicator changes to $x_{c,d}'$. Then, we can obtain

$$\Gamma_d - \Gamma_d' = \alpha \cdot R + \beta \cdot U_d(X) - \varepsilon \cdot I_{d \to c} - \alpha \cdot R' - \beta$$

$$\cdot U_d(X) - \varepsilon \cdot I_{d \to c}'$$ (21)

$$= \alpha \cdot (R - R') - \varepsilon \cdot (I_{d \to c} - I_{d \to c}').$$

We denote $\Delta_1 = R - R'$ and $\Delta_2 = I_{d \to c} - I_{d \to c}'$. As we can see, $\Delta_1 \gg \Delta_2$. Finally, we conclude that

$$\Gamma_d - \Gamma_d' > 0.$$ (22)

It means that no D2D pair can acquire performance enhancement by changing its strategy, so we prove that our proposed game is subgame perfect. As subgame is the restriction from the perspective of history circumstances, it can lead to the Nash Equilibrium of the game directly. □

4. Resource Allocation Scheme for UFM Game Theory

4.1. Priority Searching Based Solution. The value of the utility function Γ_d varies when D2D pair chooses to reuse spectrum resource from different cellular user, and the final aim of the UFM game is to determine the order of the utility function by the size of value. According to analysis in Sections 3.2 and 3.3, the resource allocation strategy a^* has a Nash Equilibrium. It means that we can finally achieve an optimal strategy by substituting the other strategies one by one in finite times. It is similar to the establishment of preference list and iterates until acquiring the best selection among different alternatives [10]. Inspired by the one-to-one matching theory, we will show the main idea of the proposed resource allocation algorithm in detail.

Definition 2. For any D2D pairs, we define the binary priority relation set $\succ_i$ to represent the entire set of resource allocation strategies that each D2D pair i would possibly take. In our UFM game, D2D pairs can choose to reuse the resource occupied by the associated cellular users or not according to the priority set. For any D2D pairs, $a_i \succ_i a_i'$ means D2D pairs i prefer choosing c as the target resource source instead of c'.

Since the priority set is determined by the utility function, we can define the priority as follows:

$$a_i' \succ_i a_i \iff$$

$$\Gamma_i(a_i') > \Gamma_i(a_i),$$ (23)

$$\forall i \in \mathscr{D}.$$

This definition demonstrates that D2D users i are likely to reuse the spectrum resource of cellular users c as no more options can bring additional performance gains. We can set the highest priority for cellular user c in the set belonging to D2D user i. By this, a complete priority set can be obtained by repeating searching operation. For every D2D pair, we can also design an optimization resource allocation scheme based on the priority set. In this scheme, every D2D pair urges finding its own highest priority and reusing the spectrum resource shared by the corresponding cellular users.

Let us present Algorithm 1.

Based on the definitions and priority searching operation, we can obtain a final Nash-stable resource scheme a_{fin} for D2D users to solve the utility maximization problem, which is given in Algorithm 1. From the whole knowledge given above, we can see that D2D users make switching iteration following a logically standard based on an arbitrarily chosen initial resource allocation strategy a_{ini}. At the beginning of each iteration, D2D user $i \in \mathscr{D}$ is randomly chosen by the system in step (13). And, then, the selected D2D user replaces its resource allocation strategy with a_{ini} by random choosing a occupied cellular users and determine its strategies a_i and uniformly selects another social-trust cellular user $c' \in \mathscr{C}$. Then, the D2D pair will request the base station for the channel state information once establishing communication link with these two cellular users c and c'. After acquiring specified information, the BS will computes the utility function of the resource allocation strategies of a and a' and broadcast to the participant of the game model. Meanwhile, making the decision that whether to carried out the switch operation for D2D link. If $a_i \succ_i a_i'$, the switch operation will not be executed. Otherwise, the switch operation will be executed. The iteration will continue until all of the priority searching operations for each D2D pair are traversed and reach a final Nash Equilibrium scheme a_{fin}.

Different from those conventional D2D resource allocation schemes, our proposed scheme needs to select suitable community detection dataset and analyze the social-community information inside. And a priority based potential game theory is applied in our scheme. This important information is taken into consideration in our proposed scheme fully.

4.2. Uniqueness and Boundedness. According to Theorem 1, for a given history point t, the combination of strategy $a_i, a_i \in A_i$, can reach a status of being subgame perfect as reaction to the combination of strategy a_{-i}. To prove the uniqueness and boundedness of our proposed game, it is necessary to confirm that if there exist any participant $\forall \widehat{i} \in \mathscr{D}$ and its

```
(01) Input: Number of mobile users N and random resource allocation strategy a_ini.
(02) Output: A priority based resource allocation scheme a_fin.
(03) Utilize the dataset of Karate Club network
(04) Calculate the transmission rate of the D2D links and cellular links.
(05) Obtain U_d(X) and I_{d→c}
(06) if U_d(X) ≤ I_{d→c}, remove the D2D links
(07) else keep the D2D links
(08) Define the matrix of indicator x_{c,d} ∈ [0, 1]
(09) I = find x_{c,d} ≠ 0 && I = 1
(10) There is just one c cellular users qualified to share
        resources to D2D user, r = r_{c,d}
(11) else if, uniformly randomly choose one cellular users c and a
        possible cellular users c', and denote its associate resource
        sharing as a_i ∈ a_ini
(12) Calculate Γ(a'_i) and Γ(a_i), priority = 0;
(13) if a'_i ≻_i a_i; then Priority = 1;
(14) else repeat (15)~(16);
(15) if Priority == 1; then
(16) D2D pairs quit current resource occupying strategy of c, and
        turn to adapt the new resource allocation strategy of c'
(17) substitute the current resource occupying strategy a for
        strategy a', and add it to a_cur
(18) Until all of the D2D pairs complete the priority searching operation, resource
        occupying strategy switching operation and reach Nash Equilibrium a_fin
```

ALGORITHM 1: The utility function maximization D2D links redistribution algorithm.

corresponding strategy $\widehat{a}_i$ can give better reaction to the strategy combination a_{-i} than a_i and make $\widehat{a}_i \succ_i a_i$ available. So we provide the following proof relative to the uniqueness and boundedness of our proposed UFM game.

Theorem 3. *For all of the D2D pairs whose $x_{c,d} = 1$, the proposed priority searching based scheme can only obtain a unique resource allocation scheme a_{fin}.*

Proof. Based on the description in Algorithm 1, we suppose reversely that the combination of strategy a_i is not subgame perfect. And, then, there must exist certain participant i that has strategy $\forall \widehat{i} \in \mathcal{D}$ and outperforms a_i. Now, we investigate another strategy $\widetilde{a}_i$, and when $t < \widehat{t}$, $\widehat{a}_i$ is equal to $\widetilde{a}_i$, but, after $\widehat{t}$, it is equal to a_i. Then, in any subgame after the history point $\widehat{t}$, strategy $\forall \widehat{i} \in \mathcal{D}$ is at least as well as $\widetilde{a}_i$ for the reason that $\forall \widehat{i} \in \mathcal{D}$ has deviated from a_i once. We can also conclude that strategy $\forall \widehat{i} \in \mathcal{D}$ is at least as well as $\widetilde{a}_i$ after the history point t, which is contrary to the assumption that strategy $\forall \widehat{i} \in \mathcal{D}$ improves the strategy a_i. And so on, we can investigate other $\widetilde{a}_i$ to prove its equal benefit with $\forall \widehat{i} \in \mathcal{D}$ until reaching the unique resource allocation scheme a_{fin}.

Through the above analysis, we prove the uniqueness of the UFM game by Reduction to Absurdity. In each iteration in Algorithm 1, it may lead to a new resource allocation strategy. As there is only $\mathcal{C}$ in the physical domain and limited $\mathcal{D}$ D2D pairs due to the limited social relationship in the social domain, each of the D2D pairs is corresponding to $\mathcal{C}$ types of resource allocation scheme. So the priority searching operation will eventually end in limited steps. This fact assures the boundedness of our proposed UFM game based scheme. □

5. Simulation Results and Discussions

In this section, we implement the simulation results from different perspective to verify the performance of our proposed UFM algorithm and elaborate some necessary explanation for the results. Main simulation parameters have been given in Table 1. Simulations are executed in a single cell, which are within an isolated community circumstance. Path loss models are considered for cellular and D2D links, along with shadow fading model. According to the dataset of Karate club, we conduct the simulation within a $500 \, \text{m} \times 500 \, \text{m}$ area to guarantee most of the club member's activities are within this area, and 34 members of the club are randomly distributed within the BS coverage area. Meanwhile, the bandwidth of allocated resource is assigned arbitrarily within the range limitation. We compare our proposed UFM algorithm with the following resource allocation schemes: (a) distributed resource allocation (DRA), which allocates the D2D communication resource by thinking in a distributed way [37], and (b) optimal social-community aware resource allocation (OSRA), which allocates the D2D communication resource to reduce the total transmission time [38]. All the results are averaged over 10 times' trial.

Without loss of generality, on one hand, we prescribe the pathloss model between the base station and all the mobile users as COST (European Cooperation in Science and Technology) 231 Hata model [39].

$$\text{PL}_{\text{CU}} = 36.7 + 35 \times \lg(d) . \tag{24}$$

Meanwhile, we prescribe the pathloss model between different cellular users and D2D users as Xia model [40], given as follows:

TABLE 1: System simulated parameters in the performance evaluation.

Parameter	Value
Coverage radius of BS	500 m
Distance of D2D	20 m~50 m
Noise figure	9 dB at device
Transmission power	BS: 46 dBm; device: 23 dBm
Maximum D2D transmitter power	23 dBm
Range of bandwidth	10 MHz~20 MHz
Communication demand	50 W
Interference threshold	5.6×10^{-6} W
n, s, z, τ	1
α, β	20

$$PL = \begin{cases} 66.5 + 40 \times \log(d), & d > 50 \\ 100.7 + 20 \times \lg(d), & d < 50. \end{cases} \quad (25)$$

Since we assume the inner distance of D2D pair remains in close standards and relatively close, the free space model can be given by

$$PL = 38.4 + 20 \times \lg(d). \quad (26)$$

Moreover, we consider the case of fast fading model for Rayleigh fading. In different situation, we adopt a different fading model to investigate. In this way, the evaluation of the average performance is objective. We also set a great number of criterions for our simulation: the maximum power state of D2D users is set at 23 dBm, and the maximum interference which mobile users can tolerate is assumed to be 5.0×10^{-6}. Before investigating the system performance based on our proposed UFM game, we tend to show the joint influence of the power interference caused by spectrum sharing and social characteristics in each social community illustrated in Figure 4.

In this section, we analyze the sum power interference and sum social utility, respectively, as the number of cellular users varies. The case of 10 cellular users means the situation of system whose spectrum resource is in short supply. In this situation, D2D users possibly have to share the spectrum resource of the same users, while the case of 30 cellular users means D2D pairs have many resource-occupying choices. The results indicate that the sum power interference decreases with the trend of the number of cellular users increasing as the sum social utility stay in quite a stable level. And when the number of cellular users in the system exceeds 18, the influence from social utility will surpass the influence from power interference. And then we evaluate the system sum rate and sum time with different number of cellular users using the proposed UFM algorithm and the other two advanced schemes which is illustrated in Figures 5 and 6.

Figure 5 compares the sum rate of the three algorithms under the isolated scenarios, in which we set the number of cellular users varied in the range of [10, 30]. From Figure 5, we observe that, by removing some interference-intolerable D2D links, significant performance enhancement can be
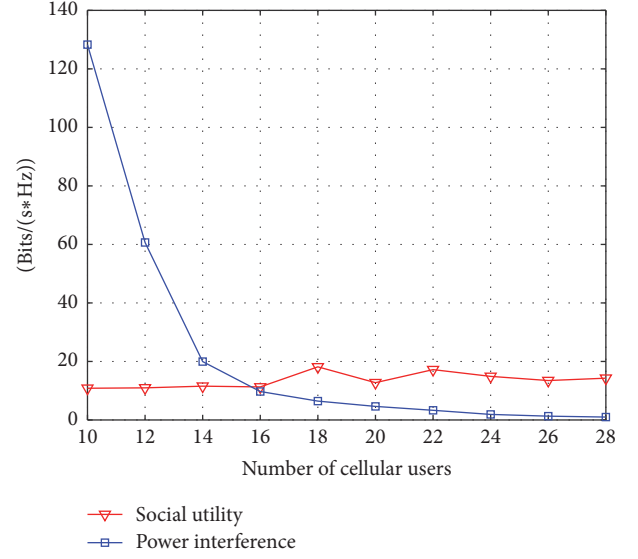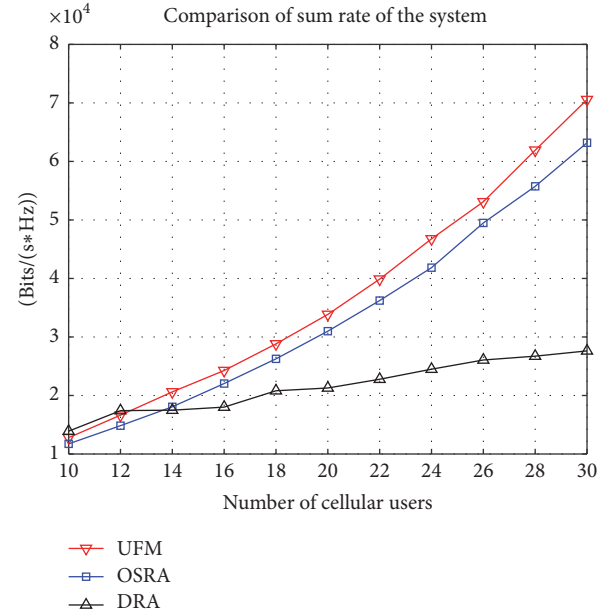

FIGURE 4: Comparison of the joint interference.

FIGURE 5: Transmission rate comparison of different resource allocation algorithms with different number of cellular users.

achieved when the cellular users are relatively sufficient. But, in the situation that cellular users are not sufficient, performances of the two are roughly equal. The reason is that the excessive reuse relationships of frequency with the same cellular user will cause unbearable interference to the cellular users. According to our algorithm, the D2D link will be removed automatically in both schemes.

Figure 6 compares the sum transmission time of the three algorithms under the isolated scenarios. From Figure 6, we can observe that, in the case that some unnecessary D2D links has been removed, the UFM algorithm still provides quite a considerable reduction of transmission time. That is, because
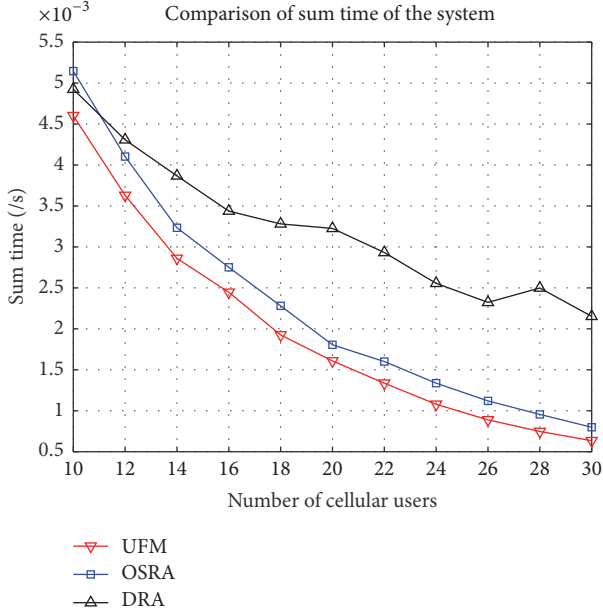
FIGURE 6: Transmission time comparison of different resource allocation algorithms with different number of cellular users.

FIGURE 7: Transmission rate comparison of different resource allocation algorithms with different number of D2D pairs.

we allow D2D users to continue to acquire content via cellular communication when D2D communication comes across link interruption. So, the sum transmission time will not be affected greatly.

For the purpose of evaluating the system performance while the number of D2D users varies within a certain range, we set geographical scope as 300 m × 300 m around the BS and suppose the number of cellular users is 10. As illustrated in Figures 7 and 8, the variation range of number of D2D pairs is [5, 30]; the result demonstrates that our proposed UFM game always attains the best performance with the increase of D2D users, compared to the OSRA and DRA. This is because, in the algorithm of DRA or OSRA, there exist little coordination measures to restrict D2D pairs to select their resource and it is inevitable to establish some high-interference links between D2D pairs and cellular users. In our proposed algorithm, UFM game effectively coordinates both social relationship and power interference and then decides whether to access the spectrum resource of certain cellular users, not in a random way. In these circumstances, we can avoid many high-risk links and attain a better system performance in terms of the evaluation of the sum transmission rate. At this point, we can summarize that our proposed scheme precedes the other two schemes in a relatively comprehensive scale.

6. Conclusion and Future Work

This paper studies game-theory based social-aware resource allocation in the D2D communication underlaying cellular network based on the realistic social network. By considering the power interference and social utility in the physical and social domain, respectively, a game-theoretic based utility function maximization scheme has been proposed. Also, to
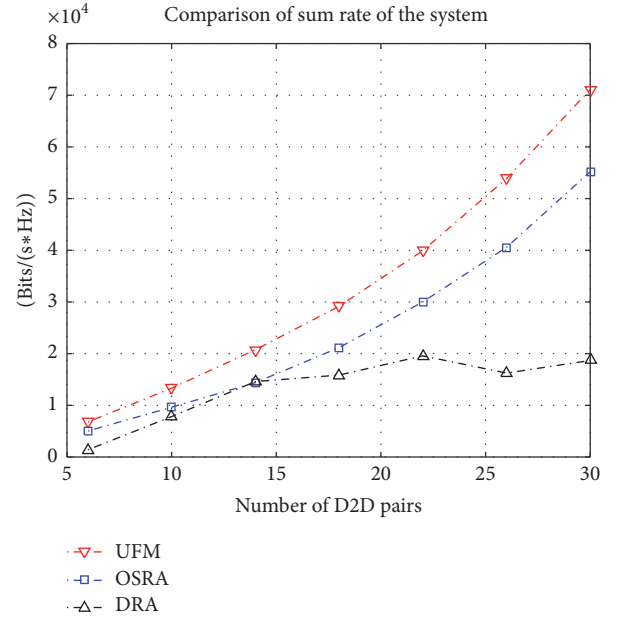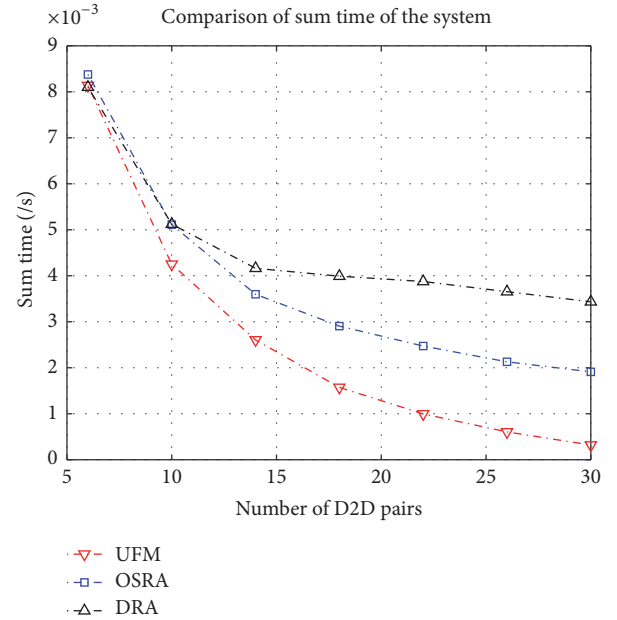

FIGURE 8: Transmission time comparison of different resource allocation algorithms with different number of D2D pairs.

demonstrate the optimality of our proposed scheme, this paper provides evidence for the existence of Nash Equilibrium theoretically. Meanwhile, a priority searching operation based resource allocation scheme is designed to implement the Nash Equilibrium of the proposed UFM game. The proposed UFM scheme is numerically shown having superiority over traditional DRA and OSRA scheme: the performances of sum rate and total transmission time are better than the OSRA and DRA algorithm through massive simulation

result, suggesting that the proposed scheme is more ideal for joint social-aware resource scenarios considering the social characteristics. Nevertheless, some issues related to further system optimization remain to be addressed, such as power allocation of mobile nodes and cluster formation of social community.

Notations

$\mathcal{N}$:	Set of mobile users
$\mathcal{C}$:	Set of cellular users
$\mathcal{D}$:	Set of D2D pairs
Φ:	The UFM game
$\succ_i$:	Set of utility priority
$I_{d\to c}$:	Interference from dth D2D to cth cellular signal
$I_{c\to d}$:	Interference from cth cellular signal to dth D2D
$U_d(X)$:	Social utility of dth D2D pairs
$\Gamma_d(X)$:	Utility function of dth D2D pairs
$x_{c,d}$:	Indicator of resource reusing relations
x_d^*:	The Nash Equilibrium of dth D2D pair
X_d:	Set of all feasible strategies in UFM game.

Conflicts of Interest

The authors declare no conflicts of interest related to the publication of this paper.

Acknowledgments

References

[1] Y. Cao, T. Jiang, and C. Wang, "Cooperative device-to-device communications in cellular networks," *IEEE Wireless Communications Magazine*, vol. 22, no. 3, pp. 124–129, 2015.

[2] J. Liu, N. Kato, J. Ma, and N. Kadowaki, "Device-to-device communication in LTE-advanced networks: a survey," *IEEE Communications Surveys & Tutorials*, vol. 17, no. 4, pp. 1923–1940, Fourthquarter 2015.

[3] A. Asadi, Q. Wang, and V. Mancuso, "A survey on device-to-device communication in cellular networks," *IEEE Communications Surveys & Tutorials*, vol. 16, no. 4, pp. 1801–1819, 2014.

[4] H. Nishiyama, M. Ito, and N. Kato, "Relay-by-smartphone: realizing multihop device-to-device communications," *IEEE Communications Magazine*, vol. 52, no. 4, pp. 56–65, 2014.

[5] M. Zhou, Y. Tang, Z. Tian, L. Xie, and W. Nie, "Robust neighborhood graphing for semi-supervised indoor localization with light-loaded location fingerprinting," *IEEE Internet of Things Journal*, vol. PP, no. 99, pp. 1-1.

[6] K. Doppler, M. Rinne, C. Wijting, C. B. Ribeiro, and K. Hug, "Device-to-device communication as an underlay to LTE-advanced networks," *IEEE Communications Magazine*, vol. 47, no. 12, pp. 42–49, 2009.

[7] J. Liu, H. Nishiyama, N. Kato, and J. Guo, "On the outage probability of device-to-device-communication-enabled multichannel cellular networks: an RSS-threshold-based perspective," *IEEE Journal on Selected Areas in Communications*, vol. 34, no. 1, pp. 163–175, 2016.

[8] M. Zhou, Y. Tang, W. Nie, L. Xie, and X. Yang, "GrassMA: graph-based semi-supervised manifold alignment for indoor WLAN localization," *IEEE Sensors Journal*, vol. 17, no. 21, pp. 7086–7095, 2017.

[9] J. Liu, S. Zhang, N. Kato, H. Ujikawa, and K. Suzuki, "Device-to-device communications for enhancing quality of experience in software defined multi-tier LTE-A networks," *IEEE Network*, vol. 29, no. 4, pp. 46–52, 2015.

[10] C. Xu, L. Song, Z. Han et al., "Efficiency resource allocation for device-to-device underlay communication systems: a reverse iterative combinatorial auction based approach," *IEEE Journal on Selected Areas in Communications*, vol. 31, no. 9, pp. 348–358, 2013.

[11] L. Ferdouse, W. Ejaz, K. Raahemifar, A. Anpalagan, and M. Markandaier, "Interference and throughput aware resource allocation for multi-class D2D in 5G networks," *IET Communications*, vol. 11, no. 8, pp. 1241–1250, 2017.

[12] T. D. Hoang, L. B. Le, and T. Le-Ngoc, "Cooperative device-to-device communications in cellular networks," *IEEE Transactions on Wireless Communications*, vol. 15, no. 10, pp. 7099–7113, 2016.

[13] M. Andrews, K. Kumaran, K. Ramanan, A. Stolyar, P. Whiting, and R. Vijayakumar, "Providing quality of service over a shared wireless link," *IEEE Communications Magazine*, vol. 39, no. 2, pp. 150–154, 2001.

[14] L. Wang, L. Liu, X. Cao, X. Tian, and Y. Cheng, "Sociality-aware resource allocation for device-to-device communications in cellular networks," *IET Communications*, vol. 9, no. 3, pp. 342–349, 2015.

[15] V. Shah and A. O. Fapojuwo, "Socially aware resource allocation for device-to-device communication in downlink OFDMA networks," in *Proceedings of the 2014 IEEE Wireless Communications and Networking Conference, WCNC 2014*, pp. 1673–1678, Istanbul, Turkey, April 2014.

[16] Y. Li, T. Wu, P. Hui, D. Jin, and S. Chen, "Social-aware D2D communications: qualitative insights and quantitative analysis," *IEEE Communications Magazine*, vol. 52, no. 6, pp. 150–158, 2014.

[17] F. Wang, L. Song, Z. Han, Q. Zhao, and X. Wang, "Joint scheduling and resource allocation for device-to-device underlay communication," in *Proceedings of the IEEE Wireless Communications and Networking Conference (WCNC '13)*, pp. 134–139, IEEE, Shanghai, China, April 2013.

[18] F. Tang, Z. M. Fadlullah, N. Kato, F. One, and R. Miura, "AC-POCA: anti-coordination game based partially overlapping channels assignment in combined UAV and D2D based

networks," *IEEE Transactions on Vehicular Technology*, vol. PP, no. 99, pp. 1-1.

[19] S. M. Azimi, M. H. Manshaei, and F. Hendessi, "Hybrid cellular and device-to-device communication power control: Nash bargaining game," in *Proceedings of the 2014 7th International Symposium on Telecommunications, IST 2014*, pp. 1077–1081, Tehran, Iran, September 2014.

[20] Z. Zhou, K. Ota, M. Dong, and C. Xu, "Energy-efficient matching for resource allocation in D2D enabled cellular networks," *IEEE Transactions on Vehicular Technology*, vol. 66, no. 6, pp. 5256–5268, 2017.

[21] C. Xu, C. Gao, Z. Zhou, Z. Chang, and Y. Jia, "Social network-based content delivery in device-to-device underlay cellular networks using matching theory," *IEEE Access*, vol. 5, pp. 924–937, 2017.

[22] X. Feng, G. Sun, X. Gan et al., "Cooperative spectrum sharing in cognitive radio networks: a distributed matching approach," *IEEE Transactions on Communications*, vol. 62, no. 8, pp. 2651–2664, 2014.

[23] J. Zhang, "The interdisciplinary research of big data and wireless channel: a cluster-nuclei based channel model," *China Communications*, vol. 13, no. supplement 2, Article ID 7833457, pp. 14–26, 2016.

[24] S. Mumtaz, K. M. Saidul Huq, J. Rodriguez, and V. Frascolla, "Energy-efficient interference management in LTE-D2D communication," *IET Signal Processing*, vol. 10, no. 3, pp. 197–202, 2016.

[25] N. Kayastha, D. Niyato, P. Wang, and E. Hossain, "Applications, architectures, and protocol design issues for mobile social networks: a survey," *Proceedings of the IEEE*, vol. 99, no. 12, pp. 2130–2158, 2011.

[26] J. Zhang, L. Tian, Y. Wang, and M. Liu, "Selection transmitting/maximum ratio combining for timing synchronization of MIMO-OFDM systems," *IEEE Transactions on Broadcasting*, vol. 60, no. 4, pp. 626–636, 2014.

[27] M. Zhou, Y. Wei, Z. Tian, X. Yang, and L. Li, "Achieving cost-efficient indoor fingerprint localization on wlan platform: a hypothetical test approach," *IEEE Access*, vol. 5, pp. 15865–15874, 2017.

[28] "Zachary's karate club," https://en.wikipedia.org/wiki/Zachary%27s_karate_club.

[29] D. Wu, L. Zhou, and Y. Cai, "Social-aware rate based content sharing mode selection for D2D content sharing scenarios," *IEEE Transactions on Multimedia*, vol. 19, no. 11, pp. 2571–2582, 2017.

[30] J. Huang, Y. Yin, Y. Sun, Y. Zhao, C.-C. Xing, and Q. Duan, "Game theoretic resource allocation for multicell D2D communications with incomplete information," in *Proceedings of the IEEE International Conference on Communications, ICC 2015*, pp. 3039–3044, London, UK, June 2015.

[31] Y. Xiao, K.-C. Chen, C. Yuen, and L. A. DaSilva, "Spectrum sharing for device-to-device communications in cellular networks: a game theoretic approach," in *Proceedings of the IEEE International Symposium on Dynamic Spectrum Access Networks (DYSPAN '14)*, pp. 60–71, IEEE, McLean, Va, USA, April 2014.

[32] D. Niyato and E. Hossain, "A game-theoretic approach to competitive spectrum sharing in cognitive radio networks," in *Proceedings of the IEEE Wireless Communications and Networking Conference (WCNC '07)*, pp. 16–20, Kowloon, China, March 2007.

[33] D. Monderer and L. S. Shapley, "Potential games," *Games and Economic Behavior*, vol. 14, no. 1, pp. 124–143, 1996.

[34] N. Nie and C. Comaniciu, "Adaptive channel allocation spectrum etiquette for cognitive radio networks," in *Proceedings of the 1st IEEE International Symposium on New Frontiers in Dynamic Spectrum Access Networks (DySPAN '05)*, pp. 269–278, Baltimore, Md, USA, November 2005.

[35] Y. Xing, C. N. Mathur, M. A. Haleem, R. Chandramouli, and K. P. Subbalakshmi, "Dynamic spectrum access with QoS and interference temperature constraints," *IEEE Transactions on Mobile Computing*, vol. 6, no. 4, pp. 423–433, 2007.

[36] T. Heikkinen, "A potential game approach to distributed power control and scheduling," *Computer Networks*, vol. 50, no. 13, pp. 2295–2311, 2006.

[37] Y. Li, D. Jin, J. Yuan, and Z. Han, "Coalitional games for resource allocation in the device-to-device uplink underlaying cellular networks," *IEEE Transactions on Wireless Communications*, vol. 13, no. 7, pp. 3965–3977, 2014.

[38] H. Ryu and S.-H. Park, "Performance comparison of resource allocation schemes for D2D communications," in *Proceedings of the 2014 IEEE Wireless Communications and Networking Conference Workshops, WCNCW 2014*, pp. 266–270, Istanbul, Turkey, April 2014.

[39] Y. Li, S. Su, and S. Chen, "Social-aware resource allocation for device-to-device communications underlaying cellular networks," *IEEE Wireless Communications Letters*, vol. 4, no. 3, pp. 293–296, 2015.

[40] D. I. Laurenson, D. G. M. Cruickshank, and G. J. R. Povey, "Computationally efficient multipath channel simulator for the COST 207 models," in *Proceedings of the IEE Colloquium on Computer Modelling of Communication Systems*, pp. 8/1–8/6, London, UK, May 1994.